The influence of ion-ion correlations on conductivity in concentrated ionic systems

A Thesis Presented for the
Master of Science
Degree
The University of Tennessee, Knoxville

Md. Dipu Ahmed
December 2023

Copyright © 2023 by Md. Dipu Ahmed.
All rights reserved.

ACKNOWLEDGEMENTS

I would like to take a moment to express my most profound gratitude to those who have played a vital part in the journey of my graduate research and thesis. Their faithful back, direction, and input are important, and I appreciate their inclusion all through this journey. To begin with, I would like to thank my advisor, Dr. Alexei Sokolov. His broad information, ability, and progress have shaped the course and quality of my investigation. I am genuinely thankful for his mentorship and the opportunities he has given me to develop both academically and professionally. Uncommonly, much gratitude goes to Dr. Ivan Popov, who made a huge contribution to what my graduate thinks about. His readiness to go over and past to assist me in getting the complex concepts, thoughts, instruments, and writing included in this field may be a genuine favor. His exhortations and experiences have enormously improved the quality of my work.

Thanks to my Graduate Committee members: Dr. Mark Dadmun, Dr. Fred Heberle, and Dr. Stephen Paddison, for serving on my MS committee and for their valuable suggestions and efforts to assist me in completing my MS. I would also like to recognize the important commitments of Dr. Murillo and Dr. Gaukhar. Their skill and bolster in taking the estimations vital to this think about not as it were progressed the exactness of the comes about, but too included profundity to the in general ponder. Their collaborative endeavors and specialized aptitudes are priceless resources for the project.

In expansion, I would like to express my true gratitude to all my colleagues within the Sokolov group. I feel greatly blessed to work in our group with so many talented and kind colleagues. I would like to thank Peyton Carden, Mohanad Mubashar Abdullah and Harmandeep Singh for their help and support to finish some experiments and their valuable guidelines to overcome difficult times. Their immovable backs, near fellowship, and mental trade created a fortifying environment for scholarly development. I am thankful for their fellowship, talks, and mindful exhortation, which have incredibly contributed to my individual and proficient development during graduate school.

In addition to my scholarly bolster, I am obliged to my family and companions. Their unflinching conviction in my capacities, unrestricted adoration, and steady support gave me quality and inspiration to overcome challenges and continue. I particularly need to thank my guardians and Kazi Madina Maraz for their unflinching otherworldliness, which has been a consistent source of motivation and guidance.

Finally, I would like to thank everybody who has contributed to my development and victory, whether directly or indirectly. Your bolster, whether through enthusiastic talks, useful comments, or indeed a straightforward word of support, has had a critical effect on my learning journey. I am truly thankful for your nearness and the commitments you've made.

ABSTRACT

This study delves into the fascinating realm of concentrated ionic systems, such as ionic liquids, superionic materials, organic ionic plastic crystals, and polyelectrolytes, which hold immense potential for energy storage applications. The focus is on understanding the intricate role of ionic correlations in shaping their ionic conductivity behavior. These correlations can either boost or impede conductivity, yet their underlying mechanisms remain elusive. Through extensive investigation of various materials, including ionic liquids with differing anionic masses, pure organic ionic plastic crystals, and doped systems, this research employs advanced techniques like dielectric spectroscopy and innovative momentum conservation models to quantify these correlations. Additionally, the study explores the impact of Li+ doping on the conductivity of organic ionic plastic crystals, providing valuable insights into ways to enhance their conductivity. Ultimately, this research not only contributes to the development of high-conductivity electrolytes for innovative technologies like solid-state batteries but also advances our fundamental understanding of ion transport in concentrated ionic systems.

TABLE OF CONTENTS

CHAPTER ONE INTRODUCTION AND GENERAL INFORMATION..... 1
1.1. Introduction..... 1
1.2. Thesis Outlines..... 3
CHAPTER TWO BACKGROUND KNOWLEDGE AND LITERATURE REVIEW..... 6
2.1. Basic Concept of Electrolyte 6
2.1.1. Type of Electrolytes..... 9
2.1.2. Advantage of Solid Electrolyte over Liquid Electrolyte..... 13
2.1.3. Conductivity of Solid Electrolyte: Factors Influencing and Potential Enhancements 17
2.2. Ionic correlation in concentrated ionic systems..... 21
2.2.1. why are ionic correlations important?..... 22
2.2.2. Ion-ion Correlations in Ionic Liquids 24
2.2.3. Ion-ion Correlations in Pure Organic Ionic Plastic Crystals (OIPCs) 26
2.2.4. Ion-ion Correlations in doped Organic Ionic Plastic Crystals (OIPCs)..... 28
2.2.5. Ionic Correlations in Poly-ionic Liquids (PolyILs) 30
2.3. How to Study Ion-ion Correlations?..... 32
2.4. Research Objectives..... 33
2.4.1. Intellectual merit 34
CHAPTER THREE MATERIALS AND METHODS..... 36
3.1. Studied Samples/Materials for Understanding of Ionic Correlations..... 36
3.1.1. Ionic liquids 36
3.1.2. Organic Ionic Plastic Crystals (OIPCs) 40
3.2. Experimental Techniques..... 43
3.2.1. Broadband Dielectric Spectroscopy (BDS) 43
3.2.2. Differential Scanning Calorimetry (DSC) 50
CHAPTER FOUR THE EFFECT OF ION MASS ON DYNAMIC CORRELATIONS IN IONIC LIQUIDS 55
4.1. Introduction..... 55
4.2. Experimental Results 57

4.2.1. Materials 57
4.2.2. Broadband Dielectric Spectroscopy (BDS) 57
4.3. Discussion 59
4.4. Conclusion 71
CHAPTER FIVE THE INFLUENCE OF DOPING ON CONDUCTIVITY IN ORGANIC IONIC PLASTIC CRYSTALS (OIPCS) 72
5.1. Introduction 72
5.2. Material and experimental measurements details 75
5.2.1 Materials 75
5.2.2. Analytical methods and techniques 75
5.3. Experimental Results 78
5.4. Discussion 80
5.5. Conclusion 96
CHAPTER SIX CONCLUSIONS 97
LIST OF REFERENCES 99
VITA 114

LIST OF TABLES

Table 1: The effect of doping and size of dopant on enthalpy and melting temperature at different phase transitions. 88

LIST OF FIGURES

Figure 1.1 Schematic representation of ion-ion correlations. Positive ion-ion correlations increase conductivity and negative ion-ion correlations suppress conductivity. Taken from[9] 2

Figure 2.1 Role of electrolytes during charging and discharging process of battery [20, 21] 7

Figure 2.2 Different types of electrolyte a). Liquid electrolytes b). Gel electrolyte [41]c). Solid state electrolytes[44, 45]..... 11

Figure 2.3 Major drawbacks of liquid electrolyte. a). Lower transport number of Ionic Liquid [77] b). Dendrites formation impairs the overall performance of battery [70] c). Leakage issue associated with liquid electrolyte [78] d). Expanded I-phone 3GS's Li battery due to short circuit [79] e). Explosion of battery in highway due to thermal runaway in Tesla S model car[80] 15

Figure 2.4 Comparative Analysis of ionic Conductivity in Sodium-Based Solid-State Electrolytes (SSEs) and Liquid Electrolyte Benchmark [96] 18

Figure 2.5 Comparative analysis of ionic conductivity in different lithium-ion battery electrolytes[95, 106] 20

Figure 2.6 Temperature dependence Ionicity/IHR (H-1) of some ionic liquids[7, 119, 127, 142-144]. 25

Figure 2.7 a). DC conductivity of P1224-PF6 on both heating and cooling cycle b). Diffusion coefficient of ions in different phases where no step like change during phase transitions c). Relationship of H-1 and temperature in P1224-PF6 during heating and cooling. d). Relationship of H-1 and different phases. Data from [9, 146] 27

Figure 2.8 a). DSC curve of pure P12TFSi plastic crystal to observe the phase transitions b). Conductivity comparison of pure and different % of doping [147, 148]. 29

Figure 2.9 a) The relationship of H-1 and inverse temperature in PolyILs with various mobile ions and structure. (b) The same data represented vs Tg/T scale. H^{-1} clearly decreases with the increase of mass of mobile ions. Data are collected from [9] 31

Figure 3.1 Chemical structure and general information of selected ILs: BMIM-BF4, BMIM-PF6 and BMIM-TFSI 38
Figure 3.2 Chemical structure and general information of selected OIPCs: P [1,2]-TFSI, P [1,4]-TFSI and dopant: LITFSI, BMIM-TFSI. 41
Figure 3.3 A dielectric permittivity spectrum covering a wide frequency range is provided, showing the real ε '(ω) and imaginary ε "(ω) components of permittivity for various polarization mechanisms such as ionic relaxation, dipolar, atomic, and electronic polarization[187]. 44
Figure 3.4 (a). A dielectric permittivity spectrum for non-conductive samples with single dipole relaxation with permanent. (b). Permittivity and Conductivity spectrum for ionic conductive samples[188] 47
Figure 3.5 Schematic representation of a usual conductivity spectrum. It has three regions: AC conductivity(σAC) at higher frequencies, DC conductivity(σDC) in the middle frequencies, electrode polarization effect, which is a drop caused on by the buildup of charge carriers at the electrode surface at a lower frequency [193]. 49
Figure 3.6 A DSC thermogram exhibiting the phases of melting, crystallization, and glass transition of material [196, 198] 51
Figure 3.7 Schematics of typical DSC equipment [199] 53
Figure 4.1 Conductivity spectra over a wide frequency range for the different ionic liquids: (a) [BMIM][BF4]; (b) [BMIM][PF6]; and (c) [BMIM][TFSI]. 58
Figure 4.2 (a) Temperature dependence of the DC conductivity, σ_DC: symbols present experimental data, and lines are from the MD simulations results. The inset figure in Fig 4.2(a) represents the comparison of MD results and experimental data on an expanded scale. **(b)** Temperature dependence of the conductivity relaxation time, $\tau\sigma$. The gap in experimental data for σDC and $\tau\sigma$ at low temperatures for [BMIM][PF6] and [BMIM][TFSI] is due to crystallization. 60
Figure 4.3 (a) Radial distribution functions of center of mass of cations and anions in ILs to estimate the half of the average distance between the ions, <d> rdf /2. (b) Ion's re-arrangement length estimated from Eq. (4.2) for cations (open square symbols) and anions (closed square symbols) 62

Figure 4.4 Temperature dependence of diffusion coefficient for cation and anion in ILs. Circle symbols represent our experimental data which are in good agreement with previous studies (ref [214]) Whereas PFG-NMR data are shown as a diamond symbol, MD data are shown solid and dotted lines for cation and anion respectively..... 63

Figure 4.5 Temperature dependence of the ionicity or inverse Haven ratio. Circle symbols represent our experimental data, where diffusion coefficient was estimated from the ac-dc crossover and square symbols corresponds to data, where diffusion coefficient was measured by PFG-NMR results. The dashed lines represent the average value of ionicity from the MD simulations which are in good agreement with the experimental data. 64

Figure 4.6 Distinct ion-ion contribution to conductivity normalized by σNE of three ionic liquids, where closed symbols represent our experimental data and open symbols represent data from MD simulations..... 66

Figure 4.7 The relationship between the diffusion coefficient and the cation/anion mass ratio was determined via MD simulations. 69

Figure 5.1 Chemical structure and general information of selected OIPCs: P12TFSI, P14TFSI and dopant: LITFSI, BMIMTFSI. 76

Figure 5.2 Conductivity spectra of pure and doped system at different temperature a). Pure P12TFSI b). P12TFSI+ 4.8% LITFSI c). P12TFSI+4.8% BMIMTFSI, in Fig. 5.2a, the additional steps are observed at solid state of P12TFSI, and doping reduces the additional steps in Fig 5.2b, c. 79

Figure 5.3 a) Temperature dependence of DC-conductivity of P12TFSI in solid and meted states. The red circle symbol represents conductivity measured by following PFG-NMR protocol whereas black circle is for conventional BDS measurement b) Diffusion coefficient of ions in P12TFSI. c). Temperature dependence of the inverse Haven ratio of P12TFSI in solid (Phase 1) and melted states..... 81

Figure 5.4 a). Additional steps in conductivity spectra of P12TFSI at different temperature. b). Conductivity spectra comparison of two type of measurement: conventional and PFG-NMR protocol at 20°C 83

Figure 5.5 WAXS spectra for two data sets of pure P12TFSI. a). P12TFSI (fresh sample) at 50°C and 100°C b) P12TFSI (aging sample), subjected to a 3–4-month room temperature storage period and used for conductivity measurements via the PFG-NMR protocol, was analyzed at 50°C. Calculating the ratio of weight fraction of liquid and crystalline phase ($S = WL/WC$) for a). P12TFSI (0.24) b). P12TFSI (0.94) and red dotted fitting line is obtained by using Eq. (5.1) 85

Figure 5.6 Comparison of conductivity of pure P12TFSI, with 4.8% LITFSI and 4.8% BMIMTFSI at different temperature b). DSC thermogram depicted phase transitions behavior of those systems. 87

Figure 5.7 Conductivity spectra for both pure and doped P12TFSI at solid phase shows that they coincide with each other at microscopical level. 90

Figure 5.8 Conductivity spectra of pure P12TFSIand with two doping systems at different temperatures representing different phases..... 91

Figure 5.9 WAXS measurements of pure and doped P12TFSI, a). WAXS spectra for pure and two doped P12TFSI sample at 50C to observe proportion of liquid and solid phase. Three different measurements in same condition to observe the repeatability and reproducibility among spectra and fitting those with Eq. (5.1) to determine proportion of solid and liquid phase b). Pure P12TFSI c). P12TFSI + 4.8% LITFSI d). P12TFSI + 4.8% BMIM TFSI. 93

Figure 5.10 a). Conductivity comparison of pure P14TFSI and with 4.8% LITFSI b). DSC thermogram of those systems to observe different phase transition behavior. 95

CHAPTER ONE
INTRODUCTION AND GENERAL INFORMATION

1.1.Introduction

The ongoing advancement of battery-powered consumer electronics, which come in a variety of sizes ranging from small personal devices like smartwatches and smartphones to larger electric vehicles, calls for in-depth research and development in the field of appropriate energy storage and conversion technologies. The electrolyte plays a significant role in these applications as a deciding factor that controls important aspects including durability, overall performance, and charge and discharge characteristics[1-5]. Therefore, it is imperative to conduct in-depth research and innovate regarding the electrolyte in order to enhance its characteristics and guarantee compatibility with a variety of energy storage and conversion systems.

Concentrated ionic systems have made significant contributions to the advancement of various technologies, including solid-state batteries, fuel cells, and supercapacitors. They are organic plastic ionic crystals (OPICs), ionic liquids (ILs), polymer electrolytes, and superionic ceramics. Ionic conductivity (σ_{DC}) is one of the significant physical characteristics used to describe ionic systems. By knowing the diffusion coefficient (D_i) and concentration of mobile ions (n_i), ionic conductivity can be estimated using Nernst-Einstein equation. [6, 7].

$$\sigma_{NE} = \frac{q^2}{kT}\sum_i n_i D_i \tag{1.1}$$

Where q is the charge of ion. Eq. (1.1) is applicable to only diluted solutions when each ion is assumed to contribute independently. Because of the close proximity of the ions in concentrated ionic systems and the significant ion-ion correlations that result from their interaction, the NE equation can't adequately represent the ionic conductivity. Considering these ion-ion correlations, a generalized NE equation can be written [6-8].

$$\sigma_{DC} = H^{-1}\frac{q^2}{kT}\sum_i n_i D_i \tag{1.2}$$

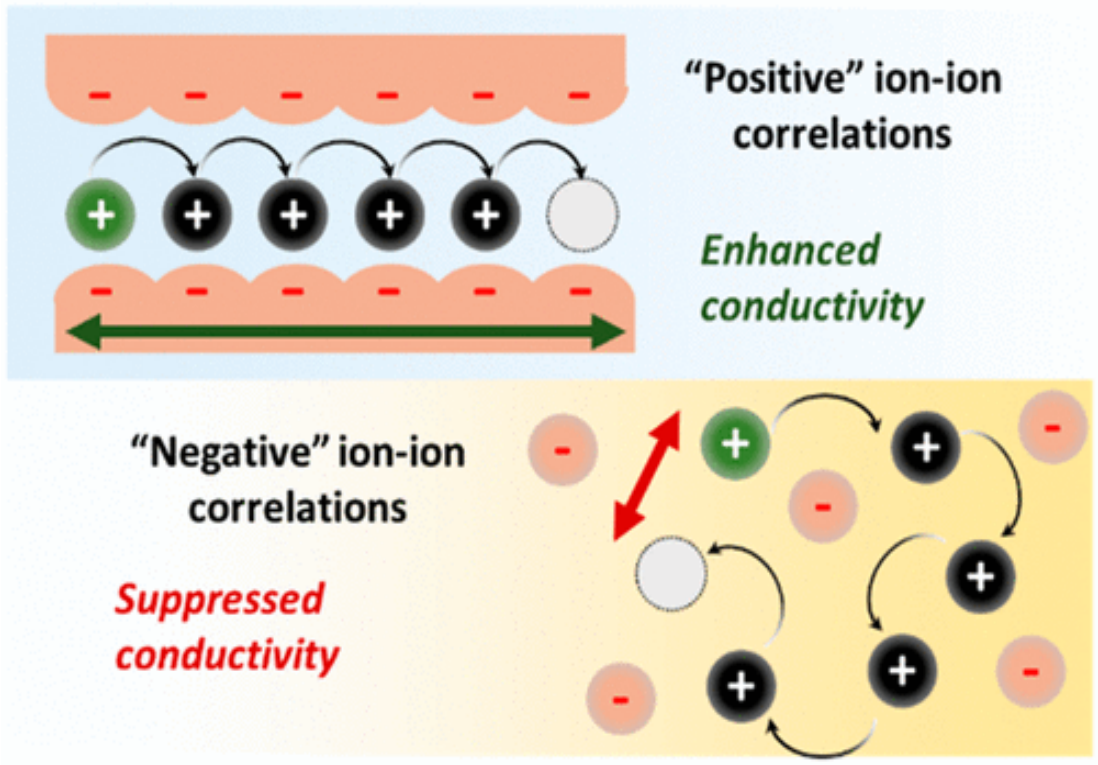

Figure 1.1 Schematic representation of ion-ion correlations. Positive ion-ion correlations increase conductivity and negative ion-ion correlations suppress conductivity. Taken from[9]

where the ratio ($H^{-1} = \sigma_{DC}/\sigma_{NE}$) of experimentally measured conductivity to the one predicted by the NE equation is known as ionicity or inverse Haven ratio [10, 11]. The conductivity of concentrated ionic systems is significantly influenced by ionic correlations, which can either be positive with charge displacement greater than that of the ions, improving conductivity, or negative with charge displacement less than that of the separate ions as a result of apparent correlated ions backflow[9, 12, 13].

Ionic correlations control H^{-1}, these correlations are known to reduce ionic conductivity in ILs(~2–3 times), in polymerized ionic liquids (an order of magnitude)[7, 12, 14], and in organic ionic plastic crystals (OIPCs) (~100 times) [9, 15] but increase conductivity in superionic glasses and crystals (~3-5 times)[16, 17]. Thus, ionic conductivity can be changed by more than two orders of magnitude by altering ionic correlations, but the reason. behind why ionic correlations greatly increase conductivity in superionic ceramics while dramatically decrease it in PolyILs and OIPCs remains unknown.

1.2.Thesis Outlines

Chapter 2 presents a comprehensive review of concentrated ionic systems, such as ionic liquids, organic ionic plastic crystals, and poly-ionic liquids. It explores the influence of ion-ion correlations on the conductivity of these systems, offering insight on the fundamental concepts. Furthermore, the chapter emphasizes the significance of solid-state batteries and discusses approaches to improve the conductivity of solid electrolytes, which is critical for enhancing battery performance. Moreover, this chapter explains the possible way including the momentum conservation approach to estimate the contribution of distinct ion-ion correlations to conductivity in these systems.

Chapter 3 focuses on the materials and experimental techniques used during the research. The chapter gives a concise summary of the selected materials, especially ionic liquids, and organic ionic plastic crystals, explaining why they were chosen and how they are important to electrochemical energy storage systems. It introduces and describes the

principles and instruments of Broadband dielectric spectroscopy (BDS), Differential Scanning Calorimetry (DSC). These techniques are critical in investigating the characteristics and behavior of the concentrated ionic systems under research. This chapter establishes the framework for the future analysis and interpretation of the study findings by offering a comprehension of the experimental methodology.

In Chapter 4 of this thesis, our original research investigates the influence of ion-ion correlations on the conductivity of ionic liquids. We introduce a novel approach based on momentum conservation that allows us to quantify the specific contribution of ion-ion correlations to the overall conductivity of ionic liquids. To validate our findings, we utilize molecular simulation data, providing further support and verification. This chapter also presents our research findings on the influence of the mass of the anion on this contribution to conductivity. We delve into the effects of the anion's size and shape on important parameters such as transport number and ionicity. These factors directly influence the strength of ion-ion correlations and, consequently, the overall conductivity of the system. Our original research work employs techniques such as differential scanning calorimetry (DSC) and broadband dielectric spectroscopy (BDS) to obtain insightful and significant findings.

Chapter 5 focuses on the investigation turns to the effects of ion-ion correlations in organic ionic plastic crystals. This section explores the intricate interplay of ion-ion correlations in both pure and doped systems, aiming to uncover the underlying mechanisms that govern their behavior. The chapter further investigates the influence of dopant size on conductivity, shedding light on how variations in dopant size can modulate the transport properties within these systems. Moreover, it conducts a comprehensive examination of the observed phase transition behavior, elucidating the role of ion-ion correlations in these transitions and their subsequent impact on conductivity properties.

Finally, Chapter 6 serves as the culmination of the significant findings derived from this research. It provides a comprehensive review of the key insights gained into the profound

nature of ion-ion correlations and their profound implications for conductivity in various concentrated ionic systems. By summarizing the contributions made towards understanding ion-ion correlations and their influence on conductivity, this chapter serves as a valuable resource for future research in this field. It concludes by offering guidelines for potential future directions, highlighting areas where further investigations can expand upon our current knowledge and contribute to the advancement of this captivating area of study.

CHAPTER TWO
BACKGROUND KNOWLEDGE AND LITERATURE REVIEW

This chapter explores the ion-ion correlations and ion dynamics seen in concentrated ionic systems such polyionic liquids, organic ionic plastic crystals, and ionic liquids as described in the body of published research. The mass and shape of the ions demonstrate significant effects on the phenomena of ionic correlations and the processes driving ion diffusion in these systems, which have a major impact on their conductivity. In particular, it has been found that the existence of ionic correlations reduces the ionic conductivity of ionic liquids (by about 2-3 times), polymerized ionic liquids (by more than an order of magnitude), and organic ionic plastic crystals (by around 100 times). On the other hand, it has been discovered that the existence of ionic correlations increases conductivity in superionic ceramics by around 3-5 times. This chapter seeks to present a thorough analysis of the distinct ionic correlations seen in these varied systems, illuminating their characteristics and significance. The idea of solid-state batteries and methods for enhancing the conductivity of solid electrolytes will both be examined concurrently within the context of this literature study. This chapter aims to improve the understanding of ion-ion correlations and solid electrolyte conductivity in the context of the systems by clarifying underlying facts and exploring previous research.

2.1. Basic Concept of Electrolyte

An electrolyte is a substance that allows electricity to flow through it by using charged particles called ions, rather than electrons. It is typically a soluble salt, acid, or base that is dissolved in a polar solvent like water. They are essential in many electrochemical systems, including batteries, fuel cells, and electrolytic cells[18-20]. Understanding the mechanism controlling conductivity of electrolytes is critical for academic reasons in the realm of energy storage and conversion. The primary function of electrolytes is to enable the movement of ions within electrochemical devices without allowing the flow of electrons. Without this characteristic, the cell would not be able to discharge properly. When a voltage is applied, positively charged ions (called cations) migrate to the negative electrode

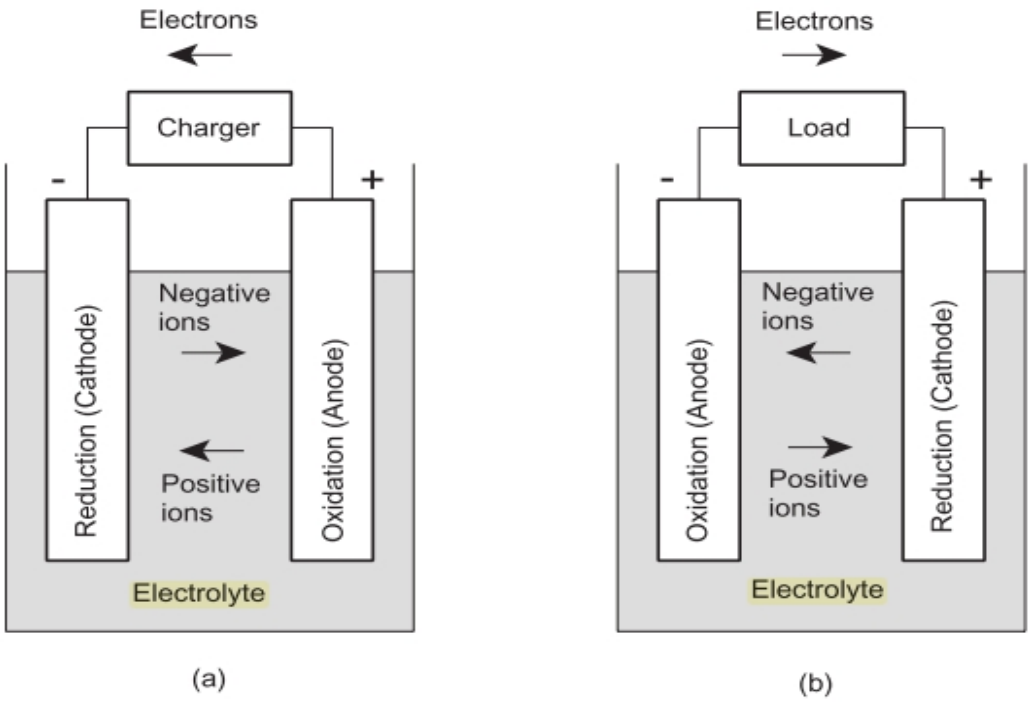

Figure 2.1 Role of electrolytes during charging and discharging process of battery [20, 21]

while negatively charged ions (called anions) travel to the positive electrode. This ion movement facilitates the flow of electric current, which is required for energy storage, conversion, or chemical reactions to occur[18-21].

The characteristics of electrolytes are critical to the performance of electrochemical systems[20, 21]. Here are some of the major features of electrolytes:

Ionic conductivity: The property of ionic conductivity determines the efficiency of ion movement within the electrolyte. A high level of ionic conductivity ensures that ions can travel rapidly between the electrodes, leading to enhanced performance of the system as a whole. It is important to note that ionic conductivity refers to the transport of electric charge rather than the physical motion of ions, although it relies on the movement of ions to facilitate this process. [20, 21].

Chemical and electrochemical stability: Chemical and electrochemical stability are critical features that any battery electrolytes e.g., Li, Na or Zn batteries including fuel cells, must have to prevent unwanted reactions and damage over time. It is critical for the electrolyte in lithium-ion batteries to retain stability[20-22] when subjected to an applied electric field and in contact with electrodes, especially when dealing with highly reactive elements like lithium metal.

The electrochemical stability window (ESW) is an important property that specifies the electrode electric potential range in which a material is neither oxidized nor reduced[23]. Determining the ESW for solvents and electrolytes is critical for electrochemical applications such as lithium-ion batteries[24]. For example, the electrolyte in lithium-ion batteries must be stable within the potential range between the anode chemical potential (around 0 V vs Li/Li+) and the cathode chemical potential[25]. If the electrolyte is not stable within this range, it might cause undesirable side reactions that degrade the electrolyte and harm the battery's performance and safety[26].

Mechanical strength: In the case of solid-state electrolytes, mechanical strength is a vital feature for maintaining the material's structural integrity[20, 27]. In electrochemical

systems, electrolytes are used in numerous manners. During the charging and discharging operations of lithium-ion batteries, they allow the reversible flow of lithium ions between the electrodes of the battery[20, 21]. Electricity is generated by the interaction of fuel and oxidant in fuel cells, which rely on electrolytes to move ions between the electrodes[20, 28]. The high energy density as well as the rapid movement of ions of supercapacitors are both made possible by electrolytes[20, 29].

The advancement of electrolytes is a focus of ongoing research and development, particularly in the fields of solid-state electrolytes[20, 27]. To develop the most advanced energy storage systems for next generation electrochemical devices possible, scientists and engineers have focused on improving the reliability, safety, and performance of electrolytes. In order to boost the efficiency, capacity, and durability of electrochemical systems, researchers are working to improve the properties and features of electrolytes[20, 21, 27]. The subject of electrochemical energy storage and conversion must be advanced by better understanding electrolytes. Researchers can find new opportunities and create innovative approaches to fulfill the expanding needs of energy storage and sustainable technologies by examining the structure and characteristics of electrolytes in greater detail[20, 21, 27].

2.1.1. Type of Electrolytes

Based on their physical condition and composition, electrolytes are categorized into several different groups, each with its own set of properties and applications. The following are the primary types of electrolytes:

Liquid Electrolytes: Liquid electrolytes are a common form of electrolyte that consists of salts dissolved in an organic solvent[30]. The solvent allows the salt to dissociate into positive and negative ions, allowing for ion conduction[31]. In lithium-ion batteries, liquid electrolytes are often used, where lithium salts dissolved in organic solvents such as ethylene carbonate or dimethyl carbonate promote the mobility of lithium ions[30]. Lithium hexafluorophosphate (LiPF6) salt is dissolved in non-aqueous solutions in these electrolytes, which are utilized in commercial lithium-ion batteries[32]. Another form of

liquid electrolyte is ionic liquids such as BMIM-BF4, BMIM-PF6 and BMIM-TFSI, which are based on organic salts that are liquid at ambient temperature[33]. Ionic liquids have distinct functions in preventing electrode material breakdown and enhancing electrolyte stability[33].

However, liquid electrolytes have several significant drawbacks and problems that limit their widespread usage in electrochemical systems. Liquid electrolytes are frequently flammable, causing safety concerns in high-energy systems such as lithium-ion batteries. If the cell is damaged or overheated, the flammable electrolyte can cause thermal runaway reactions, leading to flames or explosions[34, 35]. Moreover, Liquid electrolytes can leak or evaporate over time, resulting in electrolyte material loss, lower battery efficiency, and the danger of electrolyte exposure to the environment[36]. Electrochemical devices must also be carefully packaged and sealed to prevent leakage or evaporation. Finally, Corrosion and dendrite growth are serious problems with some liquid electrolytes, notably those used in lithium-ion batteries. Corrosion can degrade electrode materials and have a detrimental influence on overall battery performance. Dendrites, on the other hand, are branching metal formations that can form within the battery, resulting in short circuits and safety problems[37, 38]. These problems are created as a result of interactions between the liquid electrolyte and the electrode materials, as well as uneven lithium deposition during the charging and discharging process[39, 40].

Gel Electrolytes: Gel electrolytes are a liquid electrolyte variant in which the liquid component is trapped inside a gel-like polymer matrix[41]. This gel structure provides mechanical stability while preventing electrolyte flow[42]. Gel electrolytes are useful in applications requiring physical durability, such as flexible batteries or wearable devices. Gel electrolytes have become more significant in growing industries like energy storage, electronics, the environment, medicine, and others[41]. Because of their safety, flexibility, and high performance, gel polymer electrolytes (GPEs) are of significant interest in the development of high-performance rechargeable lithium metal batteries (LMBs)[43]. Gel polymer electrolytes absorb solvent components and help ions move through the polymer

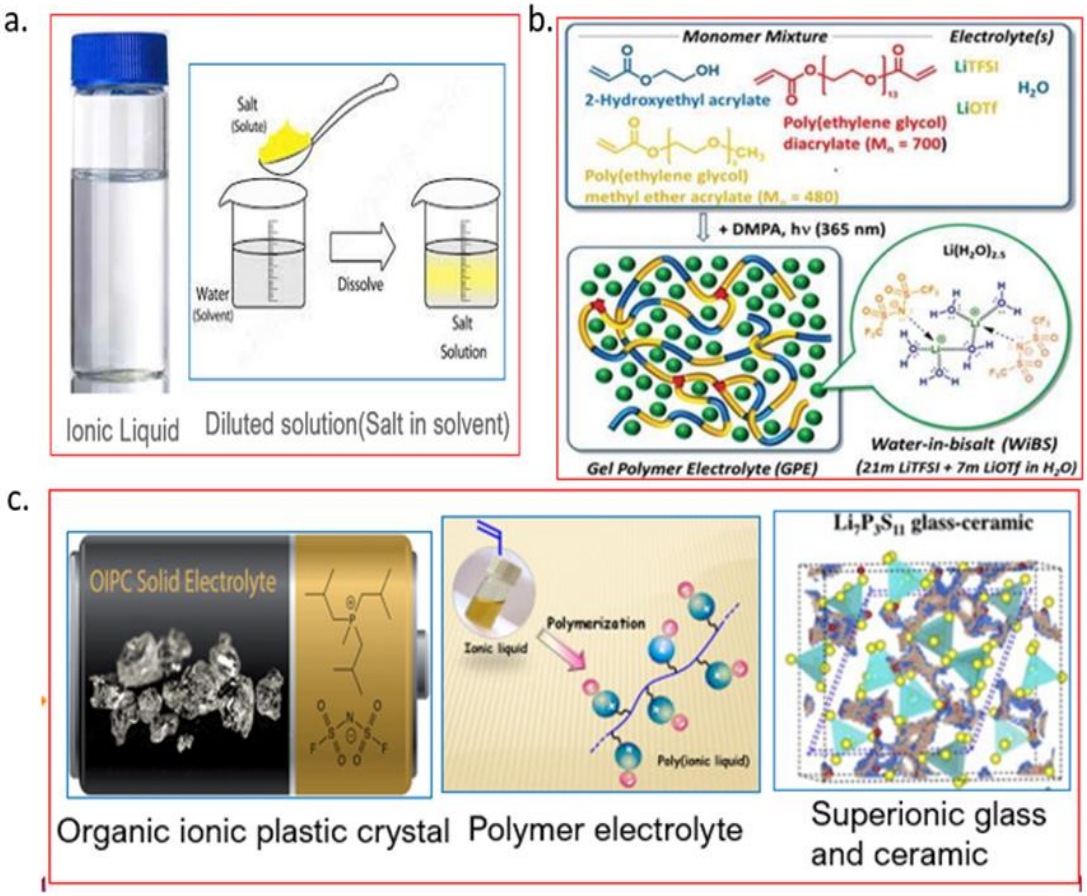

Figure 2.2 Different types of electrolyte a). Liquid electrolytes b). Gel electrolyte [41]c). Solid state electrolytes[44, 45]

matrix[43]. Gel polymer electrolytes can be used to replace present organic liquid electrolytes in lithium-ion batteries[43, 46]. A significant drawback associated with gel electrolytes is like liquids electrolyte as flammability of the solvent, leakage, etc. The limited ability of electrolyte to make effective contact with electrodes sometimes leads to higher polarization and a decrease in the speed of ion transfer within batteries, ultimately influencing the overall battery performance and efficiency[47]

Solid Electrolytes:

Solid-state electrolytes have received significant attention from the field of electrochemical energy storage and conversion due to their potential for enhanced safety, energy density, and stability when compared to liquid or gel electrolytes[44, 45]. They have the benefit of being non-flammable, which decreases the risk of thermal runaway and improves the safety of energy storage devices. Furthermore, solid-state electrolytes may provide better energy. densities, allowing for improved energy storage capacity in a smaller footprint[44, 48].

Based on their composition, solid-state electrolytes can be further classified into various material groups. The following are the primary types of solid-state electrolytes:

Organic Ionic Plastic Crystal (OIPC) Electrolytes are a form of solid-state electrolyte composed of organic compounds having a crystalline structure. Because of the presence of mobile ions inside their lattice structure, these organic crystals have strong ionic conductivity[44, 49, 50]. OIPC electrolytes provide several benefits, including excellent mechanical flexibility, a broad electrochemical stability window, and the possibility for high ion transport. They are being researched for application in solid-state batteries, supercapacitors, and other energy storage devices[44, 49-51]

Ceramic Electrolytes are made of inorganic elements for example, lithium ceramics like, lithium phosphates and lithium garnets. These materials have excellent ionic conductivity and can tolerate high temperatures, making them appropriate for demanding working conditions. Ceramic electrolytes are being widely explored for use in solid-state lithium-ion batteries, where they can improve safety, increase energy density, and enable longer

battery lifetimes[44, 52-54].Polymer electrolytes include advantages like flexibility, low cost, and high compatibility with electrode materials. They are used in lithium polymer batteries and other electrochemical devices[44, 55, 56].

Moreover, Composite electrolytes, such as polymers combined with ceramics or Polymer with Ionic Organic Polymer Conductors (IOPCs), offer improved properties for energy storage. These composites benefit from ceramics' strength and polymers' flexibility, enhancing thermal stability, ionic conductivity, and safety in lithium-ion batteries[57, 58]. This capitalizes on IOPCs' inherent ion conductivity to boost overall electrolyte performance, enabling faster charge-discharge rates and higher energy density. However, their fabrication can be intricate due to the need for precise ceramic-polymer interfaces or make a perfect balance between organic and ionic components in Polymer-IOPCs[57, 59]. Ongoing research and development activities are aimed at improving the performance and properties of electrolytes of all sorts, with the goal of advancing the area of electrochemical energy storage and conversion [21, 44, 50].

2.1.2. Advantage of Solid Electrolyte over Liquid Electrolyte

Liquid electrolytes frequently have greater ion conductivity than other forms of electrolytes. The faster ion mobility enables higher conductivity, allowing for faster charging a of batteries and their high power [60-62]. For example, Ionic liquid electrolytes (ILEs) offer great potential for high-power battery applications due to their superior conductivity. At low temperatures, such as 10 °C, they can achieve a reasonable ion conductivity of over 10^{-4} S cm^{-1}. These ILEs possess several advantageous properties, including a high intrinsic ionic conductivity at room temperature, excellent thermal stability, and good electrochemical stability within the voltage range of 4.0-5.2 V[63-65]. All six [bmim]-based ionic liquids examined in this study demonstrate relatively high ionic conductivities (σ). The conductivities are influenced by temperature, as illustrated in Fig 2.3a. At 100 °C, they exhibit conductivities exceeding 10^{-2} S cm^{-1}, while at room temperature, they range from 10^{-5} to 10^{-3} S/cm [66].However, Liquid electrolytes used in batteries present significant disadvantages, primarily related to dendrite growth, leakage,

and safety concerns, including high flammability, the risks of explosion and thermal runaway.

These limitations are crucial to address in order to ensure the safe and efficient operation of energy storage devices[67-69]. One prominent drawback of liquid electrolytes is the potential formation of dendrites, which are needle-like metallic structures that can grow within the electrolyte and bridge the electrodes[38]. This phenomenon can occur due to electrode instability, uneven current distribution, or non-uniform electrolyte composition. Dendrites compromise the battery's performance and safety by causing short circuits and impeding the proper functioning of the system. Liquid electrolytes are particularly susceptible to dendrite growth compared to other electrolyte types, making it a significant concern in battery technology[70, 71].

Furthermore, transport numbers indicate the fraction of electric current carried by specific ions in an electrolyte. In conventional batteries, low transport numbers for lithium ions, where most of the current is carried by negatively charged anions[72], can limit energy and power densities. High mobility of anions creates strong cell polarization, blocking electric field and strongly reducing the overall conductivity[73, 74]. Additionally, their weaker ionic conductivity makes them less suitable for energy storage and conversion applications. Typically, liquid electrolytes exhibit a cation transport number that is approximately 0.5, which can be considered moderately low. However, ionic liquids (ILs) lack lithium ions (Li^+). Only when ILs are infused with Li^+ do they possess it. This introduces a situation where the cation transport number is diminished because the conductivity involves a minimum of three ions. The contribution of Li^+ to conductivity is minor due to its generally limited presence in terms of concentration[75]. As a result, the transport numbers of ionic liquids restrict their effectiveness as electrolytes in batteries, emphasizing the need to consider this factor when evaluating their suitability for such purposes[76].

Leakage is another challenge associated with liquid electrolytes. When the battery casing is damaged or compromised, the liquid electrolyte may escape, resulting in reduced

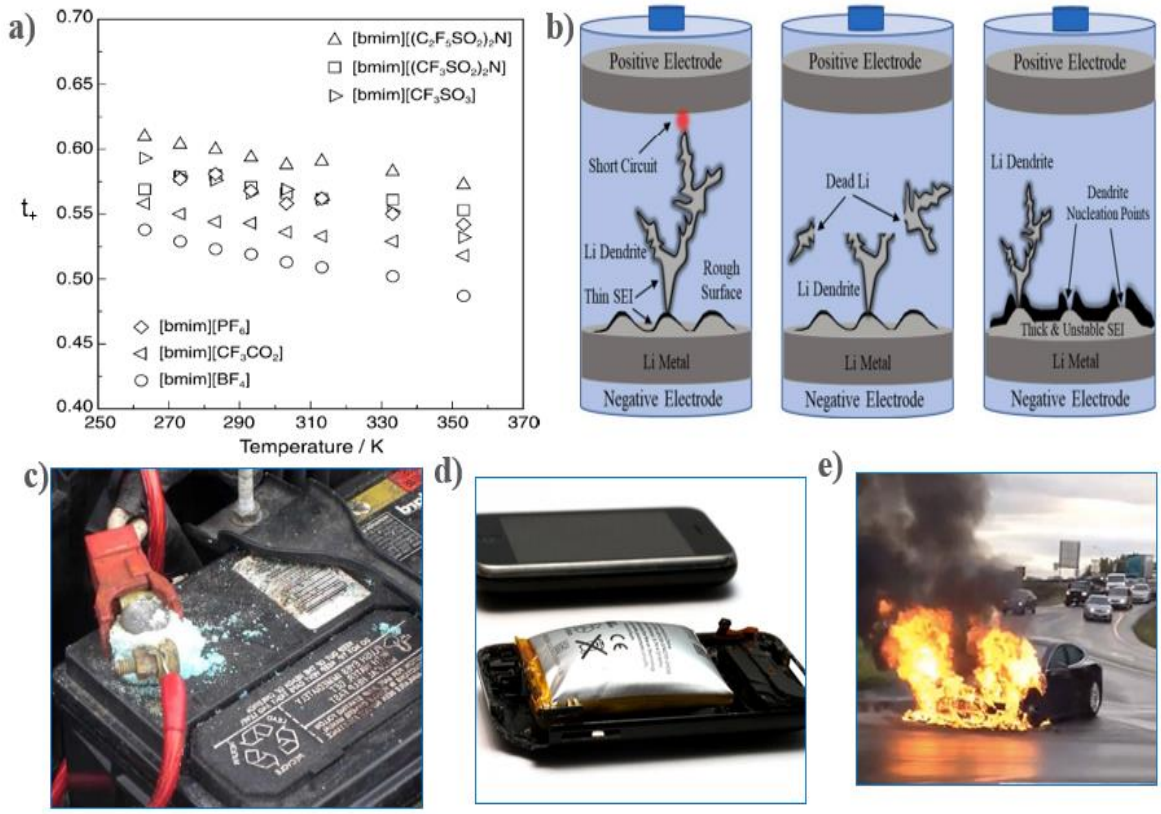

Figure 2.3 Major drawbacks of liquid electrolyte. a). Lower transport number of Ionic Liquid [77] b). Dendrites formation impairs the overall performance of battery [70] c). Leakage issue associated with liquid electrolyte [78] d). Expanded I-phone 3GS's Li battery due to short circuit [79] e). Explosion of battery in highway due to thermal runaway in Tesla S model car[80]

capacity and performance[81]. Beyond the technical implications, electrolyte leakage poses environmental risks and safety hazards. Exposure to liquid electrolytes can be corrosive and harmful, necessitating careful handling and disposal protocols[82].

Moreover, liquid electrolytes introduce safety concerns due to their flammability, especially when organic solvents are involved[83]. Under certain conditions such as high temperatures, overcharging, or physical damage, the flammable components of the electrolyte can vaporize, ignite, and contribute to thermal runaway[80, 84]. The risk of explosion, fire, and related safety hazards is particularly significant in high-energy-density applications, including electric vehicles and large-scale energy storage systems. The potential consequences of such incidents underscore the need for robust safety measures and alternative electrolyte technologies.

Thermal runaway, characterized by an uncontrollable increase in temperature within the battery, is another critical safety issue associated with liquid electrolytes. It can be triggered by internal short circuits, overcharging, or exposure to high temperatures. Once initiated, thermal runaway can propagate rapidly, leading to a cascading release of heat, the generation of gases, and the potential for catastrophic battery failure[80, 85, 86]. The prevention and mitigation of thermal runaway events are essential for ensuring the reliability and safety of energy storage systems.

To overcome the limitations of liquid electrolytes, ongoing research and development efforts are focused on alternative electrolyte technologies, such as solid-state electrolytes[87-94]. Solid-state electrolytes offer improved safety by eliminating the flammability and volatility associated with liquid electrolytes. Developing solid-state electrolytes with enhanced stability, high conductivity, and compatibility with electrode materials is a promising approach to address the challenges posed by liquid electrolytes[87-94].

2.1.3. Conductivity of Solid Electrolyte: Factors Influencing and Potential Enhancements

Solid-state batteries have emerged as a possible alternative to ordinary lithium-ion batteries, notably for electric cars. They have various advantages, including increased energy density, improved safety, shorter charging times, longer lifespan, smaller size, and greater thermal stability[87-94]. Because of their compact solid electrolytes, solid-state batteries store roughly twice as much energy as lithium-ion batteries. This results in extended driving ranges and improved performance. They are also safer, featuring non-combustible or self-ignition resistant solid electrolytes that reduce the risk of fires[88]. Solid-state batteries charge faster, reducing "range anxiety" and making them more convenient for consumers[93]. They have a longer life cycle, which lowers long-term expenses and environmental effects. Solid-state batteries are smaller and lighter, making electric cars more efficient. Finally, because of their better thermal stability, they are appropriate for use in harsh and extreme temperatures[87-94]. Solid-state batteries, in general, have significant potential for energy storage and electric vehicle applications.

The replacement of liquid electrolytes with solid alternatives improves battery safety by suppressing dendrite growth and offering superior mechanical, electrochemical, and thermal stability[87-94]. However, solid electrolytes have lower conductivity compared to liquid electrolytes due to slowed ion diffusion through the solid medium[95] . Solid electrolytes exhibit inherently lower ionic conductivity, which can limit their performance in electrochemical energy storage devices. SPEs consist of a polymer matrix, salt, some have ion attached to a polymer chain, forming a macromolecular structure[96]. They possess advantages such as low flammability, good flexibility, and are particularly suitable for flexible solid-state sodium batteries[96-98]. Polyethylene oxide (PEO) integrated with sodium salts is a widely investigated material in SPEs for solid-state sodium batteries[96, 99-101]. However, SPEs typically exhibit relatively low ionic conductivity, ranging from approximately 10^{-6} to 10^{-8} S cm^{-1} at room temperature (RT)[96, 99-101]. To address this limitation, composite polymer electrolytes (CPEs) are prepared by incorporating ceramic fillers to enhance the ionic conductivity[96, 102, 103]. This addition creates more

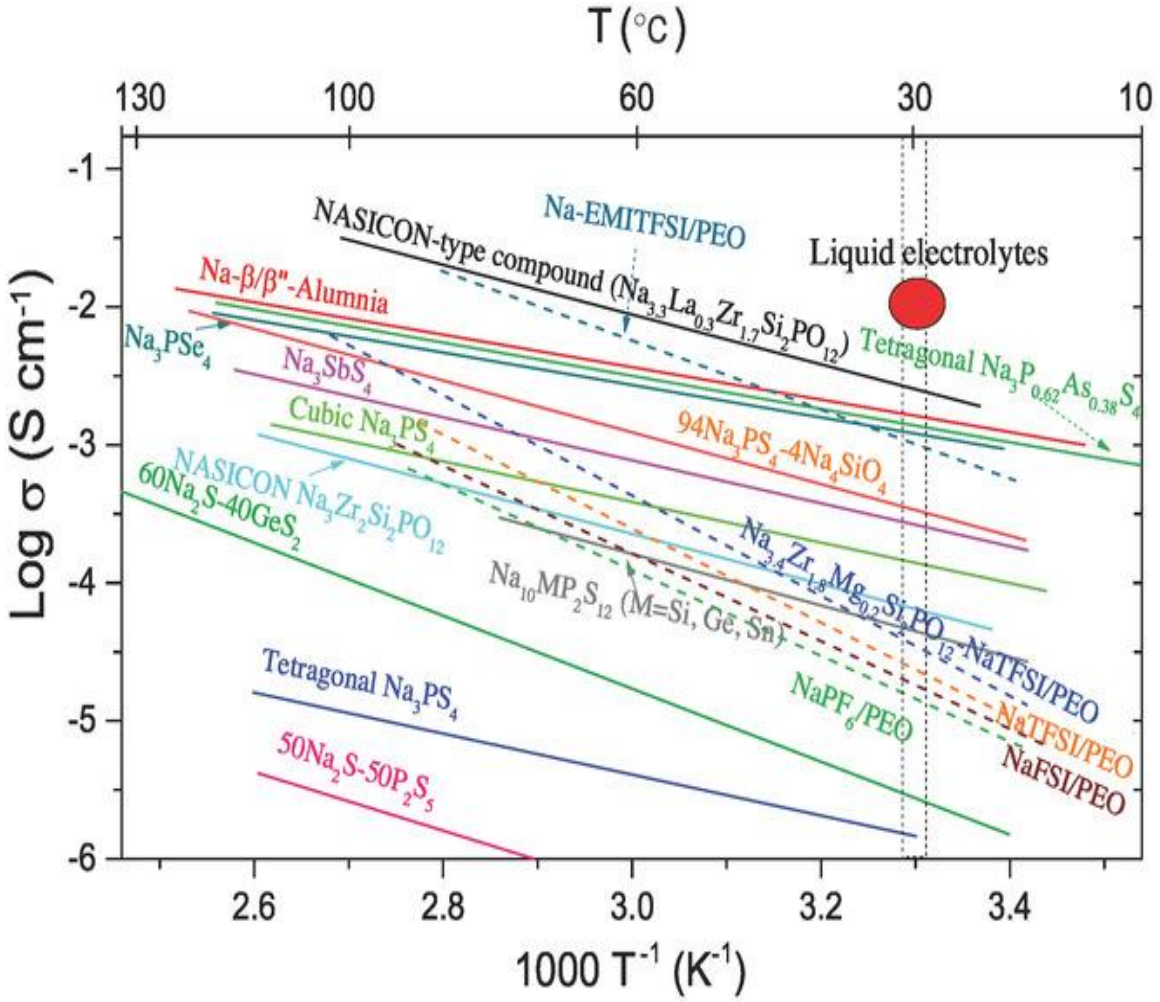

Figure 2.4 Comparative Analysis of ionic Conductivity in Sodium-Based Solid-State Electrolytes (SSEs) and Liquid Electrolyte Benchmark [96]

amorphous regions within the polymer host, thereby improving ion transport[104]. It is worth noting that inorganic solid electrolytes (ISEs) generally possess inherently high ionic conductivity at ambient temperature (10^{-3} S cm^{-1}) and exhibit high mechanical strength, which helps suppress the growth of dendrites[96]. However, ISEs currently face challenges such as high cost and complex processing, requiring further optimization[96].

The ionic conductivity of solid-state electrolytes (SSEs) at room temperature (RT) plays a crucial role in the advancement of solid-state batteries. The Fig. 2.4 highlights the representative SSEs, including Poly (ethylene oxide) (PEO), Na super ionic conductor structure (NASICON), NaN(SO2F)2 (NaFSI), NaN(SO2CF3)2 (NaTFSI), and 1-ethyl-3-methylimidazolium bis(trifluoromethanesulfonyl)imide (EMITFSI), with their respective room temperature conductivities[96]. It provides a summary of the ionic conductivity for representative sodium-ion SSEs. Unfortunately, none of the materials investigated thus far have demonstrated a high ionic conductivity at room temperature (RT), not even reaching the same level as liquid electrolytes (as indicated by the red oval in the figure) [96]. Moreover, in comparison to polymer electrolytes, inorganic solid electrolytes (ISEs) have shown a higher ionic conductivity within a relatively low temperature range. A recent discovery involves a composite electrolyte based on the Na Super Ionic Conductor (NASICON) structure, specifically $Na_{3.3}La_{0.3}Zr_{1.7}Si_2PO_{12}$. This composite electrolyte exhibited a significantly higher ionic conductivity of 3.4×10^{-3} S cm^{-1} at 25 °C[96, 105]. This finding demonstrates the potential for further development of solid electrolytes.
The conductivity of liquid electrolytes is generally higher, around 10^{-2} S cm^{-1}, compared to the most conductive solid electrolytes, which have reported conductivities on the order of 10^{-3} S cm^{-1} at room temperature. Solid electrolytes show a temperature-dependent conductivity, increasing with temperature, making them well-suited for high-temperature applications. However, conductivity decreases at lower temperatures, leading to reduced power density of solid-state batteries in cold conditions, as shown in Fig. 2.4 [95, 106].Conductivity of liquid electrolytes also have T dependence, but it is weaker.

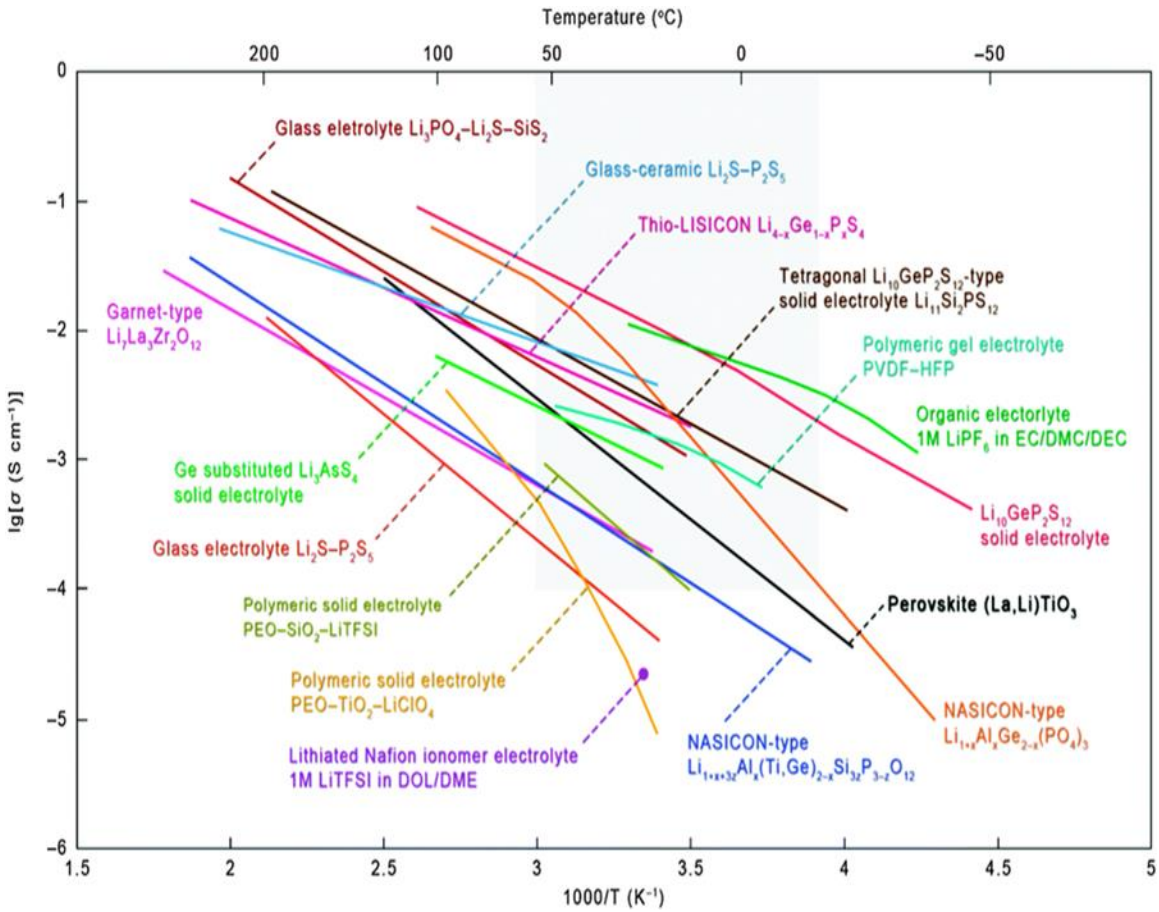

Figure 2.5 Comparative analysis of ionic conductivity in different lithium-ion battery electrolytes[95, 106]

Besides the lower ion conductivity, the high interfacial resistance between the electrode and solid electrolyte surfaces poses another challenge to ion diffusion. This resistance arises due to poor adhesion between the solid surfaces and inadequate penetration of the electrolyte into the porous electrode. In contrast, liquid electrolytes freely saturate the electrode structure, utilizing more ions stored deep within the electrode, resulting in a significantly reduced electrode-electrolyte interface when using solid electrolytes. Consequently, the number of usable ions available for charge transfer is restricted. To address this challenge, a small amount of liquid electrolyte is usually introduced at the electrode-electrolyte interface to reduce the interfacial resistance[95, 106].

2.2. Ionic correlation in concentrated ionic systems

Ion-ion correlation is a phenomenon in concentrated ionic systems in which the behavior and mobility of ions are impacted by the presence and interactions of surrounding ions[107-109]. In concentrated ionic systems, the strength of ion-ion interactions and correlations increases with higher ion concentrations, leading to a scenario where these interactions play a significant role and cannot be overlooked. These ionic correlations, depending on the context, possess the capability to suppress conductivity by a substantial factor, around 100-fold, or conversely, to elevate it by approximately 5 times [31, 107-109]. Ions move relatively freely in dilute liquids, and conductivity is essentially influenced by the mobility of individual ions. Ion-ion correlations, on the other hand, might have kind of backflow in concentrated solutions, limiting their effective mobility and resulting in poorer conductivity[31, 108, 110, 111].

Because of the complexity of the interactions involved, understanding, and measuring ion-ion correlation in concentrated ionic systems is a difficult undertaking [107-109, 112]. To analyze and describe ion-ion correlations, experimental techniques like conductivity measurements, spectroscopy, and scattering methods are frequently used in conjunction with theoretical models and molecular simulations [107-109, 112].Thus, a profound understanding of these intricate correlations holds a pivotal role in the advancement of strategies aimed at enhancing the conduction of ions [31, 107, 112].

2.2.1. Why are ionic correlations important?

If the diffusion coefficients of positive and negative ions are known as [6, 8, 16]

$$D_+ = \frac{1}{3}\int_0^\infty \langle \boldsymbol{v}_+(0)\boldsymbol{v}_+(t)\rangle dt \quad and \quad D_- = \frac{1}{3}\int_0^\infty \langle \boldsymbol{v}_-(0)\boldsymbol{v}_-(t)\rangle dt \tag{2.1}$$

then the conductivity can be calculated using the Nernst-Einstein equation. The Nernst-Einstein conductivity equation is given by the following equation[6, 7]:.

$$\sigma_{NE} = \frac{q^2}{k_B TV}(N_+ D_+ + N_- D_-) \tag{2.2}$$

where q represents the ion charge, k_B is the Boltzmann constant, T is the temperature, V is the volume of the system, N+ and N- are the concentrations of positive and negative ions, and D+ and D- are their respective diffusion coefficients.

However, the conductivity of a system is determined by the current-current correlation function, which can also be expressed in terms of the velocity-velocity correlations of all the ions [6, 8, 16].

$$\sigma_{DC} = \frac{1}{3Vk_BT}\int_0^\infty \langle \vec{J}(0)\cdot\vec{J}(t)\rangle\, dt, \quad \text{where } \langle \vec{J}(0)\cdot\vec{J}(t)\rangle = \langle \textstyle\sum_i q_i\vec{v}_i(0)\cdot\sum_j q_j\vec{v}_j(t)\rangle \tag{2.3}$$

V denotes the system's volume. It is crucial to highlight that the Nernst-Einstein equation, which assumes no correlations between the motions of various ions, holds valid only when no such correlations exist. In diluted solutions, where the correlations between ions are negligible, the Nernst-Einstein equation is commonly used to predict conductivity. However, in concentrated ionic systems where the motion of ions is highly correlated, the Nernst-Einstein equation becomes inadequate in accurately estimating conductivity because diffusion is a self-correlation function, while conductivity includes also distinct ion-ion correlations. In these concentrated systems, the behavior of ions becomes interdependent, meaning that the motion of one ion is influenced by the presence and movements of other ions. This strong correlation between ions results in deviations from the assumptions made in the Nernst-Einstein equation. As a result, the predicted

conductivity based on the equation disagrees with the actual conductivity observed in these systems.

The Nernst-Einstein equation, which predicts the conductivity of molten salts and ionic liquids based on known ion diffusion, often overestimates the actual conductivity observed in these systems. This discrepancy has been recognized for many decades[9, 13, 14, 77, 113-128]. Interestingly, the opposite effect has been observed in superionic glasses and crystals, where the measured ionic conductivity is higher than what is expected from the Nernst-Einstein equation[16, 17, 129-138].

To understand and characterize these effects, researchers introduced the inverse Haven ratio, H^{-1}, calculated as the ratio of the measured conductivity (σ_{DC}) to the conductivity estimated by the Nernst-Einstein equation (σ_{NE}). The inverse Haven ratio is sometimes called ionicity in these systems. The ionic conductivity in general can be separated into four terms [9, 124, 139]:

$$\sigma_{DC} = \sigma_{NE} + \sigma_{+-} + \sigma_{++}^{d} + \sigma_{--}^{d}, \ \ where \ \ \sigma_{NE} = \sigma_{+}^{s} + \sigma_{-}^{S} \tag{2.4}$$

Here σ_{+}^{s} and σ_{-}^{s} represent the contribution from the self-correlation of cations and anions, respectively; σ_{++}^{d} and σ_{--}^{d} are the distinct cation-cation and anion-anion correlations, respectively, while σ_{+-} is the contribution of cation-anion correlations to the conductivity. Hence, the inverse Haven ratio can be defined as:

$$H^{-1} = \frac{\sigma_{DC}}{\sigma_{NE}} = 1 + \frac{\sigma_{+-} + \sigma_{++}^{d} + \sigma_{--}^{d}}{\sigma_{NE}} \tag{2.5}$$

Ionicity, or the inverse Haven ratio, provides valuable insights into the influence of ion-ion correlations on conductivity. When H^{-1} is less than 1, ion-ion correlations suppress conductivity, as observed in ionic liquids and molten salts. In diluted solutions, H^{-1} is equal to 1, indicating negligible or compensated ion-ion correlations. However, H^{-1} greater than 1 indicates enhanced conductivity due to favorable ion-ion interactions, commonly observed in glass and ceramic materials. Understanding the role of ion-ion

correlations in conductivity is crucial for optimizing materials for various applications, including energy storage.

2.2.2. Ion-ion Correlations in Ionic Liquids

Ionicity (H^{-1}) is always less than one for ILs, and this drop is generally attributed to the production of ion pair-like coupled motion of anion and cation. [119, 140]. This ion pairs do not carry a net charge so that these ion pairs contribute to ion diffusion but have no effect on conductivity [9]. However, recent simulation studies have raised doubts on this hypothesis, claiming that the reduction in H^{-1} for molted salts and ionic liquids is produced by the correlated movements of ions of the same type (cation-cation and anion-anion correlations) rather than the ion pairs themselves[124]. They suggested that anion-cation correlations improve ionic conductivity whereas anion-anion and cation-cation correlations are the primary causes of conductivity decrease based on the experimental investigations of ILs by Harris & Kanakubo[12, 127, 141]. The latest review[138] also underlined the same idea that same ion correlations have a significant impact in lowering conductivity of various concentrated ionic solution and ionic liquids. All these studies mentioned above have focused on the significance of ionic correlations and electrostatic interaction of ions in experimentally measured conductivity of ILs.

The fact that the ionicity for every system in Fig. 2.6 is less than one shows that ionic correlations have a negative impact on the conductivity. Additionally, it demonstrates that ionicity reaches its maximum at a particular temperature. The change of ionicity at lower temperatures observed in earlier research was related to the ion pairs' dissociation energy, but we now realize that ion pairs don't have influence on ionicity in ILs. H^{-1} is controlled by ion-ion correlations, which is caused by electrostatic interactions between the ions. However, high temperature measurements indicated that H^{-1} also decreased with increasing temperature. We don't know why it decreases also at high T, but one of the possible explanations assumes changes in hydrophobic interactions and ions aggregation [114, 117, 142]. All these results point to the fact that H^{-1} is maximal at a specific temperature

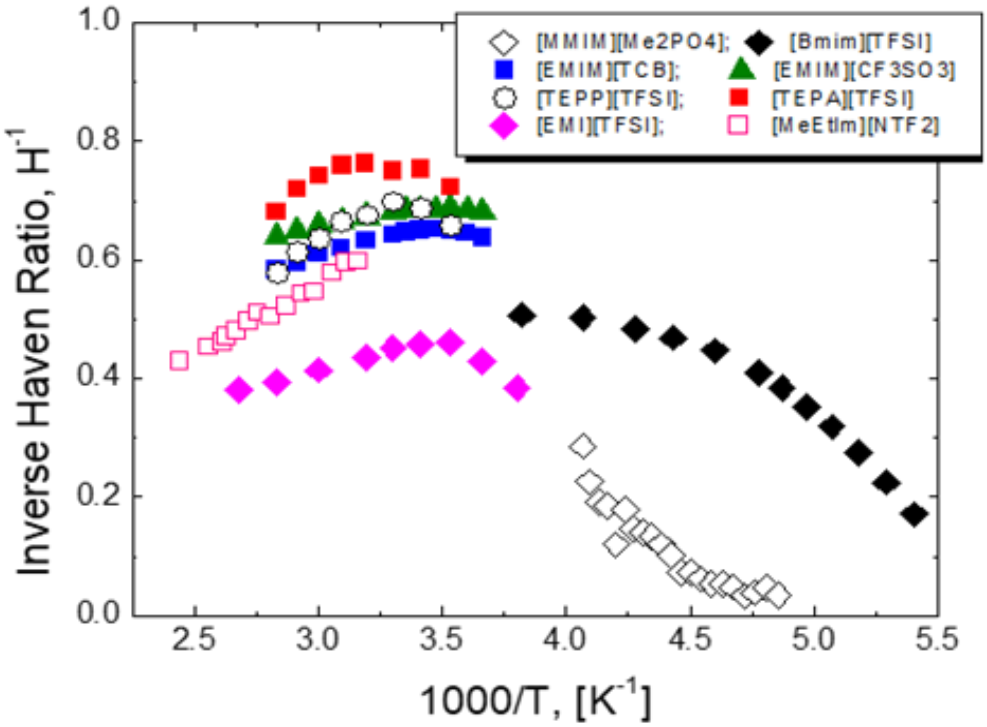

Figure 2.6 Temperature dependence Ionicity/IHR (H-1) of some ionic liquids[7, 119, 127, 142-144].

(Fig. 2.6), suggesting that several processes may be controlling the correlations between ion dynamics in ILs.

2.2.3. Ion-ion Correlations in Pure Organic Ionic Plastic Crystals (OIPCs)

Organic Ionic Plastic Crystals (OIPCs) are a unique class of materials that exhibit interesting ion-ion correlation behavior. Fig. 2.7 illustrates the temperature dependence of conductivity, diffusion coefficient and the inverse Haven ratio (H^{-1}) in a specific plastic crystal composed of P1224 cations and PF6 anions. Regarding the OIPC material under investigation, both the conductivity and diffusion coefficient experience a reduction when the temperature is decreased. However, a captivating contrast emerges in their responses during phase transitions. The conductivity displays abrupt, stair-like shifts at each phase transition, signifying rapid changes in its magnitude. Conversely, the diffusion coefficient diminishes as temperature decreases, yet it lacks the pronounced and sudden shifts observed in conductivity across various phases. In this system, the cations are immobilized or "frozen," while all the anions remain mobile[9, 145].

The analysis of OIPCs reveals a remarkable effect on ionicity, as the conductivity in these materials is significantly lower (25-100 times) than what would be expected from uncorrelated ionic conductivity calculated using the Nernst-Einstein equation and measured ion diffusion. The observed ionicity varies up to ~0.5 in the Fig. 2.7d indicates the presence of overall negative ionic correlations in the system[9]. Furthermore, there is an additional reduction in the inverse Haven ratio (H^{-1}) specifically associated with the decrease in conductivity between Phase 2 and Phase 3 at a temperature of 333K. This intriguing phenomenon cannot be explained solely by the diffusion of ion pairs, as only a small fraction of the cations exhibits mobility in this OIPC [9, 145].

In OIPCs, the restricted mobility of one ion (in this case, the cation) leads to increased correlations in the dynamics of the mobile counter ions (anions). This finding is highlighted by the fact that OIPCs exhibit lower ionicity and H^{-1} values compared to conventional ionic

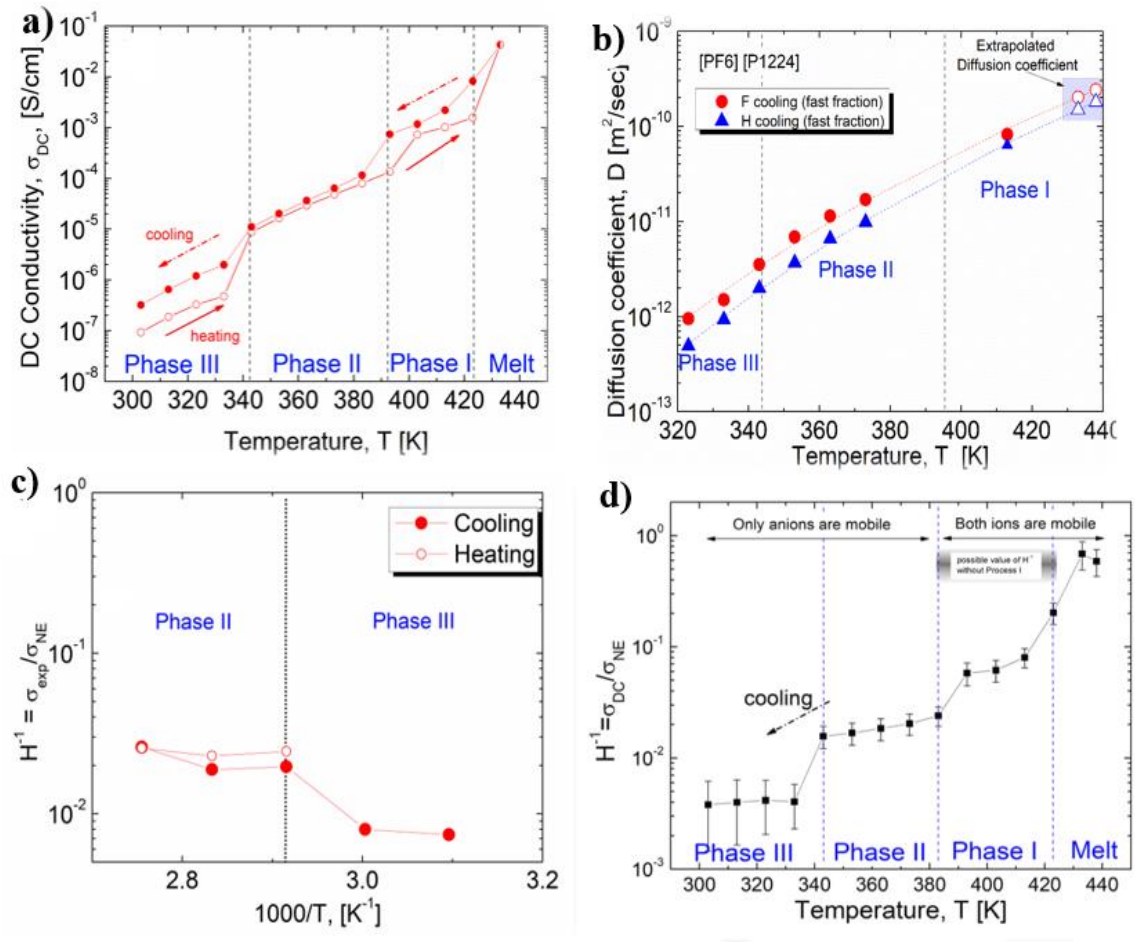

Figure 2.7 a). DC conductivity of P1224-PF6 on both heating and cooling cycle b). Diffusion coefficient of ions in different phases where no step like change during phase transitions c). Relationship of H-1 and temperature in P1224-PF6 during heating and cooling. d). Relationship of H-1 and different phases. Data from [9, 146]

liquids (ILs) [9, 146].This observation suggests that even though ions are undergoing motion, they do not significantly contribute to the overall conductivity of the material at these transition points and in different phases the correlations are different [9, 146].

Overall, the results suggest that the interplay between ion mobility and correlations is crucial in understanding the unique behavior of OIPCs. By restricting the mobility of one ion while keeping the others mobile, OIPCs exhibit enhanced ion-ion correlations, resulting in reduced conductivity compared to their IL counterparts. Further research is needed to delve deeper into the underlying mechanisms governing ion dynamics and correlations in OIPCs, offering new insights into their fascinating properties.

2.2.4. Ion-ion Correlations in doped Organic Ionic Plastic Crystals (OIPCs)

An intriguing aspect of investigating the role of dopant in OPICs involves the addition of small amounts of doped salts, such as Li+ or Na+. This phenomenon is exemplified in Fig. 2.8, which illustrates the case of incorporating Li TFSI into the plastic crystal P12TFSI, resulting in a significant increase in conductivity, particularly in phases 1 and 2, where conductivity is enhanced by up to three orders of magnitude. It is important to note that both LITFSI and P12TFSI share the same anion (TFSI), and Li acts as the cationic dopant [147, 148].

Examining Fig. 2.8(a), we observe that the phase transition from phase 3 to 2 in P12TFSI occurs at 290K, while the transition from phase 2 to 1 takes place over a broader temperature range, between 308K and 318K. Importantly, the addition of Li salts as dopants does not significantly alter the shape or location of these transitions [149].

Several hypotheses have been proposed to explain the observed enhancement in conductivity upon doping, including the presence of defects or vacancies within the crystal structure, changes in free volume, and the potential existence of a liquid-like phase in doped OIPCs[150-152]. However, to the best of my knowledge, the ion-ion correlations

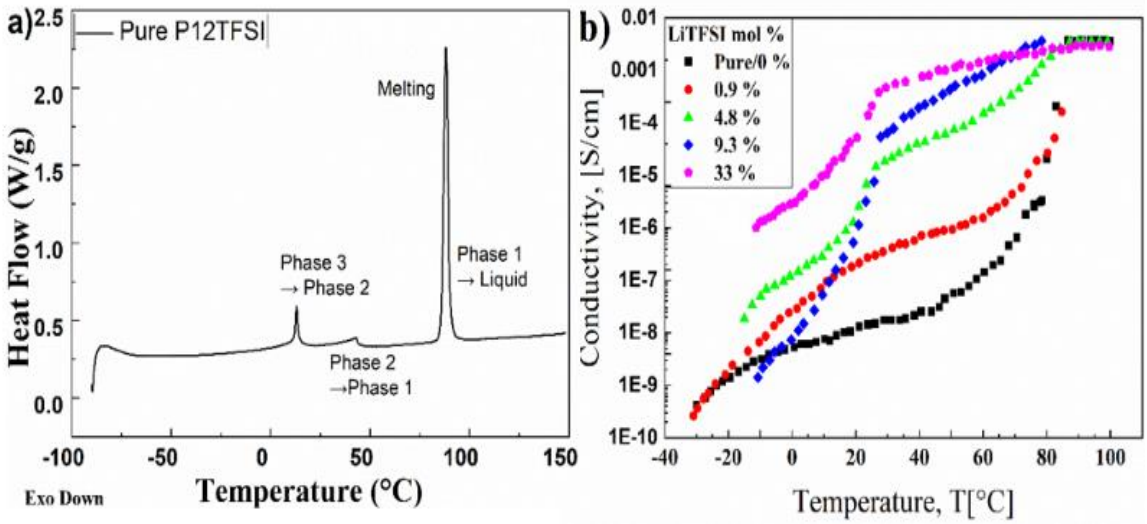

Figure 2.8 a). DSC curve of pure P12TFSi plastic crystal to observe the phase transitions b). Conductivity comparison of pure and different % of doping [147, 148].

that govern the ionicity in these doped systems have not yet been fully elucidated. Previous studies [150-152]have primarily focused on demonstrating the conductivity increase upon doping with small salts, a comprehensive explanation for this effect has yet to be provided.

Therefore, further investigations are required to understand the underlying mechanisms behind the conductivity enhancement in doped OIPCs. Exploring the nature of ion-ion correlations in these systems holds promise for unraveling the factors contributing to the observed conductivity changes and gaining a deeper understanding of the unique behavior exhibited by doped OIPCs.

2.2.5. Ionic Correlations in Poly-ionic Liquids (PolyILs)

Polymerized ionic liquids, known as PolyILs, offer intriguing insights into the behavior of ion-ion correlations and their impact on conductivity. In PolyILs, one ion is immobilized by attaching it to the polymer, while the other ion remains mobile. Researchers have observed that lighter mobile ions in PolyILs exhibit weaker correlations and higher values of the inverse Haven ratio (H^{-1}) [7, 9], as illustrated in Fig. 2.9

Conversely, the correlations between the cation and anion in PolyILs are positive, suggesting that they should enhance conductivity. Surprisingly, however, a significant decrease in conductivity is observed due to the negative correlations between the mobile ions [9]. Previous investigations [9]. have also revealed that heavier mobile ions in PolyILs display stronger negative correlations, consistent with the momentum conservation hypothesis. Yet, the temperature dependence of H^{-1}, as depicted in Fig. 2.9, still lacks a clear explanation. Simulations conducted on polymer electrolytes have emphasized the role of electrostatic interactions in determining distinct ion correlations [153-155].

Examining the influence of mobile ion size on ion-ion correlations in PolyILs proves to be intriguing. To account for temperature variations, H^{-1} values are compared at scaled temperatures relative to the glass transition temperature (Tg) of each system, as shown in Fig. 2.9b[9, 156, 157]. Although the available data is limited, it suggests a strengthening

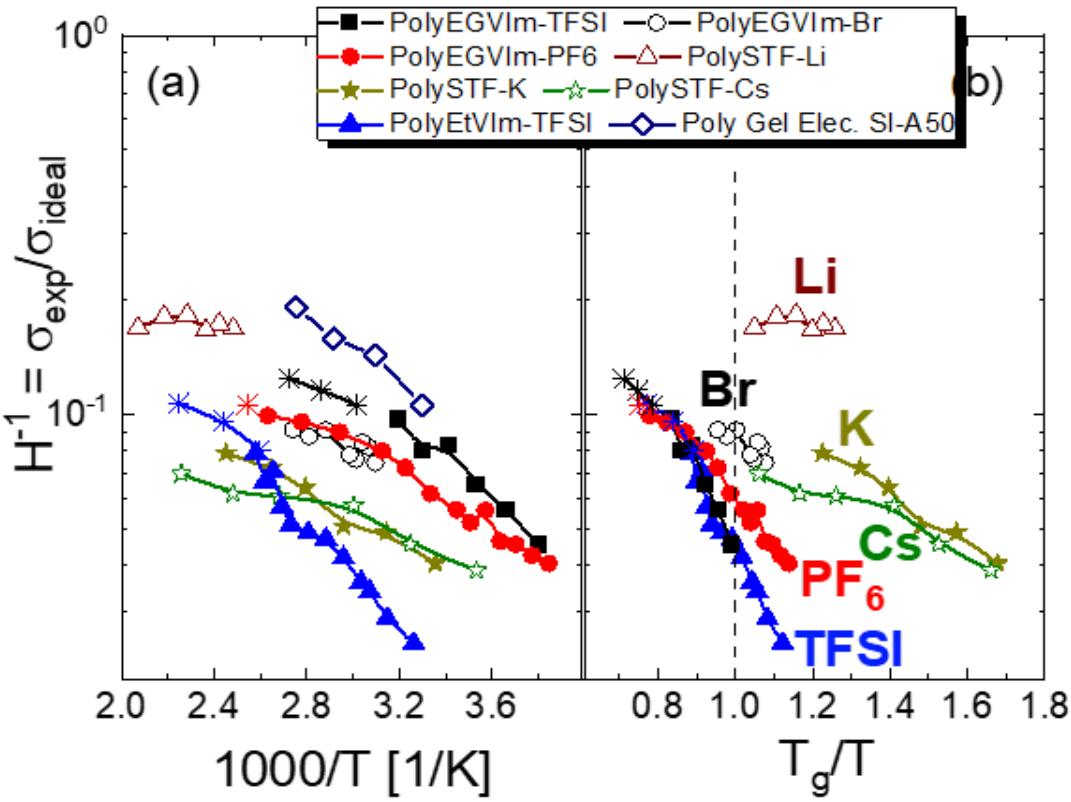

Figure 2.9 a) The relationship of H-1 and inverse temperature in PolyILs with various mobile ions and structure. (b) The same data represented vs Tg/T scale. H^{-1} clearly decreases with the increase of mass of mobile ions. Data are collected from [9]

of negative ion-ion correlations with an increase in mobile ion size. Specifically, for smaller Li ions, H^{-1} (Tg) is approximately 0.2. For intermediate size ions like Br, Cs, and K, H^{-1} (Tg) decreases to around 0.08-0.09. Furthermore, for the larger PF6 ion, H^{-1} (Tg) is approximately 0.06, and it further decreases to 0.04-0.05 for the largest TFSI ion studied (Fig. 2.9 b) [9, 156, 157]. Importantly, these findings are based on employing the same polymerized IL such as PolyEGVIm with mobile anions of varying sizes (Br, PF6, and TFSI), and polyanion – PolySTF and with different cation size Li, K, Cs. The results clearly demonstrate a decrease in H^{-1} (Tg) as the size of the mobile anion increases. This observation can be qualitatively explained by the momentum conservation model, where the motion of smaller (lighter) mobile ions can be more readily compensated by the slower motion of the heavier poly-ion, thus reducing the negative correlations among the mobile ions[9, 156, 157].

2.3. How to Study Ion-ion Correlations?

The study of ion-ion correlations in concentrated ionic systems is critical for understanding the behavior, characteristics of these systems and for design of ionic systems with high conductivity. However, it is still a challenging fact to estimate distinct ion-ion correlation contribution to conductivity of those systems. Until recently, Molecular Dynamic (MD) simulations have been the primary method used to estimate the contribution of distinct ion-ion correlations to conductivity. It offers a powerful tool for investigating ion transport and correlations in ionic systems[158-160]. Through detailed computational analyses, researchers can explore the behavior of ions in concentrated environments and understand how factors like temperature, pressure, and salt concentration influence their interactions[161]. These simulations provide valuable insights into the underlying principles governing ion dynamics and can contribute to advancements in various fields, including battery technology and fuel cells.

Recently a new proposal has emerged for experimental measurements of three correlation parameters: σ_{+-}^{d}, σ_{++}^{d}, σ_{--}^{d} [162]. It is important to note that this approach is complex and challenging, as it requires electrodes that contain only one type of ion, such as lithium

(Li). So far, this method has been applied to a limited number of lithium conductive systems. Another approach which was proposed in [9, 139, 163] is based on a combination of experimental measurements of conductivity and diffusion and theoretical models. The main idea of this approach considers the fact that the total momentum of all ions is conserved.

$$M_+ \sum_i \vec{v}_{i+}(t) + M_- \sum_i \vec{v}_{i-}(t) = 0 \tag{2.6}$$

This additional simple equation allows to resolve the distinct ion-ion correlations and provides the explicit way to estimate them from experimental data. Using experimentally obtained conductivity (σ_{DC}), diffusivities, and masses of ions, the model calculates different contributions to the conductivity of ILs [9, 124].

$$\sigma_{++}^{d} = \sigma_{DC}\left(\frac{Z_+ m_-}{Z_+ m_- - Z_- m_+}\right)^2 - \sigma_+^s, \qquad \sigma_+^s = \frac{e^2 n}{kT} x_+ z_+^2 D_+$$

$$\sigma_{--}^{d} = \sigma_{DC}\left(\frac{Z_- m_+}{Z_- m_+ - Z_+ m_-}\right)^2 - \sigma_-^s, \qquad \sigma_-^s = \frac{e^2 n}{kT} x_- z_-^2 D_-$$

$$\sigma_{\pm} = -2\sigma_{DC}\frac{Z_+ Z_- m_+ m_-}{(Z_+ m_- - Z_- m_+)^2} \tag{2.7}$$

Here, e is the charge of electron, n is the total ion pairs concentration. m-, m_+ are the masses of anions and cations where X-, X_+ and Z- and Z_+ are the mole fractions and charge numbers of anions and cations, respectively. Recently, this approach was used to estimate each term of distinct ion-ion correlations in polymerized ionic liquids [9] and concentrated ionic solutions [124, 141]. In the case of ionic solution additional terms accounting for momentum of the solvent molecules should be included [164]. However, the obtained estimations of distinct ion-ion correlations from experimental data using this approach were never compared to results of model independent MD studies.

2.4. Research Objectives

The primary objective of this research is to gain a deep molecular-level understanding of ion-ion correlations in both liquid and solid systems. The main hypothesis suggests that momentum conservation plays a crucial role in these correlations, particularly in ionic liquids, poly-ionic liquids, polymers, and plastic crystals. Another hypothesis, consistent

with the momentum conservation idea, proposes that immobilizing one of the ions leads to stronger correlations in the dynamics of the mobile counter-ions.

The overall goal of this thesis study is to investigate the influence of momentum conservation on ionic correlations in various materials, including plastic crystals, ionic liquids, and poly-ionic liquids. The focus is on enhancing our comprehension of ion dynamics and transport properties, with a specific emphasis on their influence on conductivity. The research aims to address three key research questions:

1) What is the fundamental mechanism underlying ion-ion correlations and how do they affect conductivity in these systems?

2) How does the mass of the anion influence ion dynamics, and to what extent does the momentum conservation model explain the observed behavior?

3) What roles do ionic correlations play in both pure and doped organic ionic plastic crystals (OIPCs), and how does doping impact conductivity and ion dynamics in these systems?

To investigate the proposed hypotheses and gain a deeper understanding of the mechanisms governing ionic correlations, collaboration with experts in molecular dynamics simulations is proposed. The experimental work is conducted by the author, while Dr. Paddison's research group provided atomistically detailed simulations of the same systems.

2.4.1. Intellectual merit

In terms of Intellectual merit, unraveling the intricacies of ionic correlations that control conductivity in concentrated ionic systems holds great significance. It has implications for the synthesis and design of new liquid and solid electrolytes with significantly improved ionic conductivity, potentially leading to enhanced performance, energy, and power

density in solid-state batteries. Furthermore, the findings can impact the fields of flow batteries and supercapacitors. In a broader context, this research has the potential to deepen our understanding of collective dynamic phenomena in other soft materials.

CHAPTER THREE
MATERIALS AND METHODS

This chapter delves into the characterization of ionic liquids and organic ionic plastic crystals, which have garnered significant attention in recent years due to their unique properties and potential applications. To fully comprehend their properties and potential applications, it is crucial to characterize their structural, thermal, and electrochemical properties. This chapter provides an in-depth description of the experimental techniques and procedures used to characterize ionic liquids, pure, and doped systems of organic ionic plastic crystals.

3.1. Studied Samples/Materials for Understanding of Ionic Correlations

This study investigated the influence of ionic correlations on ionic conductivity in concentrated ionic systems. We analyzed the conductivity of three ionic liquids with different anionic masses but the same cation, as well as several pure organic ionic plastic crystals. We also examined doped systems of organic ionic plastic crystals with Li+ and BMIM+ ions.

The findings of this study provide valuable insights for enhancing ionic conductivity in electrolytes, with implications for various electrochemical applications. By systematically varying the anionic mass while keeping the cation constant, we were able to determine the relative contribution of the different parameters (such as ion mass, volume, and immobilization of one of the ions) to the conductivity of the ionic liquids. Additionally, by doping the organic ionic plastic crystals with Li+ and BMIM+ ions, we were able to observe how the Li+ and BMIM+ ions interact with the host material.

3.1.1. Ionic liquids

Ionic liquids are a group of materials made completely of ions that are notable for their intriguing characteristics and wide range of uses in electrochemical energy systems.

Numerous distinctive characteristics of these materials stand out, including low volatility, good thermal stability, a large electrochemical window, and strong ionic conductivity. They are very desirable for many electrochemical energy applications because of their characteristics[165-167].

Ionic liquids have a low volatility, which means they have little vapor pressure and don't evaporate under typical working circumstances. This is one of their major benefits. They are excellent for applications where containment and safety are crucial considerations because of this feature, which significantly improves safety and lowers the chance of leakage[168, 169]. High thermal stability is another significant characteristic of ionic liquids. They can tolerate high temperatures without breaking down or evaporating, which is beneficial in energy devices that work in challenging environments. Ionic liquids may be used in high-temperature applications for their stability, which also helps the devices' long-term dependability and endurance[140, 170].

Additionally, ionic liquids have a large electrochemical window, which allows them to resist high voltages without experiencing unfavorable reactions. In electrochemical energy devices, where high-energy reactions take place, this feature is crucial. Ionic liquids' extensive electrochemical stability enables the use of high-energy electrode materials and promotes effective charge storage and transmission[171, 172].

Furthermore, ionic liquids have high ionic conductivities that allow for rapid ion movement into the substance. Due to the fact that it enables effective charge/discharge operations and improves overall device performance, this feature is essential in electrochemical energy devices. Ionic liquids are appealing electrolyte materials because of their strong ionic conductivity, which improves energy and power density for devices including batteries, supercapacitors, fuel cells, and solar cells[1, 4].

Ionic liquids can be used as electrolytes in batteries, enhancing both their performance and security. Ionic liquids' low volatility makes it possible to employ high-energy electrode

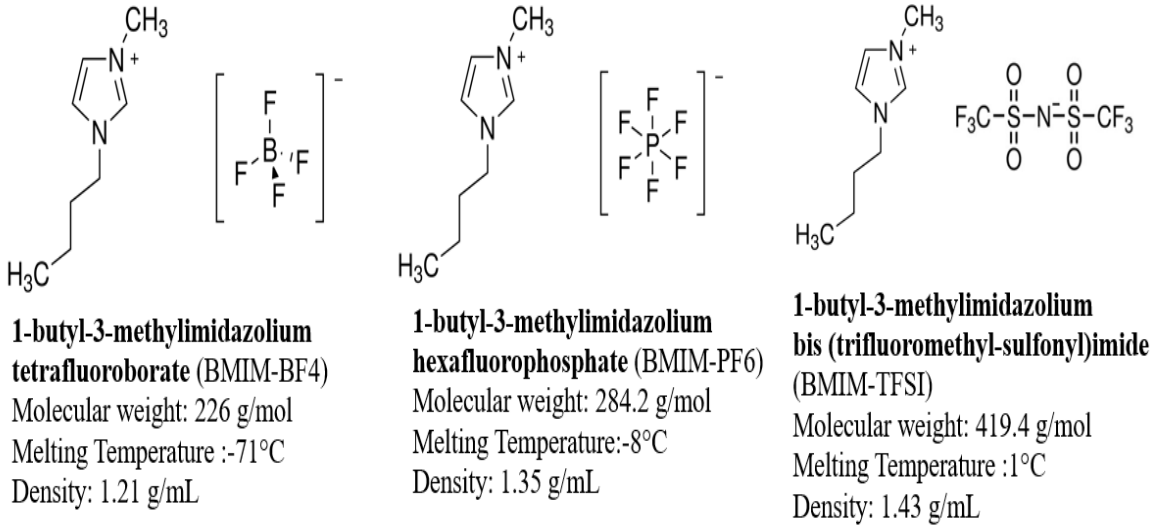

Figure 3.1 Chemical structure and general information of selected ILs: BMIM-BF4, BMIM-PF6 and BMIM-TFSI

materials, improve cycle life, and lower the danger of fire or explosion[1, 165-167, 173]. Supercapacitors also utilize ionic liquids as well since they make ideal electrolytes for their applications [174, 175]. The performance of these energy storage devices is enhanced by their broad electrochemical window and strong ionic conductivity, which together maximize energy and power density[165-167, 174, 175].

There are protic ionic liquids which are proton-conducting electrolytes that can be used in fuel cells. The high-temperature fuel cell applications are a good fit for them due to their great thermal stability and low vapor pressure as well as fuel cell performance is improved because of the efficient ion transport provided by protic ionic liquids[176-178].(For example, water with acid is better proton conductor then protic ILs but protic ILs are better at high T where water will evaporate at 100C).

In Chapter 2 and 4, our research sheds light on the unique characteristics of ionic conductivity in liquid electrolytes, particularly in the case of ionic liquids (ILs). We find that the ionic conductivity of liquid electrolytes, especially ILs, is generally higher compared to other types of electrolytes. However, an intriguing observation is made regarding the Inverse Haven ratio or Ionicity, which is found to be lower than 1 in ILs. This indicates that while the ions in ILs are in motion, they are unable to contribute significantly to the overall conductivity. It suggests that ion-ion correlations play a crucial role in suppressing the conductivity in ILs. For developing of the understanding of ionic correlations in ILs, we hypothesize that momentum conservation is one of the significant factors regulating ionic correlations in ILs and ion mass is an important variable in momentum. To investigate the ion mass effect on ion-ion correlations, we chose ionic liquids with different masses and shapes of anions where all ions are mobile. For example, we studied three imidazolium salts detailed in Fig. 3.1; BMIM-TFSI, BMIM-PF6, and BMIM-BF4 where the mass ratio of cation/anion changes from ~0.5 to ~1 and to ~1.6, and the volume ration of cation/anion changes from ~1 to ~2.3 and to ~3.3 respectively and they have the same cation but different anion.

The first question we wanted to understand is how to estimate the conductivity contributions of distinct ion-ion correlations and the anionic mass effect on these distinct ion-ion correlations. Finally, the effect of geometry and anionic mass on inverse Haven ration and cation transport number was investigated. We hypothesize that if the mass of anion is heavier than cation in any IL, most of charge will be carried by cation that why cation transport number will be higher for this IL. To verify this hypothesis, we compared my BDS measurement result and some literature data to explain more in detail their relationship with transport number and Inverse Haven Ratio (H^{-1}).

3.1.2. Organic Ionic Plastic Crystals (OIPCs)

Organic ionic plastic crystals (OIPCs) are another interesting solid-state material that exhibit properties of plastic crystals, i.e., instantaneous crystalline structure, but mobile molecular units. This leads to their plasticity while regular crystals are completely rigid but OIPCs have in addition higher ionic conductivity. They have special qualities that distinguish them distinct from other electrolytes because their main advantages is solid like structures with higher ionic conductivity [179, 180].

OIPCs are renowned for having high ionic conductivities that are on par with those of liquid electrolytes[15, 179-181]. For electrochemical energy devices to transport charges effectively, this feature is crucial. OIPCs also have a large electrochemical stability window, which means they can sustain a wide variety of voltages without degrading. The long-term dependability and durability of electrochemical energy devices depend on this feature. OIPCs are also thermally stable, which enables them to resist high temperatures without deteriorating[179]. For applications where OIPCs will be subjected to high temperatures, this feature is crucial. Finally, OIPCs have low volatility, which keeps them from fading/evaporating away rapidly. This characteristic is crucial for security and for preventing electrochemical device leaks.

OIPCs are appropriate for a range of electrochemical energy system applications, including

Selected OIPCs

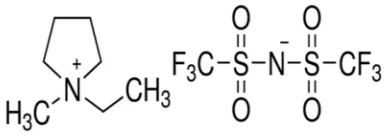

Chemical Name: P[1,2]-TFSI
1-Ethyl-1-methylpyrrolidinium bis(trifluoromethyl-sulfonyl)imide
Chemical Formula: $C_9H_{16}F_6N_2O_4S_2$
MW: 394.35 g/mol
Melting Temperature: 88 °C

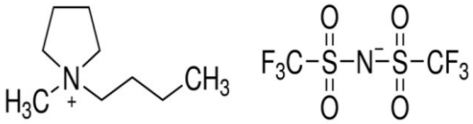

Chemical Name: P[1,4]-TFSI
1-Butyl-1-methylpyrrolidinium bis(trifluoromethyl-sulfonyl)imide
Chemical Formula: $C_{11}H_{20}F_6N_2O_4S_2$
MW:422.4 g/mol
Melting Temperature: -15 °C

Selected dopant for OIPCs

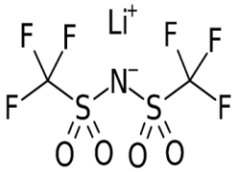

Chemical Name: LI-TFSI
Lithium bis(trifluoromethanesulfonyl)imide
Chemical Formula: $LiC_2F_6NO_4S_2$
MW: 287.075 g/mol
Melting Temperature: 236 °C

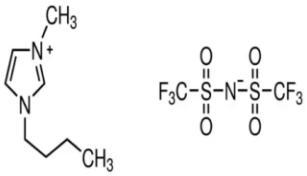

Chemical Name: BMIM-TFSI
1-Butyl-3-methylimidazolium bis(trifluoromethylsulfonyl)imide
Chemical Formula: $C_{10}H_{15}F_6N_3O_4S_2$
MW: 419.36g/mol
Melting Temperature: 1 °C

Figure 3.2 Chemical structure and general information of selected OIPCs: P [1,2]-TFSI, P [1,4]-TFSI and dopant: LITFSI, BMIM-TFSI.

dye-sensitized solar cells (DSSCs), supercapacitors, and solid-state batteries due to their properties. OIPCs can be used as electrolytes in DSSCs, which would improve their effectiveness and stability[182]. Third-generation photovoltaic technology known as DSSCs has attracted interest due to its inexpensive cost, straightforward production process, adjustable optical characteristics, and improved photoelectric conversion efficiency[183].

Additionally, OIPCs can be used in solid-state batteries as solid electrolytes, which would improve battery performance and safety[184, 185]. Solid-state batteries are a newly developed technology that provides benefits over conventional liquid electrolyte-based batteries, including increased safety, a better energy density, and a longer cycle life. In addition, supercapacitors can use OIPCs as electrolytes, which would improve their performance[186]. Supercapacitors are electrochemical energy storage devices that have fast charge/discharge cycles and high-power densities, making them appropriate for applications needing these characteristics.

Developing the understanding of ion-ion correlations in OIPCs is another interesting direction in the proposed research because the counter-ions are usually immobilized in OIPCs and most of the contributions to conductivity are done by only mobile ion. However, according to NMR all these counterions are mobile but their correlations strongly suppress conductivity [9]. Most important thing I want to understand is why H^{-1} decreases so dramatically in OIPCs in comparison to the previously described ILs. I hypothesize that the main factor inhibiting ionic conductivity in these systems is tightly correlated motions of same charged mobile ions as anion-anion and cation-cation correlations. To verify this hypothesis, I will study pyrrolidinium based plastic crystals P12TFSI and P14TFSI where P12TFSI is liquid and P14TFSI is solid at room temperature.

From Chapter 2.2 in Fig. 2.8 indicate that doping by Li salt enhances conductivity in some plastic crystal phases by 2-4 orders, but the mechanism of such strong enhancement isn’t yet understood. Main question I want to address is how and why doping of small portion

of salt able to alter conductivity by several orders of magnitude. According to my understanding and literature data [9], the negative ion-ion correlations might be responsible for the suppression of conductivity in OPICs.

The conductivity of OIPCs doped with Li salts is hypothesized to be improved due to the decrease of mobile ions correlations. This is because Li ions are very small in size and light in mass, so they can easily move between the heavier ion matrix and dissipate the total momentum to suppress negative ion correlations in OPICs.

To verify this hypothesis, the same P12TFSI and P14TFSI were doped with 4%, 10%, and 30% of Li salts. BMIMTFSI was also used as a dopant to compare with LITFSI, because BMIM is bigger in size than Li. By doping OIPCs with different concentrations of Li salts, the amount of Li ions in the material can be varied and the effect on conductivity can be observed. By comparing the results of doping with LITFSI and BMIMTFSI, the effect of dopant ion size on conductivity can be observed. If the hypothesis is correct, the conductivity of OIPCs doped with Li salts would increase as the concentration of Li salts increases.

3.2. Experimental Techniques

The concentrated ionic systems were characterized throughout the dissertation study using differential scanning calorimetry (DSC) and broadband dielectric spectroscopy. Concentrated ionic systems' conductivity and microscopic dynamics were investigated using dielectric spectroscopy. In order to determine the phase transitions temperatures and behaviors of concentrated ionic systems, differential scanning calorimetry (DSC) was performed.

3.2.1. Broadband Dielectric Spectroscopy (BDS)

Broadband dielectric spectroscopy is an experimental method that measures a material's dielectric properties as a function of the frequency of the applied external electric field[187]. It provides important information about a material's electrical response to an

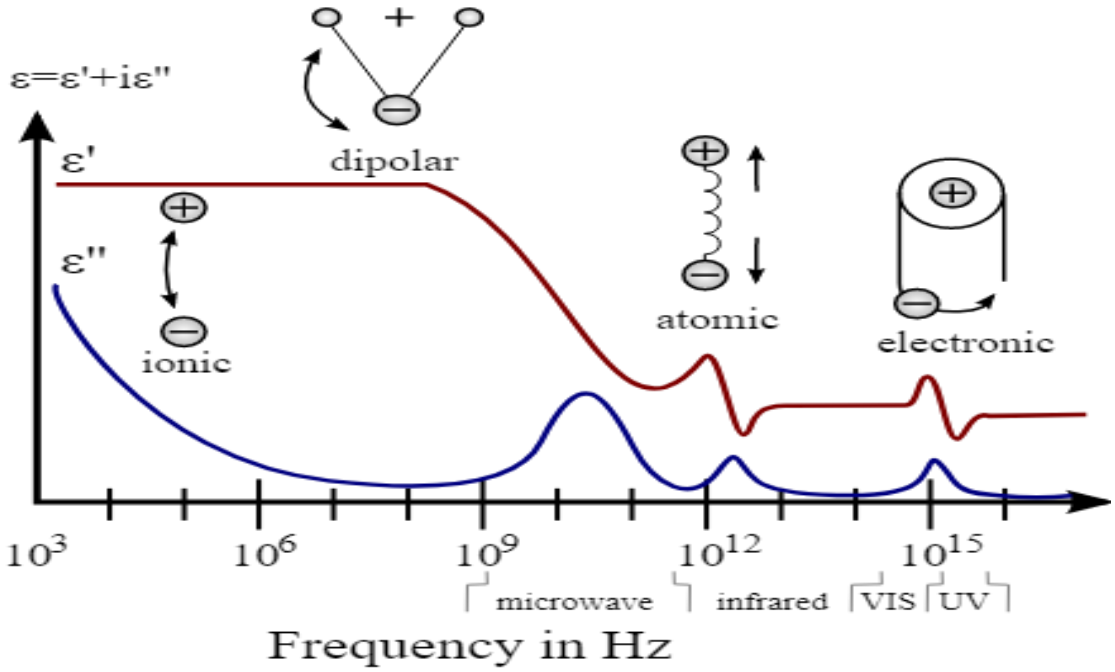

Figure 3.3 A dielectric permittivity spectrum covering a wide frequency range is provided, showing the real ε '(ω) and imaginary ε "(ω) components of permittivity for various polarization mechanisms such as ionic relaxation, dipolar, atomic, and electronic polarization[187].

applied electric field over a large frequency range from 10^{-6} Hz to several THz (10^{12}Hz)[188, 189]. It also provides information on molecular dynamics as well as important materials properties including dielectric permittivity(ε) and DC conductivity (σ_{DC})[187, 190]. When an alternating electric field is applied to any materials, the electric dipole, or free charges within the material, responds by oscillating back and forth, resulting in charge displacement and polarization of the sample. As shown in Fig 3.3, each kind of polarization has a distinct relaxation time(τ), where a quicker charge displacement process resulting in a smaller relaxation time observed at higher frequencies[188]

In ionic polarization, cation goes towards the negative electrode and anion goes to positive electrode and charge displacement of mobile ions occurred according to applied electric field. This type of displacement of mobile ions is commonly seen in electrolytes, ionic liquids, poly ionic liquids and plastic crystals. Dipolar polarization occurs in materials that have permanent dipoles that align with the electric field, causing the dipoles to reorient towards the direction of the field[188]. Atomic polarization, on the other hand, is produced by the displacement of nucleus and electronic clouds in response to an electric field. Electronic polarization is noticed when an electric field displaces the electron density relative to the nucleus in a neutral atom, resulting in a rapid process that can be observed at a higher frequency [187]. Interfacial polarization, which is induced by charge buildup at the interface of two mediums with differing conductivities, is another significant kind of polarization. This is a typical phenomenon in multicomponent or multiphase material, when charges accumulate at the interface between different components or phases of the materials[188].

Basic working principle:

BDS is an experimental technique that involves measuring AC current and voltage, as well as a phase shift between them. It is commonly used to assess the dielectric characteristics of materials. To perform BDS measurements, a sample material, which can be solid or liquid, is commonly placed between two electrodes that form a capacitor and is subjected to a voltage (V) with variable frequency (ω). The corresponding current's magnitude and

phase are then determined. By evaluating the complex voltage and current, the complex impedance of the sample material is calculated[191].

The primary goal of BDS is to measure the complex permittivity spectra ε*(ω) and conductivity spectra σ*(ω) of a given sample material. The impedance spectrum of the sample capacitor can be calculated using the equation below.

$$Z^*(\omega) = Z'(\omega) + j\,Z''(\omega) = V^*(\omega)/I^*(\omega) \tag{3.1}$$

The Complex capacitance C*(ω) of sample is calculated from complex impedance Z*(ω).

$$C^*(\omega) = \frac{1}{j\omega\, Z^*(\omega)} \tag{3.2}$$

The complex capacitance C*(ω) of the sample material is directly related to the permittivity spectrum, where C_0 represents the capacity of the empty capacitor in the absence of the sample material[192]. The complex permittivity spectrum ε*(ω) can be calculated using the following equation.

$$\varepsilon^*(\omega) = \varepsilon'(\omega) - j\,\varepsilon''(\omega) = C^*(\omega)/C_0 \quad \text{and } C_0 = \varepsilon_0 \frac{A}{d} \tag{3.3}$$

where A is the area of one electrode, d is the distance between electrodes, and $\varepsilon_0 = 8.854*10^{-12}$ F/m is known as vacuum permittivity. It should be emphasized that ε*(ω) generally contains a permittivity contribution from molecular dipoles as well as a conductivity contribution from free charge carriers[191] [192]. The complex conductivity spectrum is then calculated from ε*(ω).

$$\sigma^*(\omega) = j\omega\varepsilon_0(\varepsilon^*(\omega) - 1) \tag{3.4}$$

The complex dielectric permittivity and conductivity spectrum:

A dielectric permittivity spectrum for a material with a single permanent dipole relaxation is shown in Figure 3.4(a). The imaginary part of the complex permittivity, ε''(ω) is related to the dielectric loss function, whereas the real, ε'(ω) indicates dielectric storage. At higher frequencies ($\omega \gg 1/\tau$), the dipoles can't change their orientation, have only fluctuations

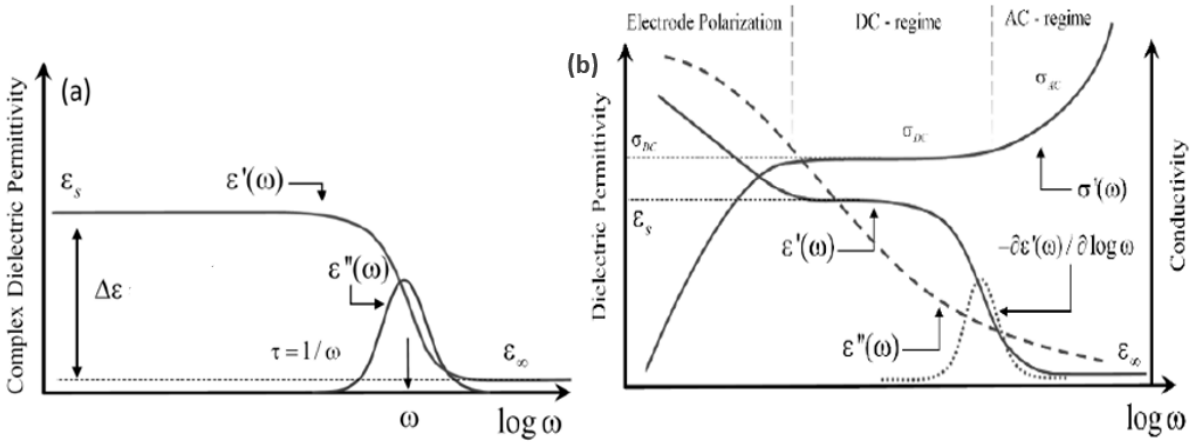

Figure 3.4 (a). A dielectric permittivity spectrum for non-conductive samples with single dipole relaxation with permanent. (b). Permittivity and Conductivity spectrum for ionic conductive samples[188]

with small angle for the fastest process, such as electronic polarization, may responds to the external field, creating the high-frequency limit, ε_∞.

At lower frequencies ($\omega \ll 1/\tau$), all dipoles align with the external electric field, resulting in maximum dielectric polarization and a static dielectric permittivity, ε_S. Moreover, at intermediate frequencies ($\omega \sim 1/\tau$) more dipoles can reorient and $\varepsilon'(\omega)$ increases with decreasing frequency. However, each cycle results in dipole rotating and dissipating energy, $\varepsilon''(\omega)$ become maximum only when the average rotation time of dipoles, ($\tau \sim 1/\omega$), approximately coincides with the cycle of the external electric field. Usually, the parameter is called a relaxation time, $\tau = \frac{1}{\omega} = \frac{1}{2\pi f}$ where f is the frequency of applied external electrical field[188].

The conductivity spectrum of ionic conductive materials can be divided into three regions, as shown in Fig. 3.4(b): (i) a frequency-dependent AC conductivity regime at high frequencies, σAC; (ii) a plateau level of DC conductivity regime at intermediate frequencies, σDC; and (iii) a decrease in conductivity due to charge carrier accumulation at the electrode surfaces at lower frequencies, known as the electrode polarization (EP) effect. In these systems, the dipole moment is determined by the shifting of positive and negative ions in response to an applied external electric field [188]. A step like function in the real part of dielectric permittivity($\varepsilon'(\omega)$) is associated with local ion rearrangements but the process is not clearly visible in the imaginary part of dielectric permittivity ($\varepsilon''(\omega)$) because it is always covered by the tail of DC conductivity. However, conductivity does not have any contribution to the real part of dielectric permittivity($\varepsilon'(\omega)$) and EP effect appears in $\varepsilon'(\omega)$ only at lower frequency. Furthermore, one can recover the conductivity loss process from derivative analysis of the real part of the dielectric permittivity in log scale ($\frac{\partial \varepsilon'(\omega)}{\partial \log \omega}$), It gives the loss peak and ionic relaxation time, $\tau^\sigma = 1/\omega_{max}^\sigma$, can be estimated from the corresponding frequency of maximum peak (ω_{max}^σ). The regime displays the current, known as direct current or DC-current, which is independent of the frequency of the applied electrical field[188].

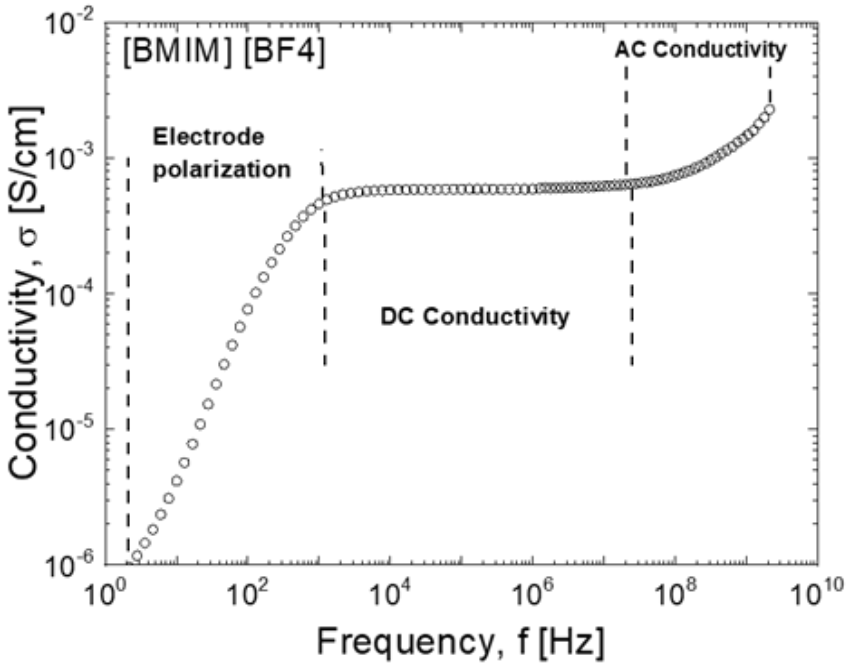

Figure 3.5 Schematic representation of a usual conductivity spectrum. It has three regions: AC conductivity(σAC) at higher frequencies, DC conductivity(σDC) in the middle frequencies, electrode polarization effect, which is a drop caused on by the buildup of charge carriers at the electrode surface at a lower frequency [193].

Based on Random barrier model (RBM), conductivity spectra can be described with the Eq. 5 [7, 194, 195].

$$\ln\left(\frac{\sigma*(\omega)}{\sigma_{DC}}\right) = \frac{i\omega\tau_\sigma\sigma_{DC}}{\sigma*(\omega)}\left(1+\frac{8}{3}\frac{i\omega\tau_\sigma\sigma_{DC}}{\sigma*(\omega)}\right)^{-1/3} \quad (3.5)$$

Here σ∗(ω) is a complex conductivity; σ_{DC} is a DC-conductivity, and τ_σ is a conductivity relaxation time. It describes the characteristic time for ac-dc crossover when charge sub-diffusive region, $\langle r2(t)\rangle \sim t^{\alpha}$ with α<1, crosses over to a usual diffusion region $\langle r2(t)\rangle \sim t$ (here$\langle r2(t)\rangle$ is the charge mean-squared displacement).

Overall, the investigation utilized the Broadband Dielectric Spectroscopy (BDS) method to analyze conductivity spectra. To encompass a wide range of frequencies, two spectrometers were employed. One of these was the Alpha-A analyzer from Novocontrol, covering frequencies spanning from 10^{-1} Hz to 10^{6}Hz. The experimental setup involved a measurement cell with a lower electrode designed as a cap, while an upper electrode was separated by a sapphire window to prevent electrical contact between them. The fixed dimensions for the electrode distance were 0.4 mm with a diameter of 10.2 mm. During measurements, a voltage amplitude of 0.1 V was applied. Prior to the actual measurements, a standard calibration procedure was meticulously carried out.

3.2.2. Differential Scanning Calorimetry (DSC)

Differential scanning calorimetry is a method of thermal analysis that measures difference in heat flow to a sample and to a reference material by heating or cooling them under controlled conditions. The fundamental function of the DSC calorimeter is to precisely quantify the amount of heat that enters or exits the sample when temperature changes. The sample and reference temperatures remain almost equal throughout the entire measurement event. The DSC equipment consists of a measurement chamber with a reference pan and a sample pan, as well as a computer that monitors and controls the temperature and heat flow of the sample and reference pans[196, 197].

Basic working principle:

To monitor phase transitions in the sample, the sample and reference must be kept at equal

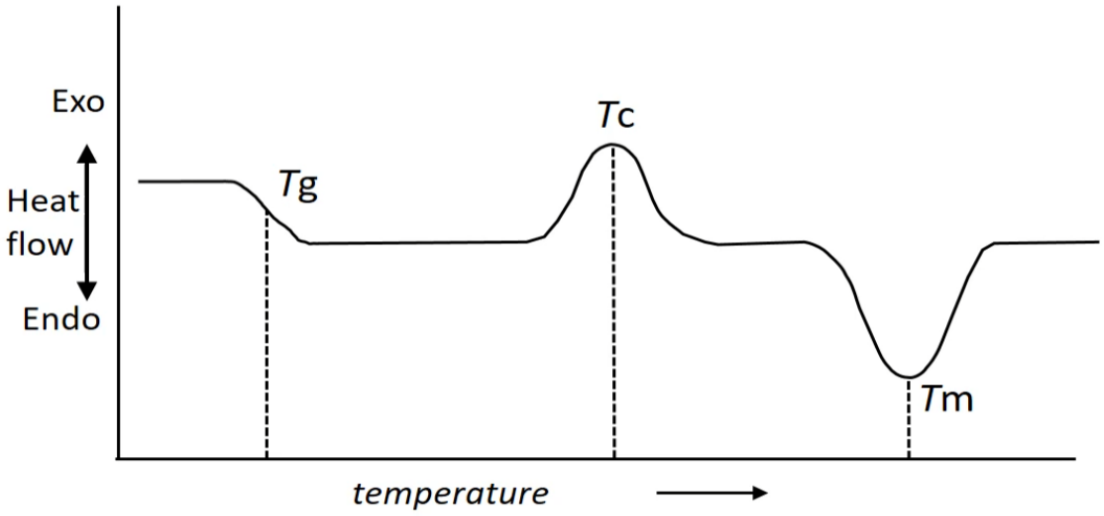

Figure 3.6 A DSC thermogram exhibiting the phases of melting, crystallization, and glass transition of material [196, 198]

temperatures. Depending on the type of transition process, which can be exothermic or endothermic, this can be accomplished by applying more or less heat to the sample than is required for the reference or an empty sample pan. For example, if a solid sample is heated at a constant rate and then converted to a liquid, additional heat must be delivered to the sample to raise its temperature since the sample absorbs heat as it transitions from solid to liquid. However, if the sample goes through an exothermic process, such as crystallization, less heat is required to raise its temperature. As a result, the DSC measurements may quantify the amount of heat generated or absorbed during a transition process by comparing heat flow changes between the sample and reference.

The glass transition temperature (T_g) of sample materials also can be measured from DSC thermogram where T_g is a point when samples alter their state like going from a glass like rigid solid to a viscous liquid state. It is also an endothermic process; sample is absorbing more heat during this transition compared to a reference pan and a step like change appears. Furthermore, Crystallization gives an exothermic peak and melting point of sample give endothermic peak during the phase transition shown in Fig. 3.6 [196-198]

Instrumentation of DSC:

In our research, we utilized two DSC instruments, namely DSC 2500 models manufactured by TA Instruments. These instruments employ a heat flux DSC method, which involves a single furnace where the sample and reference materials are simultaneously heated or cooled under precise temperature control represented in Fig. 3.7. During the analysis, the sample is placed in an aluminum pan, while an empty reference pan is also included in the furnace setup. The pans are positioned on thermoelectric disks surrounded by the furnace. As the temperature of the furnace changes, heat is transferred to both the sample and reference materials. To measure the difference in heat flow between the sample and reference, area thermocouples are used, following the principles of the thermal equivalent of Ohm's law.

The heat flow observed in the sample can be described by the following equation:

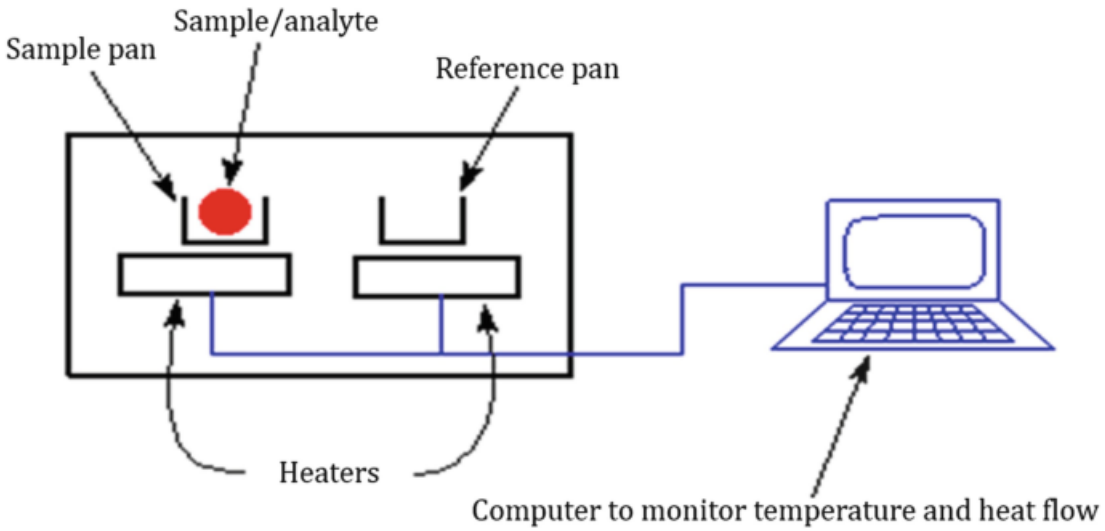

Figure 3.7 Schematics of typical DSC equipment [199]

$$q = Cp\ dT/dt + f\ (T, t) \tag{3.6}$$

In this equation, Cp represents the specific heat capacity of the sample, and dT/dt refers to the heating or cooling rate applied. The term f (T, t) represents the kinetic response of the material at a particular temperature or time. Notably, any thermal transitions occurring within the sample, such as crystallization, melting, or glass transition, are characterized by distinct changes in Cp. These thermal events are visually represented in the resulting DSC curves, as shown in Fig. 3.6.

CHAPTER FOUR

THE EFFECT OF ION MASS ON DYNAMIC CORRELATIONS IN IONIC LIQUIDS

This chapter is based on the manuscript submitted for publication in “The Journal of Physical Chemistry Part B” (Manuscript ID: jp-2023-055689) with title "The effect of ion mass on dynamic correlations in ionic liquids." Authors: Ahmed, Md. Dipu; Zhu, Zhenghao; Khamzin, Airat; Paddison, Stephen; Sokolov, Alexei; Popov, Ivan. I performed the dielectric measurements over a wide range of frequencies and analyzed the data with help from Dr. Popov. Z.Z., and S.J.P. performed molecular dynamic simulations. All authors contributed to the discussion of the results.

Ionic liquids (ILs) are a class of liquid salt with distinct properties such as high ionic conductivity, low volatility, and a broad electrochemical window, which make them appealing for use in energy storage applications. The ion-ion correlations are one of the key factors that play a critical role in the ionic conductivity of ILs. In this work, we present the study of the impact of ion mass on ion-ion correlations in ILs, applying a combination of broadband dielectric spectroscopy measurements and molecular dynamics simulations. We examined three ILs with the same cation but different anions to consider three different cases of cation-anion masses: $M_+ > M_-$, $M_+ \approx M_-$, and $M_+ < M_-$. We applied the momentum conservation approach to estimate the contribution of distinct ion-ion correlations from experimental data and obtained a good agreement with direct calculations of distinct ion-ion correlations from molecular dynamic simulations. Our findings reveal that relative ion mass has a strong effect on the distinct ion-ion correlations, leading to swapping of relative amplitude of distinct cation-cation and anion-anion correlations.

4.1. Introduction

Room-temperature ionic liquids (ILs) are promising materials for various electrochemical energy storage applications such as batteries and supercapacitors [140, 200, 201]. ILs demonstrate high intrinsic conductivity and low flammability, higher thermal and

electrochemical stabilities in comparison to conventional salt solutions with carbonate solvents [202-205]. Due to these characteristics, they meet most of the criteria for electrochemical devices with improved performance and safety [206]. One of the key fundamental properties of any ionic system is its ionic conductivity. The ionic conductivity of concentrated ionic systems is significantly influenced by the ion-ion correlations. Chapter 2 delves into a comprehensive explanation of these distinct ionic correlations and their consequential impact on conductivity. This discussion was expounded through Equations (2.1) to (2.5). Notably, it is still challenging to estimate these distinct ionic correlations by direct experiment, however some available approaches such as molecular dynamic simulation and momentum conservation model were described in chapter 2.3.

To verify validity of the momentum conservation approach, we performed experimental and computational studies of ILs with different ion masses. We chose ILs with the same cation, 1-butyl-3-methylimidazolium ([BMIM], M_+≈139g/mol), but different anions, BF_4 (M_-≈ 87g/mol), PF_6 (M_-≈145 g/mol), and bis(trifluoromethane)sulfonimide (TFSI)(M_-≈280g/mol). These ILs present the cases when $M_- < M_+$ (BMIM-BF4), $M_- \approx M_+$(BMIM- PF6) and when $M_- > M_+$ (BMIM- TFSI). Experimental data were used to estimate distinct ionic correlations based on the momentum conservation approach, and the results were compared to MD simulations, where distinct ion-ion correlations were directly calculated. This comparison revealed good quantitative agreement between experimental and simulation results. In particular, the cation-cation correlations provide a more negative contribution to conductivity than the anion-anion correlations in BMIM-BF4 with $M_- < M_+$, while in BMIM-TFSI with $M_- > M_+$, the anion-anion correlations contribute more negatively to conductivity than the cation-cation correlations. At the same time the cation-anion correlation has a positive contribution to conductivity in all three ILs. We also discussed how momentum conservation approach depends on choice of coordinate system.

4.2. Experimental Results

4.2.1. Materials

1-Butyl-3-methylimidazolium tetrafluoroborate [BMIM][BF4], 1-Butyl-3-methylimidazolium hexafluorophosphate [BMIM][PF6], and 1-Butyl-3-methylimidazolium bis (trifluoromethylsulfonyl)imide [BMIM][TFSI] were purchased from Sigma Aldrich and used as purchased. The samples were opened and loaded into acell for conductivity measurements inside a glove box in an inert atmosphere.

4.2.2. Broadband Dielectric Spectroscopy (BDS)

Broadband Dielectric Spectroscopy (BDS) was employed to conduct measurements on conductivity spectra. To cover a wide frequency spectrum extending from 0.1 Hz up to 3 GHz, two spectrometers were used. Specifically, the Alpha-A analyzer by Novocontrol was used to measure frequencies within the range of 10^{-1} Hz to 10^{6} Hz, while an Agilent RF Impedance Material Analyzer, E4991A, alongside WinDETA Software from Novocontrol, covered the range from ~10^{5} to ~$3*10^{10}$ Hz. The experimental setup involved a cell configuration comprising a bottom electrode in the form of a cap and an upper electrode, which was separated from the cap using a sapphire window to prevent electrical contact. This setup maintained a fixed electrode distance of 0.4 mm and a diameter of 10.2 mm. During measurements, a voltage amplitude of 0.1 V was applied. Both the coaxial line and the cell were meticulously calibrated using standard procedures. Temperature stabilization was ensured using a Quattro temperature controller from Novocontrol, allowing for precise measurements within a temperature range from 10^{-1} Hz to 10^{9} Hz. The measured samples were allowed to stabilize for 20 minutes at each temperature to ensure accuracy within ±0.2 K, followed by rapid cooling to avoid crystallization at lower temperatures. The conductivity spectra across all studied systems in Fig. 4.1b displayed three distinct regions: firstly, a frequency-dependent AC conductivity phase at high frequencies (σ_{AC}); secondly, a plateau-like DC conductivity phase at intermediate frequencies (σ_{DC}); and thirdly, a decline attributed to the buildup of charge carriers at the electrode surface at lower frequencies, known as the electrode polarization effect [207].

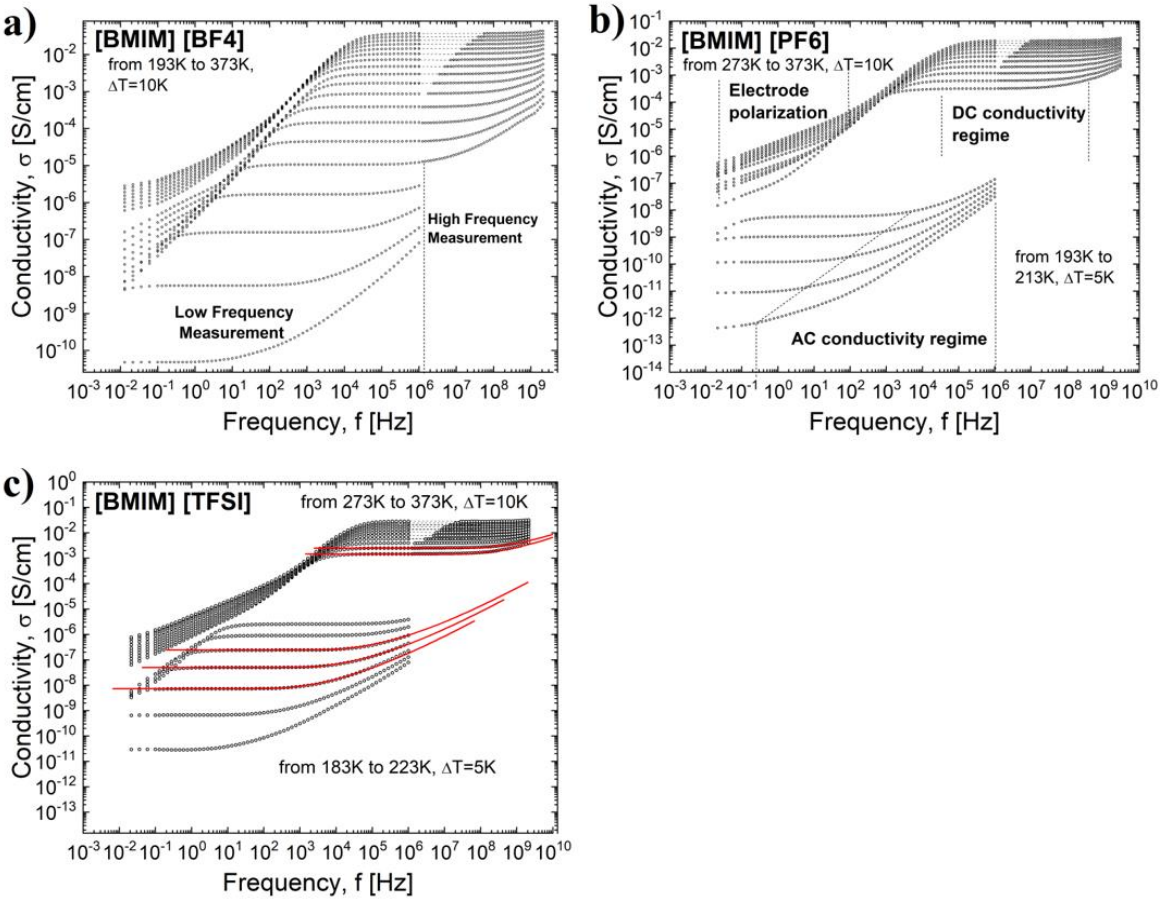

Figure 4.1 Conductivity spectra over a wide frequency range for the different ionic liquids: (a) [BMIM][BF4]; (b) [BMIM][PF6]; and (c) [BMIM][TFSI].

In Fig 4.1, the temperature gap in data of BMIM-PF6 and BMIM-TFSI is caused by samples crystallization. To determine the conductivity relaxation time, τ_σ, the conductivity spectra were fitted using Eq. (4.1). The example of fitting at different temperatures is shown in Fig. 4.1c by red solid lines. To match data from high and low frequency measurements, the electrode polarization regime in the high frequency measurements was removed, and dashed lines are only displayed to guide the eye.

4.3. Discussion

The conductivity spectra in ion conductive materials [7, 157] are usually described by the Random Barrier Model (RBM) [194, 208-210]. According to this model, charge carriers are hopping over potential energy barriers. When the barrier height distribution is constant the model results in the following prediction [195]

$$\ln\left(\frac{\sigma*(\omega)}{\sigma_{DC}}\right) = \frac{i\omega\tau_\sigma\sigma_{DC}}{\sigma*(\omega)}\left(1+\frac{8}{3}\frac{i\omega\tau_\sigma\sigma_{DC}}{\sigma*(\omega)}\right)^{-1/3} \tag{4.1}$$

Here $\sigma^*(\omega)$ is a measured complex conductivity, σ_{DC} is a DC-conductivity, and τ_σ is a conductivity relaxation time. The latter specifies the characteristic of AC-DC crossover time when charge mean-squared displacement crosses over from a sub-diffusive regime, $\langle r^2(t)\rangle \sim t^\alpha$ with $\alpha<1$ (corresponds to AC tail in conductivity spectra) to a normal diffusion regime $\langle r^2(t)\rangle \sim t$ (corresponds to DC-plateau in conductivity spectra).

Both the conductivity spectra and the conductivity relaxation process in the real part of the dielectric permittivity are described by the Eq. (4.1). The temperature dependence of σ_{DC} and τ_σ obtained from the fits are plotted in the Fig. 4.2. As it was proposed in early studies [7, 119, 157, 193, 211], conductivity relaxation process corresponds to local ion rearrangements, and knowing the conductivity relaxation time and diffusion coefficient, D, measured by pulsed field gradient nuclear magnetic resonance (PFG-NMR), we can estimate the ion rearrangement length, λ

$$\lambda = \sqrt{6D\tau_\sigma} \tag{4.2}$$

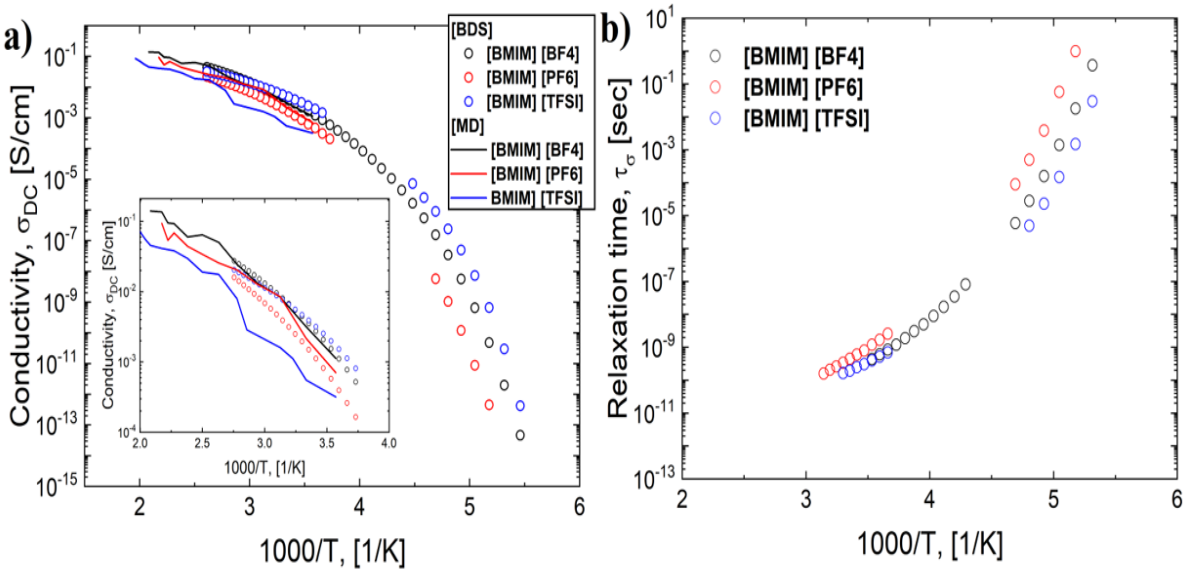

Figure 4.2 (a) Temperature dependence of the DC conductivity, σ_DC: symbols present experimental data, and lines are from the MD simulations results. The inset figure in Fig 4.2(a) represents the comparison of MD results and experimental data on an expanded scale. **(b)** Temperature dependence of the conductivity relaxation time, τ_σ. The gap in experimental data for σ_{DC} and τ_σ at low temperatures for [BMIM][PF6] and [BMIM][TFSI] is due to crystallization.

The parameter, λ, defines the characteristic length where anomalous sub-diffusion regime crosses over to a normal Fickian diffusion, and in typical ILs its value is about $\lambda \approx$ 1-3 Å [119, 212]. Using the diffusion coefficients of cation and anion [77, 213] we can estimate separately the rearrangement length for positive and negative charge carriers: $\lambda_+ = \sqrt{6D_+\tau_\sigma}$ and $\lambda_- = \sqrt{6D_-\tau_\sigma}$. These parameters for studied ILs appear in the range ≈ 1.2-1.9 Å (Fig. 4.3b). It was suggested [7] that the ion rearrangement length should be about half of the average distance between the ions estimated from their concentration, $\langle d \rangle_{conc}/2 = [(3/4\pi n)^{1/3}]/2$. However, the distance estimated from ion concentration appears slightly larger than λ, $\langle d \rangle_{conc}/2$ ~ 2.0-2.4 Å (Fig. 4.3b). The average distance between the ions can be also estimated from the radial distribution function (RDF) obtained in MD simulations (Fig. 4.3a). Half of the average distance between the ions estimated from RDF is even a bit larger than $\langle d \rangle_{conc}/2$ (Fig. 4.3b).

Although the estimated rearrangement length, λ is a bit smaller than averaged distance estimated from ion concentration and RDF function, it is worth to note that its value is almost temperature independent. This fact can be used for estimation of ion diffusion coefficient at low temperatures where slow ion dynamic is inaccessible for PFG-NMR measurements. Indeed, knowing parameter λ, we can invert the Eq. (4.2) and use τ_σ from the BDS measurements to estimate the diffusion of ions $D_\pm = \lambda_\pm^2/6\tau_\sigma$ (Fig. 4.4)[193]. Knowing diffusion coefficient, we can estimate the expected conductivity using Eq. (2.2) and calculate the inverse Haven ratio in Eq. (2.5) at low temperature to reveal how ion-ion correlations depend on temperature. Analysis of the inverse Haven ratio in the studied systems in Fig. 4.5 reveals that it stays almost constant ~0.6-0.8 at higher temperatures, and then decreases to ~0.4-0.25 upon cooling towards Tg. The decrease of H^{-1} upon cooling has been reported for many systems [7, 119], and the mechanism of this behavior remains unknown.

Although the inverse Haven ratio provides information on ion correlations, this parameter doesn't reveal any details of the mechanism dominating these correlations studied.

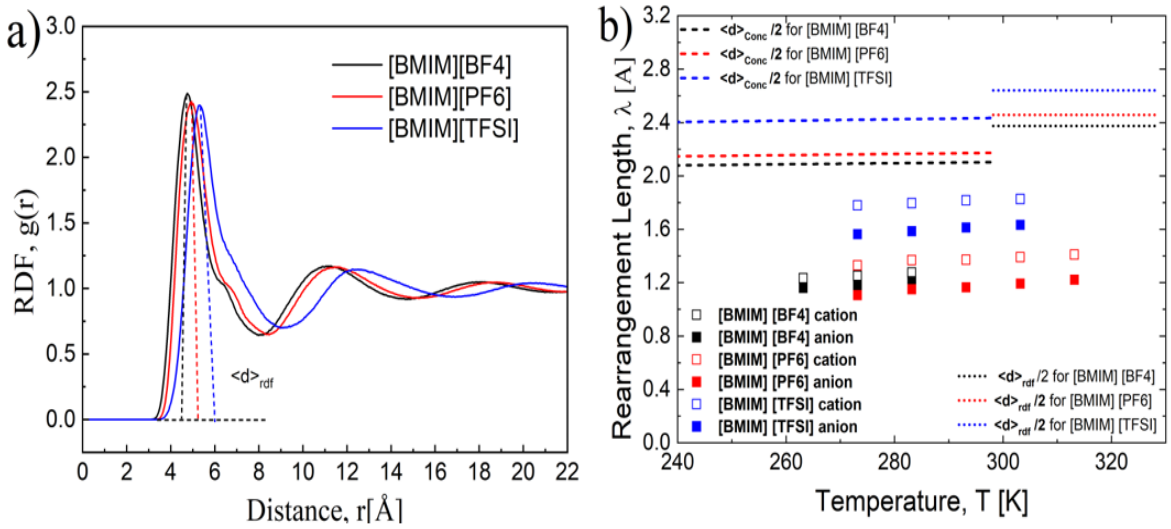

Figure 4.3 (a) Radial distribution functions of center of mass of cations and anions in ILs to estimate the half of the average distance between the ions, <d> rdf /2. (b) Ion's re-arrangement length estimated from Eq. (4.2) for cations (open square symbols) and anions (closed square symbols)

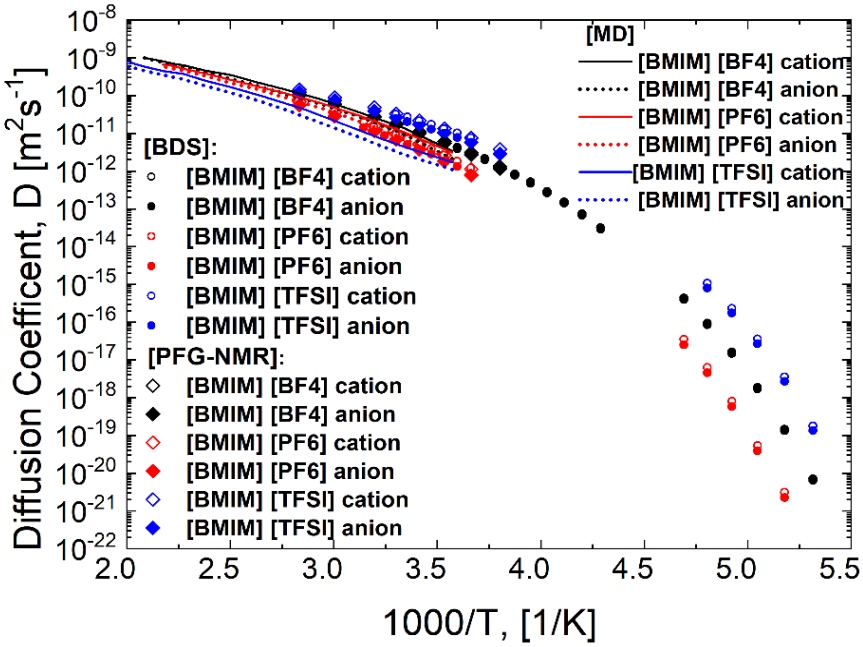

Figure 4.4 Temperature dependence of diffusion coefficient for cation and anion in ILs. Circle symbols represent our experimental data which are in good agreement with previous studies (ref [214]) Whereas PFG-NMR data are shown as a diamond symbol, MD data are shown solid and dotted lines for cation and anion respectively.

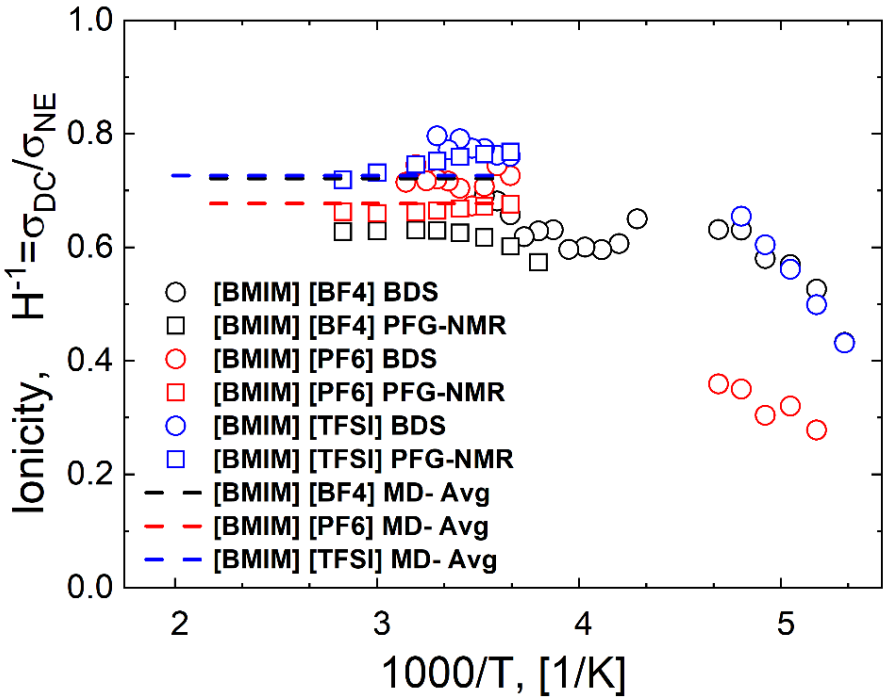

Figure 4.5 Temperature dependence of the ionicity or inverse Haven ratio. Circle symbols represent our experimental data, where diffusion coefficient was estimated from the ac-dc crossover and square symbols corresponds to data, where diffusion coefficient was measured by PFG-NMR results. The dashed lines represent the average value of ionicity from the MD simulations which are in good agreement with the experimental data.

systems. At the same time the direct experimental measurements of distinct ion-ion correlations is quite difficult [162]. However, the contributions of distinct ion-ion correlations to conductivity can be estimated based on the model proposed by Schonert and developed in papers [9, 124, 139]. The model actually takes into account only one additional assumption that the total momentum of all ions is conserved, and the velocities of cation and anions obey to the Eq. (2.6). We will discuss the validity of this assumption later. Considering the case when all ions are mobile, we can multiply Eq. (2.6) by $\vec{v}_{j+}(t)$ and $\vec{v}_{j-}(t)$ and take the average to obtain next system of equations:

$$\begin{cases} M_+(D_+^s + D_{++}^s/2) = -M_- D_{+-}^s/2, \\ M_-(D_-^s + D_{--}^s/2) = -M_+ D_{+-}^s/2 \end{cases} \tag{4.3}$$

where D_+^s, D_-^s are self-diffusion coefficients and $D_{++}^s, D_{--}^s, D_{+-}^s$ are distinct diffusion coefficients defined by the relationships:

$$D_+^s = \frac{1}{3}\int_0^\infty < \bar{v}_{i+}(t)\, \bar{v}_{i+}(0) > dt, \qquad D_-^s = \frac{1}{3}\int_0^\infty < \bar{v}_{i-}(t)\bar{v}_{i-}(0) > dt,$$

$$D_{++}^d = \frac{\varphi}{3}\int_0^\infty < v_{i+}(t)\bar{v}_{j+}(0) > dt,\ D_{--}^d = \frac{\varphi}{3}\int_0^\infty < \bar{v}_{i-}(t)\bar{v}_{j-}(0) > dt, \tag{4.4}$$

$$D_{+-}^d = \frac{\varphi}{3}\int_0^\infty < \bar{v}_{i+}(t)\bar{v}_{j-}(0) > dt = \frac{\varphi}{3}\int_0^\infty < \bar{v}_{i-}(t)\bar{v}_{j+}(0) > dt$$

here the plus/minus subscript means anion/cation, and φ is the total number of correlated ions in local area. Together with the Eq. (2.3), the Eqs. (4.4) present the closed system, which can be easily resolved [9, 124, 139, 193]. As a result, we can derive the analytical expressions for each term of contribution of ion-ion correlations in the Eq. (2.4):

$$\sigma_{++}^d = \frac{1}{4}\frac{e^2 n}{k_B T} D_{++}^d = \sigma_{DC}\left(\frac{M_-}{M_- + M_+}\right)^2 - \sigma_+^s, \qquad \sigma_+^s = \frac{e^2 n}{k_B T} D_+^s$$

$$\sigma_{--}^d = \frac{1}{4}\frac{e^2 n}{k_B T} D_{--}^d = \sigma_{DC}\left(\frac{M_+}{M_- + M_+}\right)^2 - \sigma_-^s, \qquad \sigma_-^s = \frac{e^2 n}{k_B T} D_-^s \tag{4. 5}$$

$$\sigma_{+-}^d = -\frac{1}{2}\frac{e^2 n}{k_B T} D_{+-}^d = \sigma_{DC}\frac{2M_+ M_-}{(M_- + M_+)^2}$$

This result provides a simple way to estimate distinct ion-ion correlation if DC-conductivity and self-diffusion coefficient are experimentally measured.

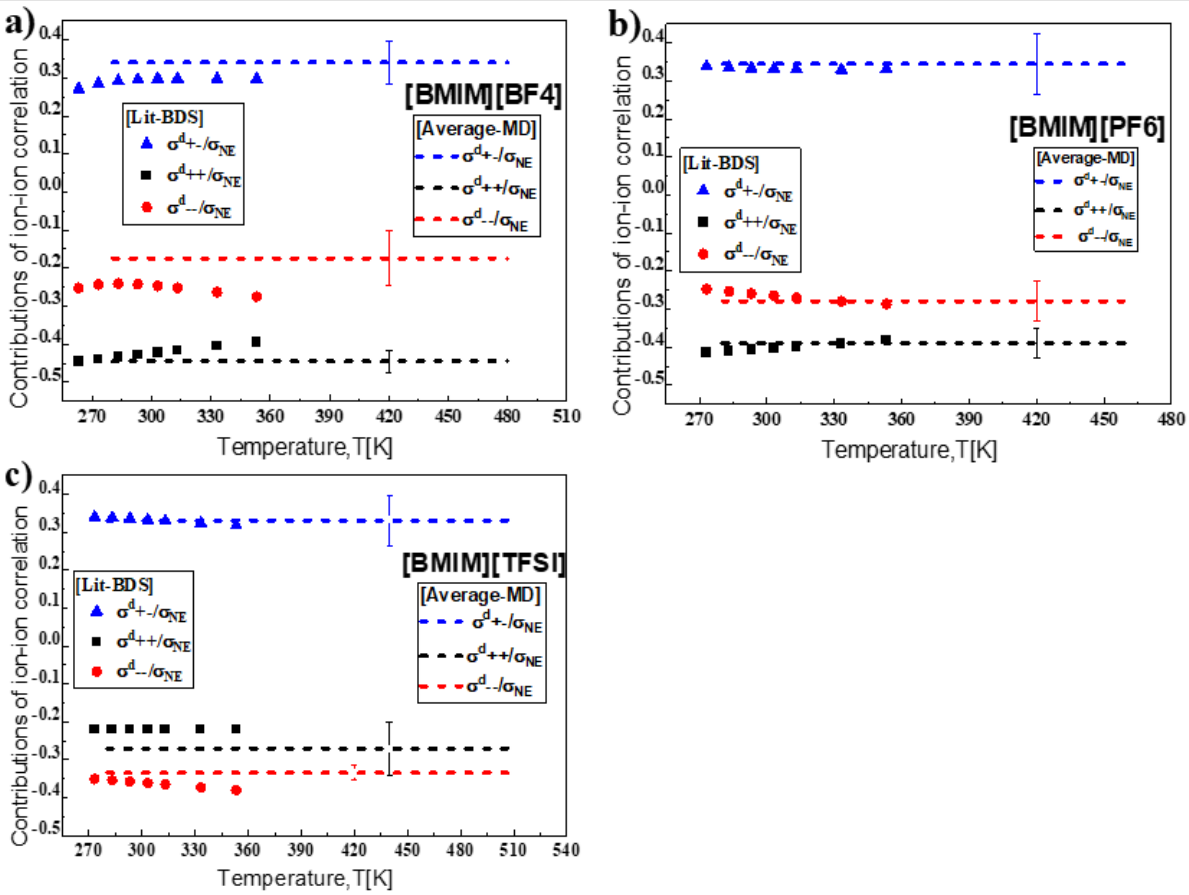

Figure 4.6 Distinct ion-ion contribution to conductivity normalized by σNE of three ionic liquids, where closed symbols represent our experimental data and dashed line represent average data from MD simulations with error bar.

According to the Eqs. (4.5), the cation-anion correlations in ionic liquids always have a positive contribution to conductivity, unlike the systems with solvent, where this type of correlation might change the sign, depending on solvent concentration [193]. This indicates that the conductivity of ionic liquids is always improved by the correlated anion-cation motion. The distinct contribution to conductivity estimated by the Eqs. (4.5) and scaled by the expected NE conductivity for the three studied ILs are shown in Figs. 4.6. These contributions appear in surprisingly good agreement with the direct calculations of these correlations in MD simulations in Figs. 4.6. These important results suggest that indeed momentum conservation might play an important role in ionic correlations in liquid electrolytes.

Both experimental and simulations results also revealed a significant role of the anion mass in these correlations (Figs. 4.6). While contribution of the anion-cation correlations to conductivity remains essentially the same, ~ +(0.3-0.4), distinct anion-anion correlations decrease from ~ - 0.2 in IL with light BF4 to ~ -(0.4-0.5) in IL with heavy TFSI, and distinct cation-cation correlations have opposite behavior with the increase of anion mass (Fig.4 6). Moreover, it can be seen from the Eqs. (4.5) that the mass of ions has direct relationship with distinct ion-ion correlation. In BMIM-BF4 the mass of the cation is larger than the mass of anion resulting in stronger negative cation-cation contributions to the conductivity (Fig. 4.6a), but BMIM-TFSI with anion mass larger than cation mass has stronger negative anion-anion contributions to conductivity (Fig. 4.6c). The independent MD simulations provide the same result of switching anion-anion and cation-cation correlations with the change of the anion mass (Figs. 4.6a, 4.6c). Surprisingly BMIM-PF6 has similar masses of anion and cation, yet cation-cation correlations appear more negative (stronger). The same result is observed in simulations (Fig. 4.6b), which adds confidence in approach of momentum conservation and Eqs. (4.5). The agreement between estimates applying the Eqs. (4.5) experimental data and the results of MD simulations justify the simple way for analysis of distinct ion-ion correlations for various ionic systems.

To better understand the impact of the mass of the anion, we artificially manipulated the

mass of BF_4^- in the MD simulations across a broad spectrum of molecular weight, while maintaining the same force field. This approach enabled us to eliminate the influence of other factors including the anion structure and charge distribution. As expected, the self-diffusion coefficient of the anion decreases with increasing mass. Similar behavior is observed also for the cation (Fig. 4.7a). It is worth noting that the self-diffusivity of the cation is consistently greater than that of the anion across all studied cases ($M_-/M_+ = 0.125 - 6.26$). This occurrence can be explained by the geometry of the cation which leads to a preferential translational motion in the plane of the ring [215, 216]. The contribution of distinct ion-ion correlations normalized by σ_{NE} as a function of the anion-to-cation mass ratio were also examined (Fig. 4.7b). We found that the correlated movement of the cations and anions positively contributes to the conductivity, while the distinct correlations between ions of the same charge result in negative contributions to the conductivity. More specifically, the negative contribution of distinct anion-anion correlation increases with increasing the mass of the anion. In contrast, the distinct cation-cation correlation shows an opposite trend. Moreover, all the distinct correlations quickly change when the anion-to-cation mass ratio is very small or very large. This is consistent with the difference between the distinct like-charged ion correlations in the case of an anion lighter than the cation (Fig. 4.6a) and the opposite situation (Fig.4.6c). It is worth noting that the distinct anion-anion correlation coincides with distinct cation-cation correlation when the ratio of the anion to cation mass (M_-/M_+) equals 1.25, rather than when the masses are identical as indicated by the green vertical line in Fig. 4.7b. This shift is consistent with stronger negative σ^d_{++} than σ^d_{--} in [BMIM][PF6] system with $M_+ \sim M_-$ (Fig. 4.6b). The shift of the crossing between the distinct ion correlations is related to the differences in diffusion coefficients of anion and cation, which may be due to the anisotropic diffusion of the cation compared to the isotropic movement of the anion as discussed above. Indeed, if we take into account the self-correlations, we obtain that $\Delta_+^{total} = (\sigma_{++}^d + \sigma_+^s)/\sigma_{NE}$ and $\Delta_-^{total} = (\sigma_{--}^d + \sigma_-^s)/\sigma_{NE}$ switch exactly at $M_- = M_+$ (Fig. 4.7b), in agreement with the Eqs.(4.5). Furthermore, the Eqs. (4.5) predict well how normalized cation-anion correlations $\sigma_{+-}^d/\sigma_{NE}$ and total contribution Δ_+^{total} and Δ_-^{total} depend on mass (solid lines in Fig 4.7b). Surprisingly, the distinct like-charged ion correlations shift from negative to slightly

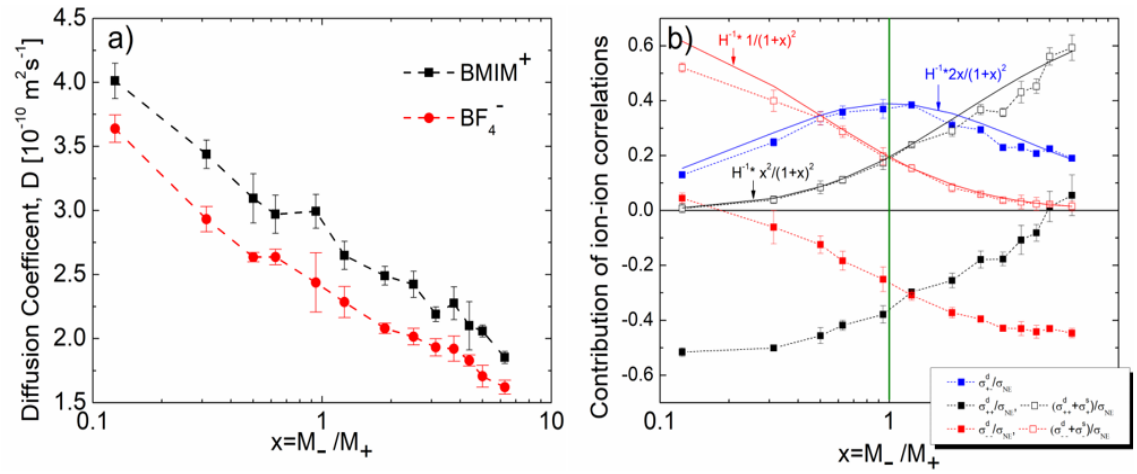

Figure 4.7 The relationship between the diffusion coefficient and the cation/anion mass ratio was determined via MD simulations.

positive values as the ratio of anion to cation masses is either significantly small or sufficiently large. The reason for this remains unclear. These findings conclusively demonstrate that disparities in anion and cation masses influence the magnitude of distinct correlations between ions. Remarkably, even the sign of these contributions can change when the masses of ions are significantly different. However, the results (Fig.4. 6 and 4.7b) also suggests that the ion mass is not the only parameter affecting these correlations. Apparently also the geometry and/or volume of the ion and their diffusion play a role.

It is important to emphasize that MD simulations explicitly assume momentum conservation (keeping no displacement for the center of mass). Momentum conservation law in the form of Eq. (2.6) is equivalent with coordinate system linked to the center of mass, where the velocity of system center mass is equal to zero, i.e.

$$\vec{v}_{CM}(t) = \frac{M_+\vec{v}_+(t) + M_-\vec{v}_-(t)}{M_+ + M_-} = 0$$

However, recent studies using electrophoretic NMR [217] suggested that momentum conservation might be broken in ILs, and instead, the conservation of local molar volumes of specific ions plays the critical role. Possibly, this happens because the electrophoretic NMR measurements and data analysis were done in the coordinate system linked to the center of volume [218]. If the density of the anion and cation differ [217], this automatically leads to breaking of momentum conservation in this coordinate system. Another important fact is that the Eq. (2.6) assumes that total momentum is conserved only for mobile ions, and is not transferred to the environment, for example to the sample cell. In the latter case, the velocity of the system's center of mass might not be equal to zero $\vec{v}_{CM}(t) \neq 0$, and we have to take into account the next type of correlations $\langle \vec{v}_{CM}(t)\vec{v}_{CM}(0)\rangle$, $\langle \vec{v}_+(t)\vec{v}_{CM}(0)\rangle$ and $\langle \vec{v}_-(t)\vec{v}_{CM}(0)\rangle$. The general equations in this case are derived in [219, 220]. The effect of these three additional terms is difficult to estimate, because it is quite challenging to measure how much momentum passed to the environment due to the movement of the ions. One of the ways to measure it is the combinations of the MD simulations, where

momentum conservation between ions is explicitly assumed, and experimentally measured distinct ion-ion correlations as proposed in [162]. This approach, however, is not applicable for ILs studied here [162].

4.4. Conclusion

In this work we studied three ILs with different anion/cation mass ratios. We have measured conductivity spectra in a wide frequency range and estimated DC-conductivity and conductivity relaxation time in wide temperature range. Based on diffusion coefficient at high temperature we estimated the ion rearrangement length marking a crossover from anomalous to normal diffusion regime. This length appears slightly lower than half of the average distance of the ions assumed in earlier studies. It is important that in the accessible temperature range this length scale appears essentially temperature independent. This enables an estimate of ion diffusion at low temperatures where it is too slow for PFG-NMR. As a result, it provides a way to estimate the inverse Haven ratio at very low temperatures. Our results indicate that H^{-1} decreases with decreasing temperature, but the mechanism of this temperature dependence requires additional investigation. Furthermore, we demonstrate that the distinct ion-ion contributions to conductivity can be estimated using a momentum conservation approach, in the center of mass coordinate system. The results from this approach were validated by our MD simulations. It was discovered that the behavior of the anion-anion and cation-cation correlations depend strongly on the anion to cation mass ratio, M_-/M_+. In the case of $M_-/M_+ > 1$ the distinct anion-anion correlations show a stronger suppression effect in the conductivity in comparison to the distinct cation-cation correlation. The opposite effect is observed in the case of $M_-/M_+ < 1$. This switching effect was also verified by our MD simulations. Detailed analysis also revealed that not only mass, but also the diffusivity of ions plays role in these correlations, emphasizing the role of ions geometry.

CHAPTER FIVE

THE INFLUENCE OF DOPING ON CONDUCTIVITY IN ORGANIC IONIC PLASTIC CRYSTALS (OIPCS)

This research focuses on analysis of conductivity and ionic correlations in organic ionic plastic crystals (OIPCs). By doping OIPCs with lithium salts, significant conductivity enhancement is observed within solid plastic crystal phases, showcasing their potential for improving battery performance. Additionally, the influence of dopant size on conductivity is investigated, revealing its role in different phases of OIPCs. Notably, the introduction of a liquid-like phase upon doping underscores its role in facilitating rapid ion movement and conductivity improvement. These findings collectively contribute to the understanding of conductivity enhancement mechanisms in doped OIPCs, offering insights for the design of more efficient and secure solid-state batteries.

5.1. Introduction

In the quest for efficient and safe energy storage solutions, solid-state batteries (SSBs) have emerged as a promising technology. These batteries, in contrast to traditional liquid electrolyte-based systems, employ solid electrolytes that offer improved stability and safety[221, 222]. However, the development and implementation of SSBs face challenges due to the properties of solid electrolytes. To address this, researchers have turned their attention to organic ionic plastic crystals (OIPCs), which hold great potential as replacements for liquid electrolytes in energy storage and other electrochemical devices. The allure of OIPCs lies in their unique properties, such as nonflammability, absence of a liquid phase, and negligible vapor pressure[15, 223-225]. These attributes make OIPCs highly attractive for the next generation of safe and efficient batteries.

In addition, many OIPCs exhibit relatively high conductivity, particularly when doped with lithium (Li) salts. This characteristic has sparked interest in leveraging doped OIPCs as a viable solution for SSBs. Upon doping with lithium salts, a majority of OIPCs demonstrate a remarkable increase in ionic conductivity within their solid plastic crystal phases [226-

228]. As a result, some of these materials have already been utilized to realize all-solid-state lithium batteries. Nevertheless, achieving a comprehensive understanding of how doping with lithium salts dramatically enhances ionic conductivity in plastic crystalline phases remains an ongoing scientific endeavor. Doping OIPCs with lithium salts, considering the common anion shared by both the lithium salt and the OIPC, allows us to effectively view the Li+ as a cationic dopant[226, 229]. This process modifies the structure of the material, introducing defects and forming solid solutions, and even eutectic liquid phases[226]. Furthermore, the charge is strongly localized on small Li ions that influences the dynamics of the matrix ions, thereby serving as another crucial factor affecting the transport mechanisms[226].

In contrast to superionic ceramics, organic ionic plastic crystals (OIPCs) suffer from limited conductivity under normal conditions, primarily due to a significant decrease in conductivity within their solid phases[230]. Previous research has revealed a fascinating behavior in OIPCs, where ion conductivity demonstrates abrupt decreases between different phases, while the diffusion coefficient of mobile ions shows relatively smooth temperature variations[231]. This peculiar phenomenon has been attributed to correlations in the movement of ions within the material.

Controlling these ionic correlations holds great potential for significantly improving the conductivity of electrolytes. In conventional ionic liquids, the reduction in conductivity, referred to as "ionicity," is typically modest, around 2-3 times[7, 12, 14]. However, in several potential electrolyte candidates for solid-state batteries (SSBs), such as poly-ionic liquids and OIPCs, ion-ion correlations have a much more pronounced impact, suppressing ionic conductivity by over 100 times[7, 9, 12, 14, 15]. This strong effect necessitates thorough and comprehensive studies to pave the way for the future development of innovative electrolyte materials. Therefore, it is important to carefully examine both the structural and phase transition behavior, as well as dynamic factors, to develop an understanding of ionic correlations in both pure and doped OIPCs, to reveal the underlying reasons for the enhancement of ion transport in Li+-doped OIPC systems.

This chapter offers a comprehensive analysis of the conductivity spectra and phase transition thermogram of pure OIPCs, namely [P 1,2]-TFSI, [P 1,4]-TFSI, as well as OIPCs doped with 4.8% LITFSI and BMIM-TFSI. BMIM is larger than Li and the role of the ion size can be observed easily. To obtain a thorough understanding of these systems, the conductivity measurements were conducted across an exceptionally broad frequency range, spanning from 0.1 Hz to approximately 30 GHz. Additionally, complementary techniques such as thermal analysis, light scattering, X-ray diffraction and PFG-NMR (in collaboration with CUNY) measurements were employed.

In this study, we aim to investigate the intricate interplay between ionic correlations, Li salt doping, and the resulting impact on conductivity and ion dynamics in OIPCs. We seek to unravel the mechanisms underlying the conductivity enhancement observed in Li+-doped OIPCs.

Through this analysis, we have uncovered intriguing aspects of OIPCs' conductivity spectra. Specifically, we observed the presence of unusual two-step conductivity spectra in these materials. Furthermore, doping with LITFSI has been found to reduce the additional step observed in the solid phase and decrease in enthalpy during different phase transitions. Moreover, we have demonstrated the effect of dopant size in OIPCs and how it influences conductivity in various phases. Additionally, our investigation has revealed a remarkable finding: the conductivity spectra for both pure OIPCs and doped OIPCs coincide at a microscopic level.

Our findings will contribute to the development of a comprehensive understanding of ionic correlations in electrolytes, paving the way for the future design and optimization of highly efficient and safe solid-state batteries.

5.2. Material and experimental measurements details

5.2.1 Materials

1-Ethyl-1-methylpyrrolidinium bis (trifluoromethyl sulfonyl) imide [P12TFSI], 1-Butyl-1-methylpyrrolidinium bis (trifluoromethyl sulfonyl) imide [P14TFSI], Lithium bis (trifluoro methane) sulfonamide [LITFSI] and *1-Butyl-3-methylimidazolium bis (trifluoromethyl sulfonyl) imide* [BMIMTFSI] were purchased from Sigma Aldrich (Shown in Fig.5.1)..

For the doping process, 4.8% mole of LITFSI and BMIMTFSI were carefully measured and added to 95.2% mole of P12TFSI and P14TFSI respectively. The mixture was then subjected to melting and thorough mixing in an oil bath at a controlled temperature of 110°C for a duration of 2 hours. All samples were opened and loaded into a cell for all measurements inside a glove box in an inert atmosphere.

5.2.2. Analytical methods and techniques

Broadband Dielectric Spectroscopy (BDS) was used to perform conductivity spectra measurements on various systems. To encompass a broad frequency range spanning from 0.01 Hz up to 3 GHz, two distinct spectrometers were utilized. For measurements within the frequency range of 10^{-2} Hz to 10^{6} Hz, the Alpha-A analyzer from Novocontrol was employed. The experimental setup comprised a cell design featuring a cap as the bottom electrode, while the upper electrode was isolated from the cap through a sapphire window, thereby preventing any electrical contact. The electrode separation was maintained at a constant 0.4 mm, with a diameter of 10.2 mm. During measurements, a voltage amplitude of 0.1 V was applied, and rigorous calibration procedures were executed prior to commencing the measurements. Within the higher frequency range of 10^{6} Hz to 3×10^{9} Hz, the Agilent RF Impedance Material Analyzer, E4991A, along with Novocontrol's WinDETA Software, was employed. To construct the measurement cell, two APC-7 connectors were utilized. The upper electrode was adapted by substituting the inner pin of one connector with a solid 3 mm diameter pin, supplemented with Teflon filling the space.

Selected OIPCs

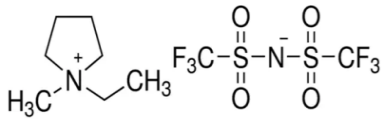

Chemical Name: P[1,2]-TFSI
1-Ethyl-1-methylpyrrolidinium bis(trifluoromethyl-sulfonyl)imide
Chemical Formula: $C_9H_{16}F_6N_2O_4S_2$
MW: 394.35 g/mol
Melting Temperature: 88 °C

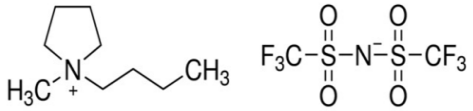

Chemical Name: P[1,4]-TFSI
1-Butyl-1-methylpyrrolidinium bis(trifluoromethyl-sulfonyl)imide
Chemical Formula: $C_{11}H_{20}F_6N_2O_4S_2$
MW:422.4 g/mol
Melting Temperature: -15 °C

Selected dopant for OIPCs

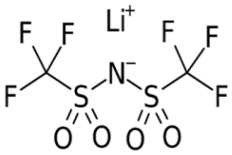

Chemical Name: LI-TFSI
Lithium bis(trifluoromethanesulfonyl)imide
Chemical Formula: $LiC_2F_6NO_4S_2$
MW: 287.075 g/mol
Melting Temperature: 236 °C

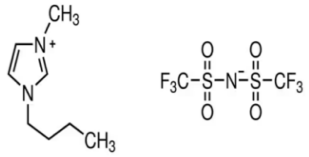

Chemical Name: BMIM-TFSI
1-Butyl-3-methylimidazolium bis(trifluoromethylsulfonyl)imide
Chemical Formula: $C_{10}H_{15}F_6N_3O_4S_2$
MW: 419.36g/mol
Melting Temperature: 1 °C

Figure 5.1 Chemical structure and general information of selected OIPCs: P12TFSI, P14TFSI and dopant: LITFSI, BMIMTFSI.

between the inner and outer components. The lower electrode was formed by removing the pin of another connector and introducing a movable metallic cylinder into the vacant central space. This arrangement facilitated the creation of a coaxial line concluding in a plate capacitor, wherein the distance between the electrodes could be adjusted. Calibration procedures, encompassing both the coaxial line and the cell itself, were meticulously undertaken through established methodologies (Open/Short/50 Ohm). The sample loading was executed between the two electrodes at a separation distance of 0.1 mm, with measurements performed using a voltage amplitude of 0.1 V. To ensure precise temperature control during measurements spanning from 10^{-2}Hz to 10^{9} Hz, a Quattro temperature controller from Novocontrol was employed. At each temperature point, a stabilization period of 20 minutes was observed to achieve a high level of precision, within ±0.2 K.

Differential Scanning Calorimetry (DSC) was used to conduct thermal behavior measurements of pure and dopes OIPCs samples using a Q2500 DSC instrument from TA Instruments. To ensure a controlled environment, the samples were carefully placed into the DSC pans within a glove box, maintaining an inert atmosphere throughout the process. To eliminate any previous thermal effects, the samples were initially subjected to isothermal equilibration at 393 K (~30 K above the melting temperature) for a duration of 10 minutes. Following this, they were rapidly cooled to 183 K and allowed to stabilize for another 10 minutes. The next step involved heating the samples from 183 K to 393 K at a controlled rate of 10 K/min. For consistency and reliability, each sample underwent the entire process twice, ensuring repeatability of the results. By employing this well-defined procedure, we aimed to obtain accurate data on the thermal properties of the samples under investigation. These DSC measurements offer valuable insights into the material's behavior and transitions at different temperature ranges, ultimately contributing to a comprehensive understanding of its characteristics.

Wide-Angle X-ray Scattering (WAXS) was performed to get information on the structural aspects of both liquid and solid phases within the samples. The primary

objectives of these experiments were two-fold: Qualitative Phase Characterization aiming to gain an understanding of the relative weight fractions of the solid and liquid phases present within the samples. Crystalline Structure Analysis: Another goal was to detect any modifications in the crystalline structure caused by introducing dopants to the plastic crystal. This encompassed potential outcomes like the emergence of new crystalline phases or alterations in the dimensions of the unit cell. The experimental conditions were set at a temperature of 50°C. This temperature was chosen to lie between two crucial points: the transition from phase 2 to phase 1, and the ultimate melting of the crystalline structure of the plastic crystals. To minimize the influence of coarse grain effects, the samples underwent a grinding process. This grinding procedure was executed promptly to minimize the exposure of the samples to ambient air. Initially, a method was employed where the samples were heated to 50°C, allowed to equilibrate for 10 minutes, and then WAXS data were gathered over a span of 30 minutes. However, it was evident that this approach led to localized heating of the samples and a significant rise in the liquid phase content, particularly in the doped samples. Consequently, a refinement in the experimental protocol was necessary. The modified procedure involved heating the samples to 50°C, followed by a 10-minute equilibration period, during which WAXS data were captured for 6 minutes. After this initial run, the sample temperature was allowed to stabilize for another 6 minutes, and subsequently, a fresh WAXS run was carried out. This sequence was repeated once more, resulting in a total of three runs (each lasting 6 minutes) for every sample.

5.3. Experimental Results

In the context of conductivity spectra, three distinct regimes have traditionally been observed[207]. Firstly, the Electrode Polarization (EP) effect occurs at low frequencies, leading to a decrease in conductivity due to the accumulation of charge carriers at the surface of the electrodes. Secondly, an intermediate frequency range shows a plateau in the DC conductivity regime. Lastly, at higher frequencies, the AC regime is observed[207].

However, when studying the P12TFSI in its solid state, an intriguing phenomenon emerges. An additional relaxation process, labeled as "Process I," appears as an extra step in the

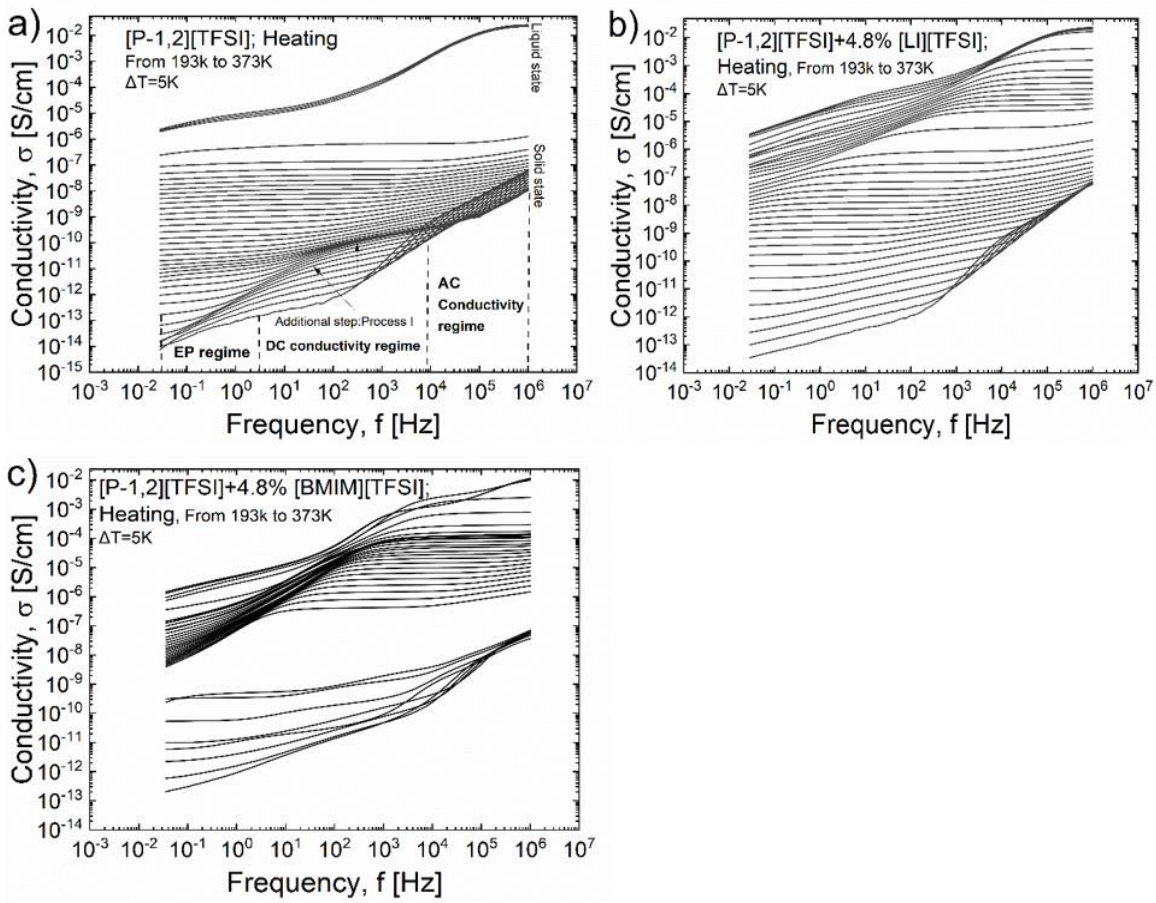

Figure 5.2 Conductivity spectra of pure and doped system at different temperature a). Pure P12TFSI b). P12TFSI+ 4.8% LITFSI c). P12TFSI+4.8% BMIMTFSI, in Fig. 5.2a, the additional steps are observed at solid state of P12TFSI, and doping reduces the additional steps in Fig 5.2b, c.

conductivity spectra at frequencies lower than the typical AC-DC crossover point (as depicted in Fig. 5.2a). This distinct behavior is prominent in solid phase and not observed in the melt phase of the material(in both pure and doped systems), as shown in Figs. 5.2, suggesting that Process I is specifically linked to unique dynamics within the crystalline structure of the OIPC[232].

5.4. Discussion

Ion-ion correlations in pure P12TFSI:

In pure P12TFSI, both cation and anion are mobile according to Pulsed Field Gradient Nuclear Magnetic Resonance (PFG-NMR) results presented in Fig.5.3b. It's important to clarify that we have two distinct sets of conductivity data for Pure P12TFSI in Fig 5.3a. The DC conductivity measured following the same protocol as PFG-NMR (Fig 5.3a in red circle), showed a distinct decrease at phase transition temperatures. Sample was melted inside glove box at 100℃ and cooled to room temperature to remove thermal history. Measurements were then performed at specific temperature: 20℃, 25℃, 30℃, 55℃, 65℃, 75℃, 90℃, and 95℃.The other set of data corresponds to our conventional conductivity measurements (Fig 5.3a in black circle) conducted during the heating cycle, ranging from -110°C to 115°C with 5°C increment for each measurement (sample was melted inside glove box in the BDS cell and waited to room temperature before starting the measurement).It's noteworthy that both sets of data closely coincide with previously published results in [147], ensuring the consistency and reliability of our findings. This conductivity increases with temperature increase showing step like increase upon crossing melting temperature from phase 1 to liquid phase. In parallel, the ion diffusivity measured by PFG NMR displayed no analogous stepwise behavior across the melting point. Notably, while the conductivity experienced a substantial reduction of approximately 2-3 orders of magnitude for red circle and 4-5 orders of magnitude for black circle within the temperature range of 95-55°C (Fig. 5.3a), the corresponding diffusion coefficients only diminished by about 2 orders of magnitude (Fig. 5.3b). Moreover, PFG NMR revealed that 100% of ions are moving with these diffusion coefficients. This intriguing disparity suggests that although the ions exhibit mobility, their contribution to conductivity remains constrained.

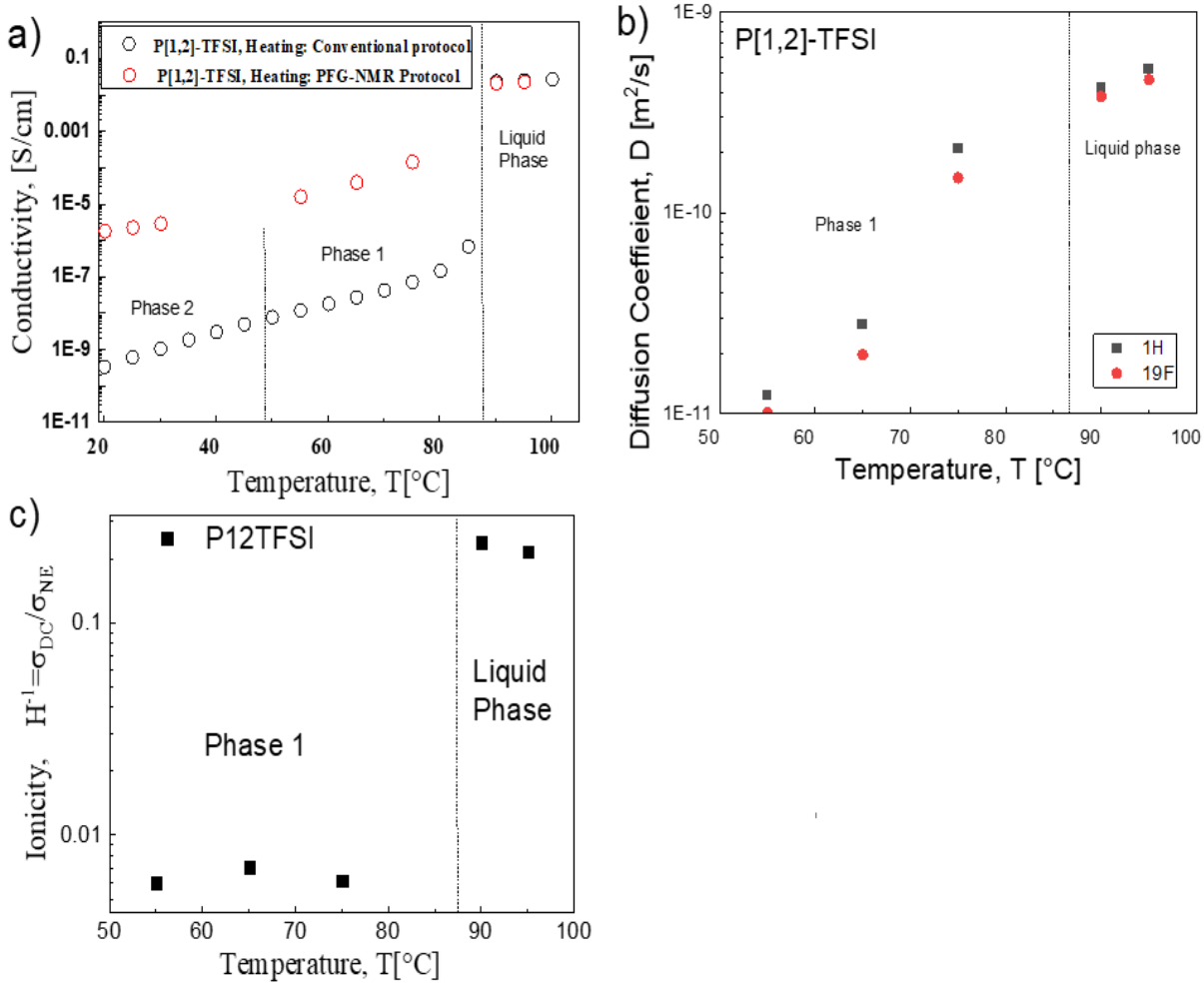

Figure 5.3 a) Temperature dependence of DC-conductivity of P12TFSI in solid and meted states. The red circle symbol represents conductivity measured by following PFG-NMR protocol whereas black circle is for conventional BDS measurement b) Diffusion coefficient of ions in P12TFSI. c). Temperature dependence of the inverse Haven ratio of P12TFSI in solid (Phase 1) and melted states

These results suggest a strong drop in the inverse Haven ratio indicating an inhibition of conductivity attributed to ion-ion correlations.

We derived the temperature-dependent inverse Haven ratio using Eq. (2.5). Analysis, illustrated in Fig. 5.3c, indicates that the inverse Haven ratio in the ionic liquid (above melting temperature) is approximately H^{-1} ~ 0.2-0.3. This value is a bit lower than in most ILs, where H^{-1} ~ 0.4-0.6[7, 119, 127, 142-144]. In the solid states, this ratio notably decreases to around 0.004-0.006 which indicates ionic correlation suppress conductivity more than 100 times in phase 1. These findings underscore the significant impact of ion-ion correlations in the solid phases of this plastic crystal. Consequently, our analysis strongly suggests that the variations in conductivity between different phases of the studied OIPC primarily stem from drops in the inverse Haven ratio. This result is consistent with earlier observation for another plastic crystal published in [9, 146].

Furthermore, in the pure P12TFSI system, the spectral characteristics resemble the liquid phase at high frequencies, followed by a pronounced step (Process 1) leading to decreased conductivity in Fig 5.2a and 5.4 This step indicates a structural transformation, impacting ion or molecule mobility and, consequently, conductivity.

Examining the conductivity spectra across diverse solid phases in the pure system, variations likely arise from shifts in crystalline structure or molecular organization. Distinct solid phases may exhibit differing ion mobility due to varied arrangements, lattice configurations, or local environments[152, 233]. Moreover, the conductivity spectra from two distinct measurement methods are illustrated in Fig. 5.4b. In the measurements of conductivity at T=20°C followed the PFG-NMR protocol, a clear AC-DC crossover is evident, with no additional step. In contrast, the spectra obtained through conventional measurements display a distinct step, and the AC-DC crossover is not as pronounced in this set of data. These differences highlight the unique characteristics captured by each measurement technique.

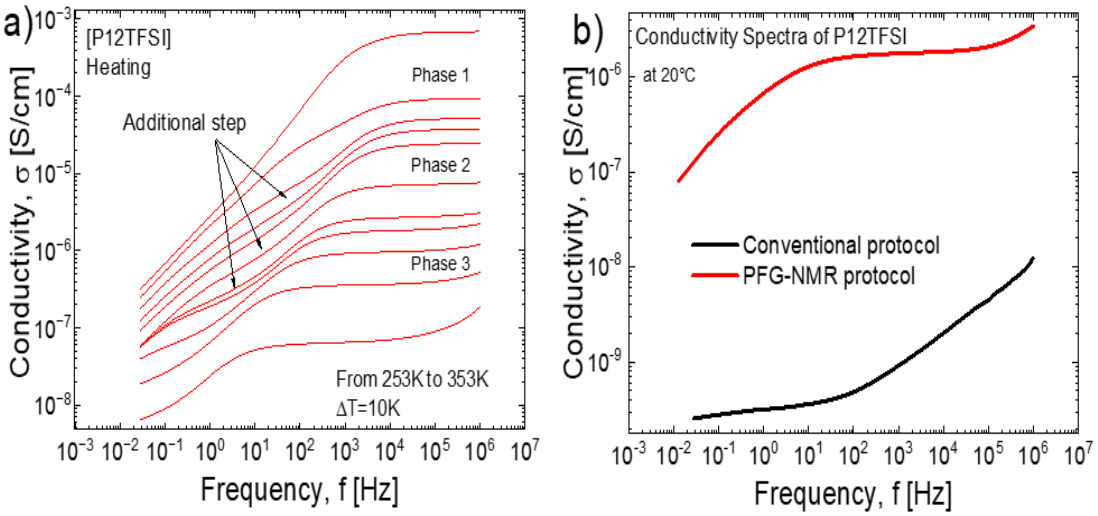

Figure 5.4 a). Additional steps in conductivity spectra of P12TFSI at different temperature. b). Conductivity spectra comparison of two type of measurement: conventional and PFG-NMR protocol at 20°C

We conducted WAXS experiments to investigate the structure factors of both liquid and solid phases in the samples. We undertook a qualitative assessment of phase weight fractions, incorporating the following considerations. Given the consistent behavior of pure P12TFSI data under the initial 30-minute exposure protocol, we adopted this approach to derive empirical standard data for both liquid and solid phases. Specifically, we collected data at 100°C for the liquid state and at 50°C for the solid plus liquid state. The liquid state data were then used to remove its contribution from the spectra of other phases. Subsequently, we employed the scaled sum of these datasets to fit data across all samples. Key considerations encompass:

Firstly, the liquid phases are the same in all samples. This assumption is based on the same conductivity for all the samples above melting temperature. Secondly, the crystalline phases are the same in all samples, including the number of chemical formulas per unit cell, the molecular weight of the unit cells and their volumes. Naturally, this assumption is not necessarily true and was only made for simplification of the analyses.

The weight fraction of phase α in a in multiphase mixture is described with the Eq. (5.1), where Wα is the weight fractions of phases α [234].

$$W_{\mathrm{c}} = W_{\mathrm{L}} \frac{S_c (ZMV)_{\mathrm{c}}}{S_L (ZMV)_L} \tag{5.1}$$

Where, S_c and S_L are the Rietveld scale factors for crystalline phases and liquid phase, respectively, and $(ZMV)_c$ and $(ZMV)_L$ are the product of the number of chemical formulas per unit cell, the molecular weights of these unit cells, and their respective volumes for phases crystalline and liquid [234, 235]. Moreover, Eq. (5.1) provides a means to determine the phase fraction within a multiphase sample, facilitating the estimation of the presence and quantity of any amorphous or unidentified phases.

When we applied Equation (5.1) to both our pure P12TFSI and then analyzed the data using WAXS spectra, we gained some interesting insights. In the case of the pure P12TFSI, specifically the intake sample in Fig 5.5a, an in-depth analysis at 50°C reveals that

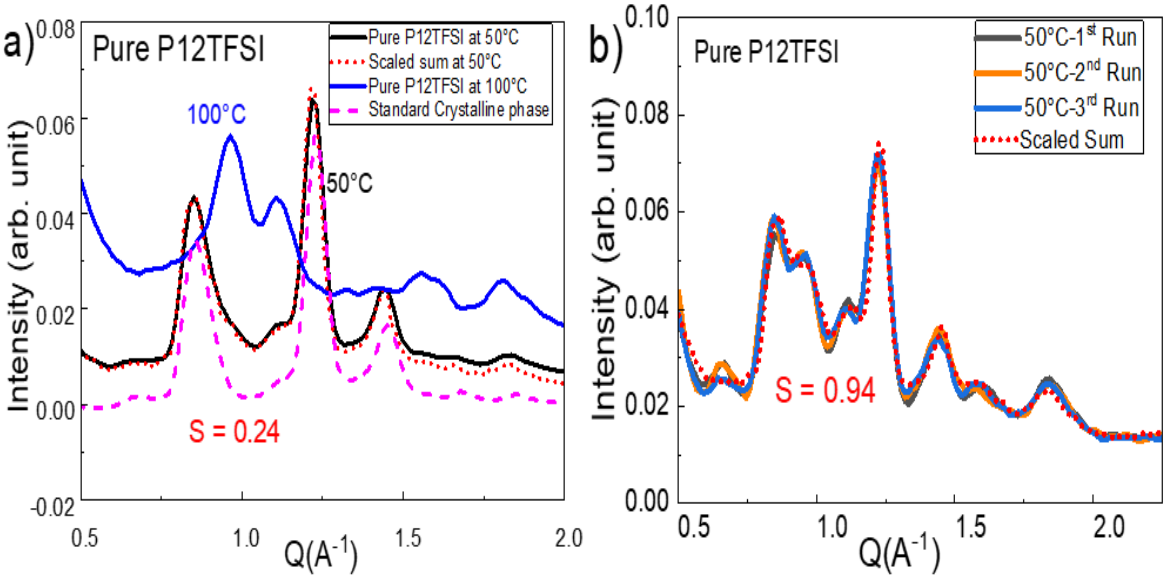

Figure 5.5 WAXS spectra for two data sets of pure P12TFSI. a). P12TFSI (fresh sample) at 50°C and 100°C b) P12TFSI (aging sample), subjected to a 3–4-month room temperature storage period and used for conductivity measurements via the PFG-NMR protocol, was analyzed at 50°C. Calculating the ratio of weight fraction of liquid and crystalline phase ($S = \frac{w_L}{w_C}$) for a). P12TFSI (0.24) b). P12TFSI (0.94) and red dotted fitting line is obtained by using Eq. (5.1)

approximately 19% of the material exhibits liquid-like structure, while the remaining 81% is crystalline. On the other hand, when considering the aging sample of pure P12TFSI as depicted in Fig 5.5b, we observe a notable shift with 48% of the material displaying liquid-like characteristics, while the solid-like phase constitutes the remaining 52%. It's important to note that these percentages are not exact measurements in absolute value; they are relative to each other and provide qualitative rather than quantitative information. We suggest that the observed difference in structure of pure P12TFSI depending on thermal history (Fig. 5.5) might be the reason for the observed difference in conductivity (Fig. 5.3a).

Role of doping and their size effect on conductivity in OIPCs:

My research in the OIPCs focuses on the interplay between P12TFSI, P14TFSI, and dopants like LITFSI or BMIM TFSI. Adding a small amount of LITFSI (around 4.8%) to P12TFSIsignificantly increases the ionic conductivity, as shown in Figure 5.6a. This boost in conductivity results from the introduction of lithium ions, which enhance ion mobility and charge movement[147, 236]. Increasing the concentration of lithium ions further improves conductivity [236, 237].Moreover, in the liquid phase, conductivity remains essentially constant, yet the decrease in conductivity upon crossing T_m is less pronounced in the doped systems.

Effect of dopant size on conductivity:

The observed phenomenon depicted in Figs. 5.6 underscores the pivotal role of doping in enhancing conductivity in the solid OIPCs, with the added dimension of dopant size influencing this relationship. Pure P12TFSI was doped with 4.8 mol% of LITFSI and 4.8 mol% of BMIMTFSI where BMIM have larger size than Li as cation[238]. In Phase 1, dopant size has little effect on conductivity, with Li and BMIM showing similar profiles. However, in Phases 2 and 3, a clear trend emerges: larger dopants like BMIM lead to increased conductivity. This suggests that dopant size plays a significant role in enhancing conductivity beyond a certain threshold. These findings enhance our understanding of the complex relationship between dopant properties and material conductivity in OIPCs.

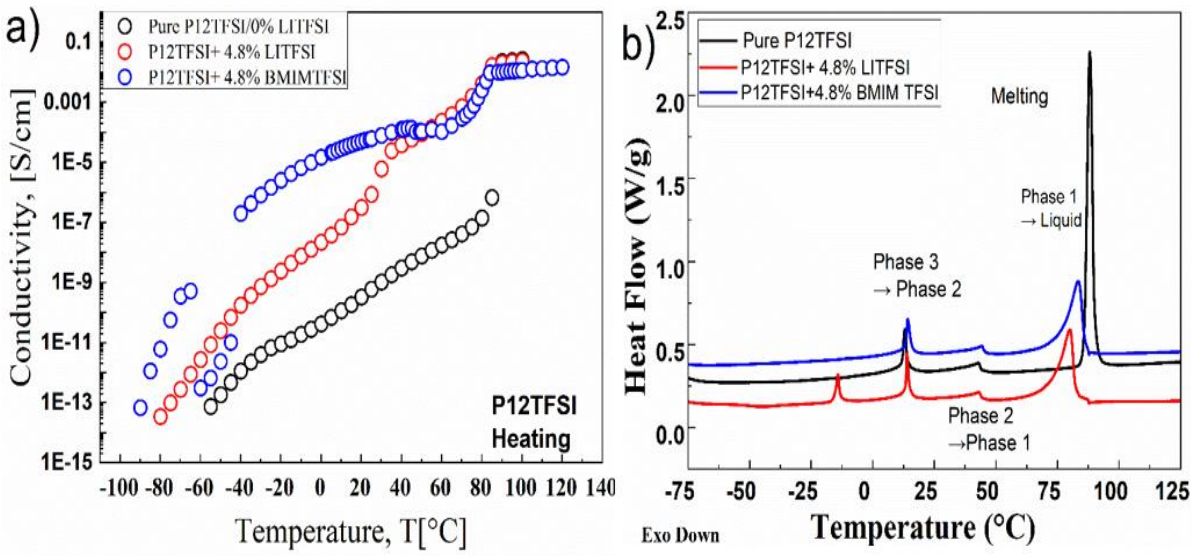

Figure 5.6 Comparison of conductivity of pure P12TFSI, with 4.8% LITFSI and 4.8% BMIMTFSI at different temperature b). DSC thermogram depicted phase transitions behavior of those systems.

Effect of doping and size of dopant on enthalpy and melting temperature:

In our calorimetric studies of P [1,2]-TFSI, an intriguing phenomenon emerges upon introducing LITFSI doping (Table 1 and Fig 5.6b). The addition of a small amount of Li salt resulted in a decrease in the material's melting temperature, along with a significant widening of its melting peak, as illustrated in Figure 5.6b.

After doping the melting peak becomes smaller and wider for both systems with BMIMTFSI and LITFSI compared to the pure system P12TFSI. Additionally, the enthalpy of melting of the doped system decreases across its phases, suggesting not complete crystallization and a significant part is in a liquid-like state (Table 1). After doping the enthalpy of melting becomes more than 30% lower than in pure sample in the melting of the Phase 1 and for rest of the phases, they follow the same trends of decreasing enthalpy. LITFSI doping lowers the melting temperature by disrupting the regular arrangement of P12TFSI molecules. It introduces heterogeneity, causing different regions to experience varied melting temperatures[239, 240].

Effect on additional relaxation process and microscopical level:

The conductivity spectra of pure and doped P12TFSIat high frequencies coincide and have similar behavior in Fig 5.7.

The dopants in doped P12TFSIdo introduce some disorder into the crystalline structure, but this disorder is not enough as a result, the additional step in the conductivity spectra of doped P12TFSI is not as prominent as the additional step in the conductivity spectra of pure P12TFSI, but it is still present. The fact that the microscopic behavior of pure and doped P12TFSI aligns remarkably suggests that the dopant forms a phase separated structure, and the rest remains the same as in pure system.

Doping P12TFSIwith LITFSI or BMIM-TFSI reduces the distinctive extra step in conductivity spectra in Figs. 5.8, attributed to dopants disrupting crystalline arrangement.

Table 1: The effect of doping and size of dopant on enthalpy and melting temperature at different phase transitions.

Sample	Phase 1 to Liquid		Phase 2 to 1		Phase 3 to 2		Phase 4 to 3	
	T(°C)	ΔH(J/g)	T(°C)	ΔH(J/g)	T(°C)	ΔH(J/g)	T(°C)	ΔH(J/g)
P12TFSI	88.07	30.06	43.29	1.65	13.09	3.74		
P12TFSI+4.8% LITFSI	78.44	20.08	42.91	1.51	13.81	3.52	14.01	2.63
P12TFSI+4.8% BMIMTFSI	83.46	20.81	44.41	1.44	14.15	2.89		

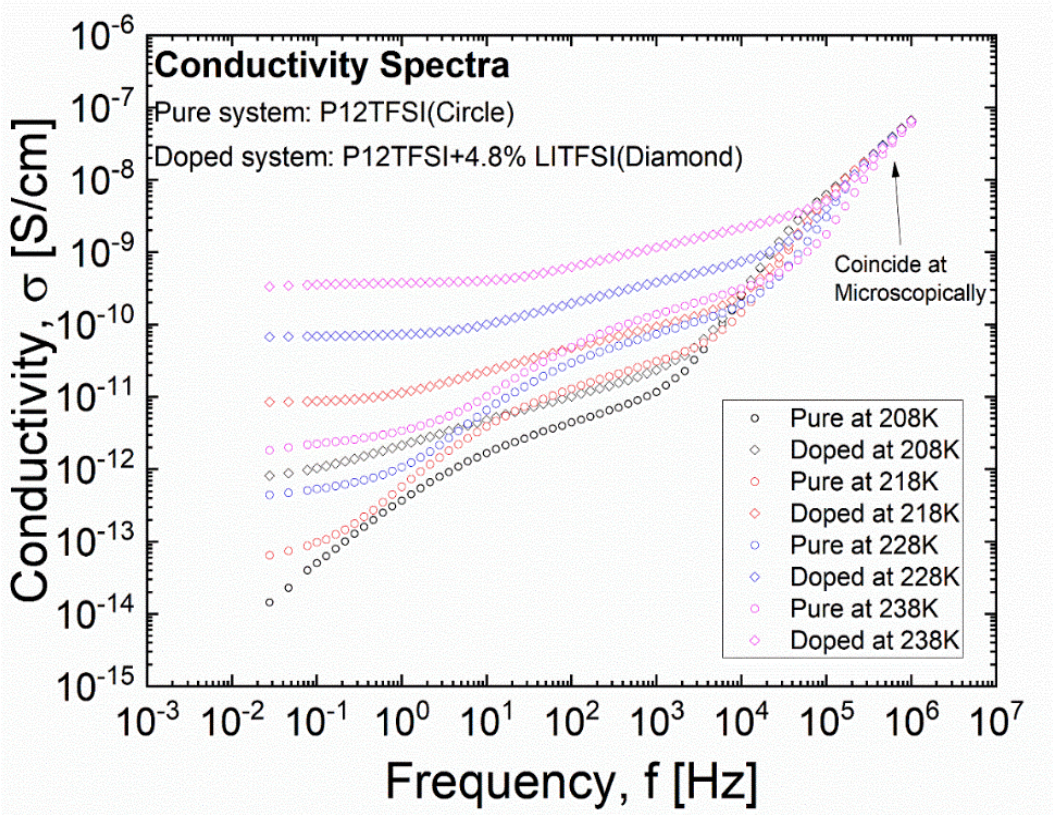

Figure 5.7 Conductivity spectra for both pure and doped P12TFSI at solid phase shows that they coincide with each other at microscopical level.

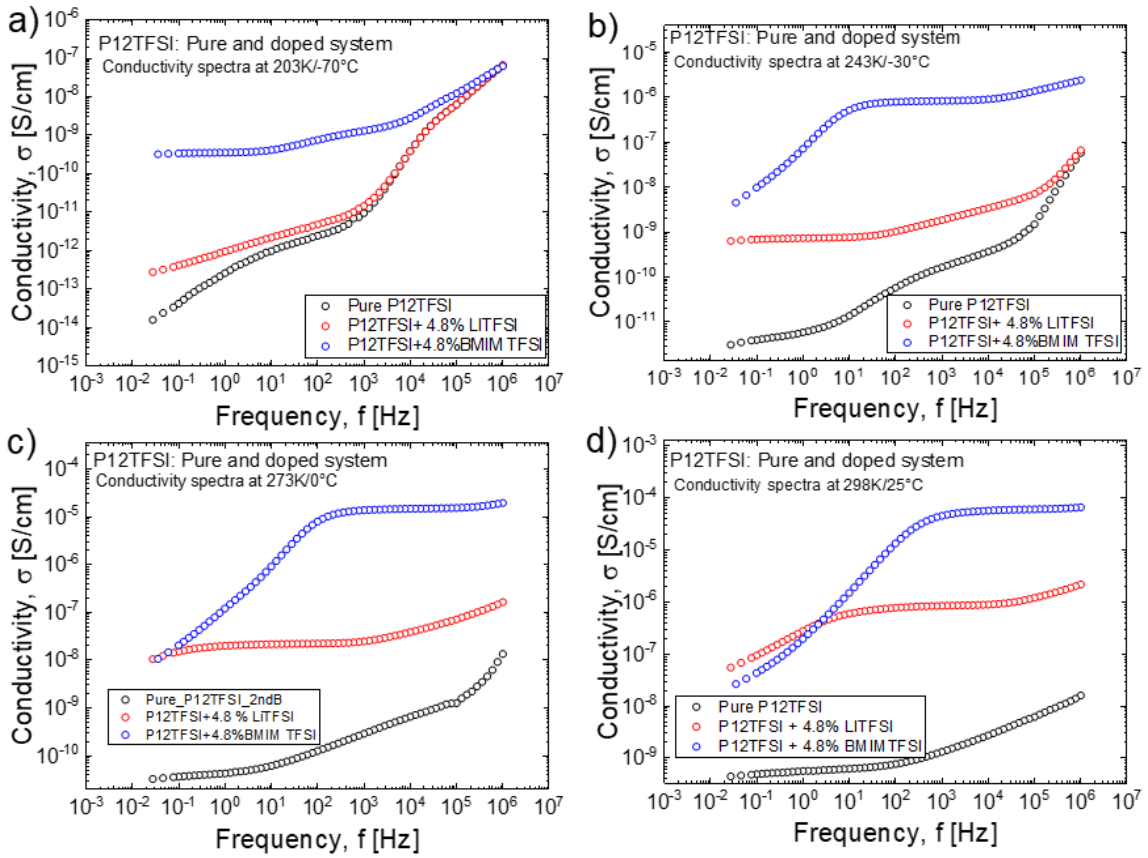

Figure 5.8 Conductivity spectra of pure P12TFSIand with two doping systems at different temperatures representing different phases.

When introducing different-sized dopants like LITFSI and BMIM TFSI at the same concentration, we observe intriguing shifts in behavior. The pure sample shows an additional step, linked to P12TFSI's arrangement and dopants' impact on material molecular dynamics and structure [226] . LITFSI disrupts this, reducing the step, and BMIM TFSI almost removes it, indicating a more profound arrangement disruption. In Phase 2, larger BMIM TFSI-doped samples have higher conductivity than LITFSI-doped ones, revealing dopant size strongly influences material conductivity. BMIM TFSI's larger ions create a better environment for ion movement, enhancing conductivity compared to smaller LITFSI ions.

Qualitative determination of weight fraction of different phases:

In our analysis of doped P12TFSI systems using Eq (5.1), intriguing results emerged. Introducing 4.8% LITFSI resulted in a composition of 53% liquid-like and 47% solid-like phases(crystalline) at 50°C. Conversely, doping with 4.8% BMIM TFSI led to a different trend, reducing the crystalline phase to 31% while increasing the liquid-like phase to 69%. Comparatively, when examining pure P12TFSI, specifically the fresh sample in Fig 5.5a at 50°C revealed that roughly 19% of the material exhibited liquid-like characteristics. Importantly, it's noteworthy that these percentages represent relative proportions rather than precise quantitative values, providing qualitative insights into the material's composition. This highlights the substantial influence of dopants, particularly their size, in augmenting the liquid-like attributes of the material compared to its pure state. Notably, larger dopants result in higher weight fractions of the liquid phase. Considering the relative sizes of the dopants, with BMIM being significantly larger than Li, it becomes evident that dopants disrupt the crystalline structure, leading to a more substantial liquid-like fraction.

To comprehensively explore ion diffusion, mobility, and intricate ionic correlations in both pure and Li-doped P12TSI, ion diffusion in our samples will be measured using PFG NMR analysis. While our existing data has already revealed a more liquid like phase upon doping, contributing to enhanced conductivity, PFG NMR provides deeper insights into ionic correlations. Through PFG NMR combined with conductivity data, we aim to reveal

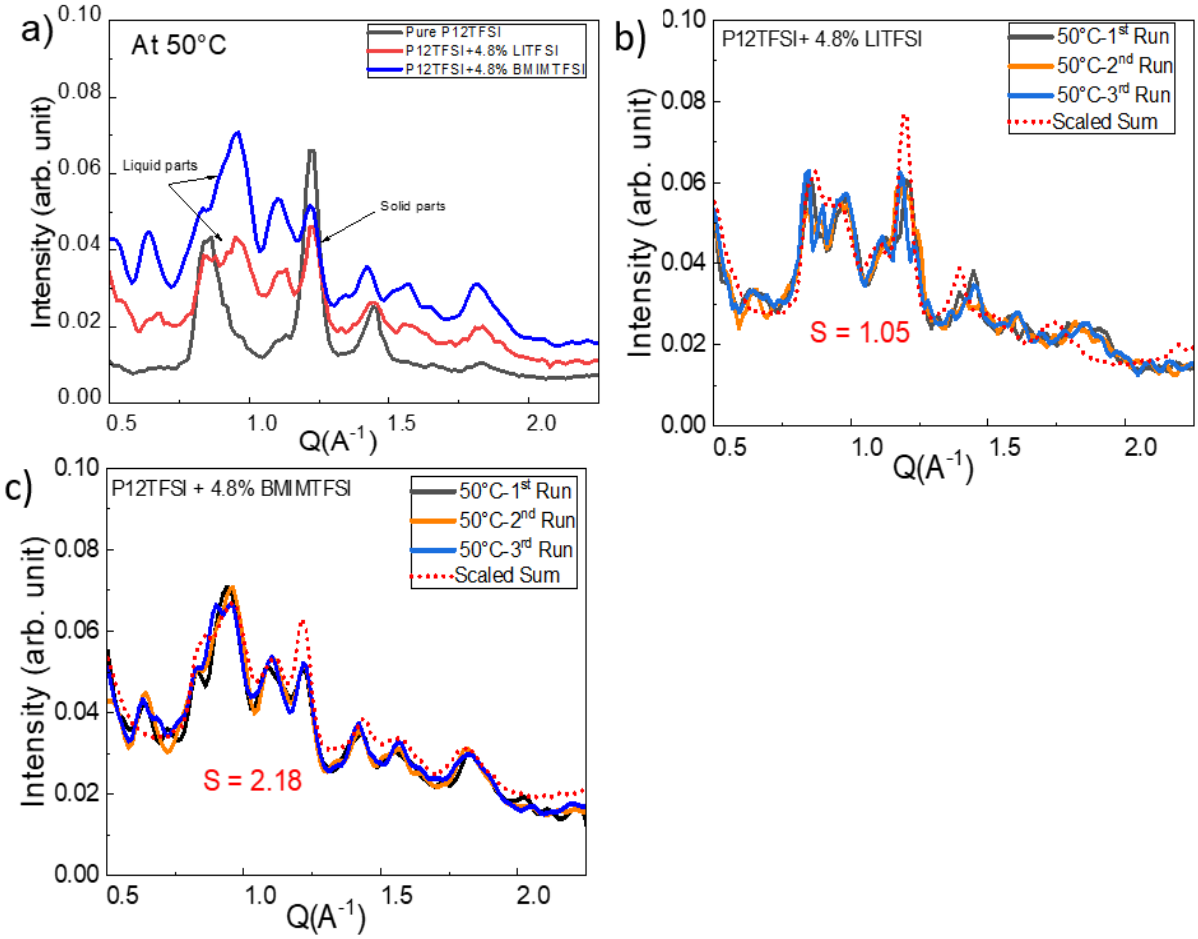

Figure 5.9 WAXS measurements of pure and doped P12TFSI, a). WAXS spectra for pure and two doped P12TFSI sample at 50C to observe proportion of liquid and solid phase. Three different measurements in same condition to observe the repeatability and reproducibility among spectra and fitting those with Eq. (5.1) to determine proportion of solid and liquid phase b). Pure P12TFSI c). P12TFSI + 4.8% LITFSI d). P12TFSI + 4.8% BMIM TFSI.

the role of the ionic correlation in OIPC's conductivity, enhancing our understanding of material dynamics. Especially interesting will be to unravel the effect of doping on ionic correlations.

Role of doping with low melting temperature OIPC, P14TFSI:

We investigated the effect of doping on another organic ionic plastic crystal (OIPC) P14TFSI with 4.8% LITFSI. P14TFSI exhibits a melting temperature of approximately -15 °C and a conductivity of 10^{-2} S/cm at 50 °C in Figs 5.10. Our findings indicate that the addition of LITFSI as a dopant did not lead to a significant increase in conductivity when it was already melted. However, the differential scanning calorimetry (DSC) thermogram revealed that the dopant reduced the melting temperature peak and decreased crystallization. This study provides valuable insights into the doping effect on the conductivity of OIPCs and their potential applications in solid-state electrolytes.

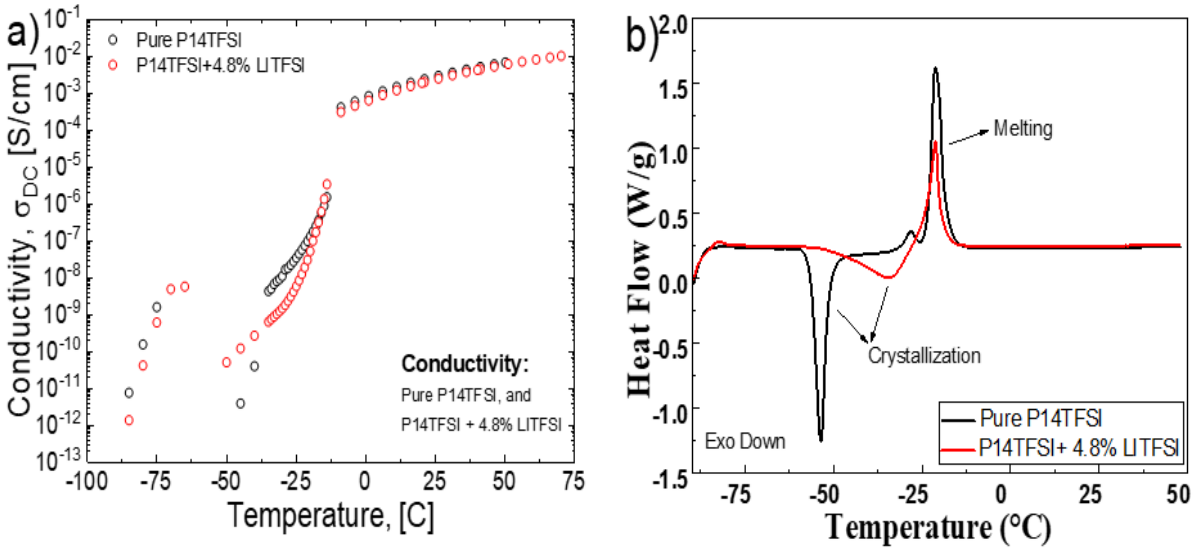

Figure 5.10 a). Conductivity comparison of pure P14TFSI and with 4.8% LITFSI b). DSC thermogram of those systems to observe different phase transition behavior.

5.5. Conclusion

In this study, our primary focus was to develop an understanding of the influence of ion-ion correlations on the conductivity of OIPCs. Additionally, we explored the effects of doping and the size of dopants on conductivity within these materials. Our studies focused on two specific OIPCs, namely P12TFSI and P14TFSI, and we used two dopants, LITFSI and BMIM TFSI, to investigate their impact on conductivity. In the solid phase, there is a significant decline in conductivity, primarily driven by ion-ion correlations, as indicated by the inverse Haven ratio. It's noteworthy that during the transition from the liquid to Phase 1, there is no distinct stepwise behavior in ion diffusion. Instead, we observe a gradual reduction in ion mobility within the solid phase, and this decrease is less pronounced compared to the drop in conductivity. Moreover, doping effectively reduces the drop in conductivity in solid phases, and the extent of this improvement depends on the size of the dopant. Larger dopant, such as BMIM, are more effective than smaller dopant Li in enhancing conductivity, especially at lower temperatures. Furthermore, our research shows that doping creates a substantial liquid-like phase within Phase 1 of the solid state and larger size of dopant give higher weight fraction of liquid. In essence, our study provides valuable insights into ion behavior in OIPCs and underscores the transformative potential of doping in shaping their conductivity characteristics. These findings hold promise for diverse practical applications, ranging from energy storage to solid-state electrolytes.

CHAPTER SIX
CONCLUSIONS

In conclusion, this study has provided valuable insights into the intricate dynamics and transport properties of imidazolium-based ionic liquids (ILs) and organic ionic plastic crystals (OIPCs). Through combination of experimental and simulation studies, we have unraveled the underlying factors that influence ionic correlations and conductivity in these systems.

Chapter 4 delved into the understanding of ion-ion correlations in distinct ILs, shedding light on the role of anion-cation mass ratios in shaping ion-ion interactions and subsequent conductivity. By employing a momentum conservation approach and validating results with molecular dynamics simulations, we established a clear role of ion mass in ionic correlations and conductivity suppression in ILs. The intriguing temperature-independent ion rearrangement length proved invaluable in estimating ion diffusion at low temperatures, previously inaccessible through traditional techniques. The findings underscore the role of ion mass, diffusivity, and their consistency with the idea of momentum conservation. Furthermore, this study offers a good model for analyzing the contributions of distinct ionic correlations to conductivity in ionic liquids. This analytical approach holds particular importance for understanding ionic correlations within concentrated ionic systems.

In Chapter 5, our focus was on elucidating the underlying mechanisms of drop in conductivity of OIPCs, with a particular emphasis on the influential role of ion-ion correlations. Additionally, this chapter provides valuable insights into how doping, and the size of dopants, impacts the conductivity within OIPCs by unraveling a transformative role of dopants in altering material dynamics and enhancing ion transport. While conductivity experiences a significant reduction, ion diffusivity decreases to a lesser extent indicating the increasing role of ionic correlations in conductivity of solid OIPCs. This suggests that ion mobility exists, but its contribution to conductivity remains constrained. The

temperature-dependent inverse Haven ratio confirms the strong influence of ion-ion correlations, particularly in the solid phases of the plastic crystal. Moreover, the primary mechanism behind the improved conductivity in the presence of dopants is the formation of a liquid-like phase. Dopants reduce enthalpy of melting by approximately 30%, resulting in a broader melting peak. In terms of size effect, larger dopant (BMIM) contributes to a higher weight fraction of liquid-like phase within the material compared to small dopant (Li).

Collectively, this comprehensive study not only contributes to the fundamental understanding of ion transport mechanisms but also presents a strategic framework for engineering advanced solid electrolytes. The newfound knowledge about ion-ion correlations, doping effects, and their interplay with material structures opens doors to innovative designs for next-generation electronic devices. As we stand at the precipice of unprecedented technological advancement, the insights derived from this research hold great promise in shaping the trajectory of mobile electronics and related industries.

LIST OF REFERENCES

1. Karuppasamy, K., et al., *Ionic Liquid-Based Electrolytes for Energy Storage Devices: A Brief Review on Their Limits and Applications.* Polymers (Basel), 2020. **12**(4).
2. Rustomji, C.S., et al., *Liquefied gas electrolytes for electrochemical energy storage devices.* 2017. **356**(6345): p. eaal4263.
3. Tian, Y., et al., *Compatibility issues between electrodes and electrolytes in solid-state batteries.* 2017. **10**(5): p. 1150-1166.
4. Jónsson, E., *Ionic liquids as electrolytes for energy storage applications – A modelling perspective.* Energy Storage Materials, 2020. **25**: p. 827-835.
5. Yin, Y., et al., *Fire-extinguishing, recyclable liquefied gas electrolytes for temperature-resilient lithium-metal batteries.* 2022. **7**(6): p. 548-559.
6. Maass, P., M. Meyer, and A. Bunde, *Nonstandard relaxation behavior in ionically conducting materials.* Physical Review B, 1995. **51**(13): p. 8164-8177.
7. Gainaru, C., et al., *Mechanism of Conductivity Relaxation in Liquid and Polymeric Electrolytes: Direct Link between Conductivity and Diffusivity.* The Journal of Physical Chemistry B, 2016. **120**(42): p. 11074-11083.
8. Roling, B., C. Martiny, and S. Brückner, *Ion transport in glass: Influence of glassy structure on spatial extent of nonrandom ion hopping.* Physical Review B, 2001. **63**(21): p. 214203.
9. Popov, I., et al., *Strongly Correlated Ion Dynamics in Plastic Ionic Crystals and Polymerized Ionic Liquids.* The Journal of Physical Chemistry C, 2020. **124**(33): p. 17889-17896.
10. MacFarlane, D.R., et al., *On the concept of ionicity in ionic liquids.* Physical Chemistry Chemical Physics, 2009. **11**(25): p. 4962-4967.
11. Zhang, Z., et al., *Ion Mobilities, Transference Numbers, and Inverse Haven Ratios of Polymeric Ionic Liquids.* ACS Macro Letters, 2020. **9**(1): p. 84-89.
12. Harris, K.R., *Relations between the Fractional Stokes−Einstein and Nernst−Einstein Equations and Velocity Correlation Coefficients in Ionic Liquids and Molten Salts.* The Journal of Physical Chemistry B, 2010. **114**(29): p. 9572-9577.
13. McDaniel, J.G. and C.Y. Son, *Ion Correlation and Collective Dynamics in BMIM/BF4-Based Organic Electrolytes: From Dilute Solutions to the Ionic Liquid Limit.* The Journal of Physical Chemistry B, 2018. **122**(28): p. 7154-7169.
14. Harris, K.R., *On the Use of the Angell–Walden Equation To Determine the "Ionicity" of Molten Salts and Ionic Liquids.* The Journal of Physical Chemistry B, 2019. **123**(32): p. 7014-7023.
15. Zhu, H., et al., *Organic Ionic Plastic Crystals as Solid-State Electrolytes.* Trends in Chemistry, 2019. **1**(1): p. 126-140.

16. Dyre, J.C., et al., *Fundamental questions relating to ion conduction in disordered solids.* Reports on Progress in Physics, 2009. **72**(4): p. 046501.
17. Marcolongo, A. and N. Marzari, *Ionic correlations and failure of Nernst-Einstein relation in solid-state electrolytes.* Physical Review Materials, 2017. **1**(2): p. 025402.
18. Petrovic, S.J.C.S.I.P., *Battery technology crash course.* 2021.
19. Winter, M. and R.J. Brodd, *What Are Batteries, Fuel Cells, and Supercapacitors?* Chemical Reviews, 2004. **104**(10): p. 4245-4270.
20. Xia, L., et al., *Electrolytes for electrochemical energy storage.* 2017. **1**(4): p. 584-618.
21. Leverick, G., *Towards comprehensive design of electrolytes for electrochemical energy storage*. 2022, Massachusetts Institute of Technology.
22. Kaiser, M.R., et al., *Structure–Property Relationships of Organic Electrolytes and Their Effects on Li/S Battery Performance.* 2017. **29**(48): p. 1700449.
23. Nam, K., et al., *Evaluation of the electrochemical stability, interfacial reaction, and molecular behavior of ether-functionalized pyrrolidinium as novel electrolyte for lithium metal battery by quantum and molecular dynamics simulations.* Applied Surface Science, 2022. **600**: p. 154077.
24. Sun, B. and E.J. Berg, *Electrochemical and Chemical Modifications of Electrode Surfaces and Interphases for Li–Ion Batteries*, in *Encyclopedia of Interfacial Chemistry*, K. Wandelt, Editor. 2018, Elsevier: Oxford. p. 680-693.
25. Richards, W.D., et al., *Interface Stability in Solid-State Batteries.* Chemistry of Materials, 2016. **28**(1): p. 266-273.
26. Abbasi, I., *Aqueous Li-Ion Batteries: Achieving Wide Electrochemical Stability and Maintaining Fast Ion Transport.* AZoM, 2021.
27. Li, M., et al., *New concepts in electrolytes.* 2020. **120**(14): p. 6783-6819.
28. Kartha, S. and P.J.P.T. Grimes, *Fuel cells: Energy conversion for the next century.* 1994. **47**(11): p. 54-61.
29. Hwang, J.Y., et al., *Next-generation activated carbon supercapacitors: a simple step in electrode processing leads to remarkable gains in energy density.* 2017. **27**(15): p. 1605745.
30. Domingues, L.S., H.G. de Melo, and V.L.J.P.C.C.P. Martins, *Ionic liquids as potential electrolytes for sodium-ion batteries: an overview.* 2023.
31. Huang, Y., et al., *Electrolytes and Electrolyte/Electrode Interfaces in Sodium-Ion Batteries: From Scientific Research to Practical Application.* 2019. **31**(21): p. 1808393.
32. Li, Q., et al., *Progress in electrolytes for rechargeable Li-based batteries and beyond.* Green Energy & Environment, 2016. **1**(1): p. 18-42.

33. Chen, R., et al., *A Comparative Review of Electrolytes for Organic-Material-Based Energy-Storage Devices Employing Solid Electrodes and Redox Fluids.* ChemSusChem, 2020. **13**(9): p. 2205-2219.
34. Hess, S., M. Wohlfahrt-Mehrens, and M. Wachtler, *Flammability of Li-Ion Battery Electrolytes: Flash Point and Self-Extinguishing Time Measurements.* Journal of The Electrochemical Society, 2015. **162**(2): p. A3084.
35. Erol, S.J.a.p.a., *A fibrous solid electrolyte for lithium-ion batteries.* 2017.
36. Liu, K., et al., *Impurity effects on ionic-liquid-based supercapacitors.* 2017. **115**(4): p. 454-464.
37. Siczek, K.J., *Chapter Eight - Negative Electrode (Anode) Materials*, in *Next-Generation Batteries with Sulfur Cathodes*, K.J. Siczek, Editor. 2019, Academic Press. p. 117-131.
38. He, L., et al., *Understanding and Preventing Dendrite Growth in Lithium Metal Batteries.* ACS Applied Materials & Interfaces, 2021. **13**(29): p. 34320-34331.
39. Aslam, M.K., et al., *How to avoid dendrite formation in metal batteries: Innovative strategies for dendrite suppression.* 2021. **86**: p. 106142.
40. Hogrefe, C., et al., *Direct observation of internal short circuits by lithium dendrites in cross-sectional lithium-ion in situ full cells.* 2023. **556**: p. 232391.
41. Zhang, H., et al., *Gel Electrolytes: Chemistry and Applications.* 2023: p. e202300360-e202300360.
42. Castillo, J., et al., *Safe, Flexible, and High-Performing Gel-Polymer Electrolyte for Rechargeable Lithium Metal Batteries.* Chemistry of Materials, 2021. **33**(22): p. 8812-8821.
43. Long, L. and S.J.M.C.A. Wang, *XiaoMandMengY 2016 Polymer electrolytes for lithiumpolymer batteries J.* **4**: p. 10038-9.
44. Yang, X., et al., *Recent advances and perspectives on thin electrolytes for high-energy-density solid-state lithium batteries.* 2021. **14**(2): p. 643-671.
45. Zhao, Q., et al., *Designing solid-state electrolytes for safe, energy-dense batteries.* 2020. **5**(3): p. 229-252.
46. Tsao, C.-H. and P.-L.J.J.o.M.S. Kuo, *Poly (dimethylsiloxane) hybrid gel polymer electrolytes of a porous structure for lithium ion battery.* 2015. **489**: p. 36-42.
47. Yang, Q., et al., *The recent research progress and prospect of gel polymer electrolytes in lithium-sulfur batteries.* Chemical Engineering Journal, 2021. **413**: p. 127427.
48. Chen, A., et al., *Manufacturing strategies for solid electrolyte in batteries.* 2020. **8**: p. 571440.
49. Jin, L., et al., *An organic ionic plastic crystal electrolyte for rate capability and stability of ambient temperature lithium batteries.* 2014. **7**(10): p. 3352-3361.

50. Pringle, J.M.J.P.C.C.P., *Recent progress in the development and use of organic ionic plastic crystal electrolytes.* 2013. **15**(5): p. 1339-1351.
51. Zhu, H., et al., *Organic ionic plastic crystals as solid-state electrolytes.* 2019. **1**(1): p. 126-140.
52. Goodenough, J.B.J.S.S.I., *Ceramic solid electrolytes.* 1997. **94**(1-4): p. 17-25.
53. Fergus, J.W.J.J.o.P.S., *Ceramic and polymeric solid electrolytes for lithium-ion batteries.* 2010. **195**(15): p. 4554-4569.
54. Li, J., et al., *Solid electrolyte: the key for high-voltage lithium batteries.* 2015. **5**(4): p. 1401408.
55. Yue, L., et al., *All solid-state polymer electrolytes for high-performance lithium ion batteries.* 2016. **5**: p. 139-164.
56. Ngai, K.S., et al., *A review of polymer electrolytes: fundamental, approaches and applications.* 2016. **22**: p. 1259-1279.
57. Yu, X. and A. Manthiram, *A review of composite polymer-ceramic electrolytes for lithium batteries.* Energy Storage Materials, 2021. **34**: p. 282-300.
58. Kalnaus, S., et al., *Design of composite polymer electrolytes for Li ion batteries based on mechanical stability criteria.* Journal of Power Sources, 2012. **201**: p. 280-287.
59. Yang, K., et al., *Organic Ionic Plastic Crystal-polymer Solid Electrolytes with High Ionic Conductivity and Mechanical Ability for Solid-state Lithium Ion Batteries.* 2018. **3**(44): p. 12595-12599.
60. Wang, Y. and W.H.J.C. Zhong, *Development of electrolytes towards achieving safe and high-performance energy-storage devices: a review.* 2015. **2**(1): p. 22-36.
61. Li, G.J.A.E.M., *Regulating mass transport behavior for high-performance lithium metal batteries and fast-charging lithium-ion batteries.* 2021. **11**(7): p. 2002891.
62. Weiss, M., et al., *Fast charging of lithium-ion batteries: a review of materials aspects.* 2021. **11**(33): p. 2101126.
63. Galiński, M., A. Lewandowski, and I.J.E.a. Stępniak, *Ionic liquids as electrolytes.* 2006. **51**(26): p. 5567-5580.
64. Armand, M., et al., *Ionic-liquid materials for the electrochemical challenges of the future.* 2009. **8**(8): p. 621-629.
65. Kim, J.-K., et al., *Improving the stability of an organic battery with an ionic liquid-based polymer electrolyte.* 2012. **2**(26): p. 9795-9797.
66. Tokuda, H., et al., *Physicochemical properties and structures of room temperature ionic liquids. 1. Variation of anionic species.* 2004. **108**(42): p. 16593-16600.
67. Chen, Y., et al., *A review of lithium-ion battery safety concerns: The issues, strategies, and testing standards.* Journal of Energy Chemistry, 2021. **59**: p. 83-99.

68. Liu, B., et al., *Safety issues caused by internal short circuits in lithium-ion batteries.* 2018. **6**(43): p. 21475-21484.
69. Wen, J., Y. Yu, and C.J.M.e. Chen, *A review on lithium-ion batteries safety issues: existing problems and possible solutions.* 2012. **2**(3): p. 197-212.
70. Foroozan, T., S. Sharifi-Asl, and R.J.J.o.P.S. Shahbazian-Yassar, *Mechanistic understanding of Li dendrites growth by in-situ/operando imaging techniques.* 2020. **461**: p. 228135.
71. Aslam, M.K., et al., *How to avoid dendrite formation in metal batteries: Innovative strategies for dendrite suppression.* Nano Energy, 2021. **86**: p. 106142.
72. Shah, F.U., et al., *Transport and Association of Ions in Lithium Battery Electrolytes Based on Glycol Ether Mixed with Halogen-Free Orthoborate Ionic Liquid.* Scientific Reports, 2017. **7**(1): p. 16340.
73. Besner, S., et al., *Effect of anion polarization on conductivity behavior of poly(ethylene oxide) complexed with alkali salts.* Macromolecules, 1992. **25**(24): p. 6480-6488.
74. Klein, R.J., et al., *Modeling electrode polarization in dielectric spectroscopy: Ion mobility and mobile ion concentration of single-ion polymer electrolytes.* The Journal of Chemical Physics, 2006. **124**(14).
75. Tong, J., et al., *The effect of concentration of lithium salt on the structural and transport properties of ionic liquid-based electrolytes.* 2020. **7**: p. 945.
76. Wang, X., Y. Chi, and T. Mu, *A review on the transport properties of ionic liquids.* Journal of Molecular Liquids, 2014. **193**: p. 262-266.
77. Tokuda, H., et al., *Physicochemical Properties and Structures of Room Temperature Ionic Liquids. 1. Variation of Anionic Species.* The Journal of Physical Chemistry B, 2004. **108**(42): p. 16593-16600.
78. Lückhoff, C., *When can a car battery leak?*, in *AutoTrader*. 2018, AutoTrader.
79. TECH, H., *Top Reasons Why Samaprtphone Batteries Explode, and How You Can Prevent It from Happening.* HT TECH, 2022.
80. staff, A.N.E., *Tesla Model S probed by U.S. after three fires in five weeks*, in *Automotive News Europe*. 2013, Crain Communication.
81. Pigłowska, M., et al., *Challenges for Safe Electrolytes Applied in Lithium-Ion Cells-A Review.* Materials (Basel), 2021. **14**(22).
82. Mrozik, W., et al., *Environmental impacts, pollution sources and pathways of spent lithium-ion batteries.* 2021. **14**(12): p. 6099-6121.
83. Hess, S., M. Wohlfahrt-Mehrens, and M.J.J.o.T.E.S. Wachtler, *Flammability of Li-ion battery electrolytes: flash point and self-extinguishing time measurements.* 2015. **162**(2): p. A3084.
84. Roth, E.P. and C.J.J.T.E.S.I. Orendorff, *How electrolytes influence battery safety.* 2012. **21**(2): p. 45.
85. Tran, M.-K., et al., *A review of lithium-ion battery thermal runaway modeling and diagnosis approaches.* 2022. **10**(6): p. 1192.

86. Lyu, P., et al., *Recent advances of thermal safety of lithium ion battery for energy storage.* 2020. **31**: p. 195-220.
87. Block, A. and C.H.J.J.o.c.p. Song, *Exploring the characteristics of technological knowledge interaction dynamics in the field of solid-state batteries: A patent-based approach.* 2022. **353**: p. 131689.
88. Bates, A.M., et al., *Are solid-state batteries safer than lithium-ion batteries?* Joule, 2022. **6**(4): p. 742-755.
89. Chen, R., et al., *Approaching practically accessible solid-state batteries: stability issues related to solid electrolytes and interfaces.* 2019. **120**(14): p. 6820-6877.
90. Aizat Razali, A., et al., *State-of-the-Art of Solid-State Electrolytes on the Road Map of Solid-State Lithium Metal Batteries for E-Mobility.* 2023.
91. Albertus, P., et al., *Challenges for and Pathways toward Li-Metal-Based All-Solid-State Batteries.* ACS Energy Letters, 2021. **6**(4): p. 1399-1404.
92. Yu, X., et al., *Battery safety: From lithium-ion to solid-state batteries.* 2023. **21**: p. 9-14.
93. Tahir, Y., et al., *A state‐of‐the‐art review on topologies and control techniques of solid‐state transformers for electric vehicle extreme fast charging.* 2021. **14**(9): p. 1560-1576.
94. Li, C., et al., *An advance review of solid-state battery: Challenges, progress and prospects.* 2021. **29**: p. e00297.
95. Kelly, T., *Solid-State Lithium Ion Batteries - The Challenges*, in *Knowledge & Education in Intertek Blog*. 2019, Intertek Group plc.
96. Zhao, C., et al., *Solid-State Sodium Batteries.* 2018. **8**(17): p. 1703012.
97. Chen, R., et al., *The pursuit of solid-state electrolytes for lithium batteries: from comprehensive insight to emerging horizons.* 2016. **3**(6): p. 487-516.
98. Alamgir, M. and K.J.J.o.t.E.S. Abraham, *Li ion conductive electrolytes based on poly (vinyl chloride).* 1993. **140**(6): p. L96.
99. Ma, Q., et al., *A new Na [(FSO 2)(n-C 4 F 9 SO 2) N]-based polymer electrolyte for solid-state sodium batteries.* 2017. **5**(17): p. 7738-7743.
100. Qi, X., et al., *Sodium bis (fluorosulfonyl) imide/poly (ethylene oxide) polymer electrolytes for sodium‐ion batteries.* 2016. **3**(11): p. 1741-1745.
101. Moreno, J.S., et al., *Composite PEOn: NaTFSI polymer electrolyte: Preparation, thermal and electrochemical characterization.* 2014. **248**: p. 695-702.
102. Croce, F., et al., *Nanocomposite polymer electrolytes for lithium batteries.* 1998. **394**(6692): p. 456-458.
103. Song, S., et al., *A hybrid polymer/oxide/ionic-liquid solid electrolyte for Na-metal batteries.* 2017. **5**(14): p. 6424-6431.
104. Armand, M.J.S.S.I., *Polymer solid electrolytes-an overview.* 1983. **9**: p. 745-754.
105. Zhang, Z., et al., *A self‐forming composite electrolyte for solid‐state sodium battery with ultralong cycle life.* 2017. **7**(4): p. 1601196.

106. Zhao, Y., et al., *A chemistry and material perspective on lithium redox flow batteries towards high-density electrical energy storage.* Chemical Society Reviews, 2015. **44**(22): p. 7968-7996.
107. Lee, S.S., et al., *Ion correlations drive charge overscreening and heterogeneous nucleation at solid-aqueous electrolyte interfaces.* Proc Natl Acad Sci U S A, 2021. **118**(32).
108. Nürnberg, P., et al., *Superionicity in Ionic-Liquid-Based Electrolytes Induced by Positive Ion–Ion Correlations.* Journal of the American Chemical Society, 2022. **144**(10): p. 4657-4666.
109. Gregory, K.P., et al., *Understanding specific ion effects and the Hofmeister series.* 2022. **24**(21): p. 12682-12718.
110. Chauhan, R., et al., *Theory-Enabled High-Throughput Screening of Ion Dissociation Explains Conductivity Enhancements in Diluted Ionic Liquid Mixtures.* 2023.
111. Li, Z., et al., *Ionic Conduction in Polymer-Based Solid Electrolytes.* Adv Sci (Weinh), 2023. **10**(10): p. e2201718.
112. Huang, Y., B. Shao, and F. Han, *Solid-State Batteries: An Introduction*, in *Solid State Batteries Volume 1: Emerging Materials and Applications*. 2022, ACS Publications. p. 1-20.
113. Zhang, Y. and E.J. Maginn, *Direct Correlation between Ionic Liquid Transport Properties and Ion Pair Lifetimes: A Molecular Dynamics Study.* The Journal of Physical Chemistry Letters, 2015. **6**(4): p. 700-705.
114. Turton, D.A., et al., *Dynamics of Imidazolium Ionic Liquids from a Combined Dielectric Relaxation and Optical Kerr Effect Study: Evidence for Mesoscopic Aggregation.* Journal of the American Chemical Society, 2009. **131**(31): p. 11140-11146.
115. Tokuda, H., et al., *How Ionic Are Room-Temperature Ionic Liquids? An Indicator of the Physicochemical Properties.* The Journal of Physical Chemistry B, 2006. **110**(39): p. 19593-19600.
116. Tokuda, H., et al., *Physicochemical Properties and Structures of Room-Temperature Ionic Liquids. 3. Variation of Cationic Structures.* The Journal of Physical Chemistry B, 2006. **110**(6): p. 2833-2839.
117. Tokuda, H., et al., *Physicochemical Properties and Structures of Room Temperature Ionic Liquids. 2. Variation of Alkyl Chain Length in Imidazolium Cation.* The Journal of Physical Chemistry B, 2005. **109**(13): p. 6103-6110.
118. Thompson, M.W., et al., *Scalable Screening of Soft Matter: A Case Study of Mixtures of Ionic Liquids and Organic Solvents.* The Journal of Physical Chemistry B, 2019. **123**(6): p. 1340-1347.
119. Sangoro, J.R., et al., *Charge transport and mass transport in imidazolium-based ionic liquids.* Physical Review E, 2008. **77**(5): p. 051202.
120. Philippi, F., et al., *Transport properties and ionicity of phosphonium ionic liquids.* Physical Chemistry Chemical Physics, 2017. **19**(34): p. 23015-23023.

121. Pabst, F., et al., *Molecular dynamics of supercooled ionic liquids studied by light scattering and dielectric spectroscopy.* Chemical Physics, 2017. **494**: p. 103-110.
122. Noda, A., K. Hayamizu, and M. Watanabe, *Pulsed-Gradient Spin−Echo 1H and 19F NMR Ionic Diffusion Coefficient, Viscosity, and Ionic Conductivity of Non-Chloroaluminate Room-Temperature Ionic Liquids.* The Journal of Physical Chemistry B, 2001. **105**(20): p. 4603-4610.
123. Molinari, N., et al., *Transport anomalies emerging from strong correlation in ionic liquid electrolytes.* Journal of Power Sources, 2019. **428**: p. 27-36.
124. Kashyap, H.K., et al., *How Is Charge Transport Different in Ionic Liquids and Electrolyte Solutions?* The Journal of Physical Chemistry B, 2011. **115**(45): p. 13212-13221.
125. Horwitz, G., et al., *Mobility-viscosity decoupling and cation transport in water-in-salt lithium electrolytes.* Electrochimica Acta, 2020. **359**: p. 136915.
126. Harris, K.R. and M. Kanakubo, *Revised and Extended Values for Self-Diffusion Coefficients of 1-Alkyl-3-methylimidazolium Tetrafluoroborates and Hexafluorophosphates: Relations between the Transport Properties.* The Journal of Physical Chemistry B, 2016. **120**(50): p. 12937-12949.
127. Harris, K.R. and M. Kanakubo, *Self-Diffusion Coefficients and Related Transport Properties for a Number of Fragile Ionic Liquids.* Journal of Chemical & Engineering Data, 2016. **61**(7): p. 2399-2411.
128. Harris, K.R. and M. Kanakubo, *High pressure studies of the transport properties of ionic liquids.* Faraday Discussions, 2012. **154**(0): p. 425-438.
129. Bychkov, E., *Superionic and ion-conducting chalcogenide glasses: Transport regimes and structural features.* Solid State Ionics, 2009. **180**(6): p. 510-516.
130. Isard, J.O., *The Haven ratio in glasses.* Journal of Non-Crystalline Solids, 1999. **246**(1): p. 16-26.
131. Murch, G.E., *The haven ratio in fast ionic conductors.* Solid State Ionics, 1982. **7**(3): p. 177-198.
132. Yokota, I., *On the Deviation from the Einstein Relation Observed for Diffusion of Ag+ Ions in α-Ag2S and Others.* Journal of the Physical Society of Japan, 1966. **21**(3): p. 420-423.
133. Jain, H., N.L. Peterson, and H.L. Downing, *Tracer diffusion and electrical conductivity in sodium-cesium silicate glasses.* Journal of Non-Crystalline Solids, 1983. **55**(2): p. 283-300.
134. Adeli, P., et al., *Boosting Solid-State Diffusivity and Conductivity in Lithium Superionic Argyrodites by Halide Substitution.* Angewandte Chemie International Edition, 2019. **58**(26): p. 8681-8686.
135. Bron, P., et al., *Li10SnP2S12: An Affordable Lithium Superionic Conductor.* Journal of the American Chemical Society, 2013. **135**(42): p. 15694-15697.

136. Hussain, F., P. Li, and Z. Li, *Theoretical Insights into Li-Ion Transport in LiTa2PO8.* The Journal of Physical Chemistry C, 2019. **123**(32): p. 19282-19287.
137. Sinitsyn, V.V., et al., *Transport properties of LaF3 fast ionic conductor studied by field gradient NMR and impedance spectroscopy.* Journal of Physics and Chemistry of Solids, 2003. **64**(7): p. 1201-1205.
138. Vargas-Barbosa, N.M. and B. Roling, *Cover Feature: Dynamic Ion Correlations in Solid and Liquid Electrolytes: How Do They Affect Charge and Mass Transport? (ChemElectroChem 2/2020).* ChemElectroChem, 2020. **7**(2): p. 363-363.
139. Schoenert, H.J., *Evaluation of velocity correlation coefficients from experimental transport data in electrolytic systems.* The Journal of Physical Chemistry, 1984. **88**(15): p. 3359-3363.
140. Watanabe, M., et al., *Application of Ionic Liquids to Energy Storage and Conversion Materials and Devices.* Chemical Reviews, 2017. **117**(10): p. 7190-7239.
141. Harris, K.R., *Can the Transport Properties of Molten Salts and Ionic Liquids Be Used To Determine Ion Association?* The Journal of Physical Chemistry B, 2016. **120**(47): p. 12135-12147.
142. Stolwijk, N.A. and S. Obeidi, *Combined analysis of self-diffusion, conductivity, and viscosity data on room temperature ionic liquids.* Electrochimica Acta, 2009. **54**(5): p. 1645-1653.
143. Every, H.A., et al., *Transport properties in a family of dialkylimidazolium ionic liquids.* Physical Chemistry Chemical Physics, 2004. **6**(8): p. 1758-1765.
144. Seki, S., et al., *Relationships between center atom species (N, P) and ionic conductivity, viscosity, density, self-diffusion coefficient of quaternary cation room-temperature ionic liquids.* Physical Chemistry Chemical Physics, 2009. **11**(18): p. 3509-3514.
145. Jin, L., et al., *Structure and transport properties of a plastic crystal ion conductor: diethyl (methyl)(isobutyl) phosphonium hexafluorophosphate.* 2012. **134**(23): p. 9688-9697.
146. Popov, I. and A.J.B.o.t.A.P.S. Sokolov, *Collective ion dynamics in Organic Ionic Plastic Crystals.* 2023.
147. MacFarlane, D.R. and M. Forsyth, *Plastic Crystal Electrolyte Materials: New Perspectives on Solid State Ionics.* Advanced Materials, 2001. **13**(12-13): p. 957-966.
148. MacFarlane, D.R., J. Huang, and M. Forsyth, *Lithium-doped plastic crystal electrolytes exhibiting fast ion conduction for secondary batteries.* Nature, 1999. **402**(6763): p. 792-794.
149. Forsyth, M., J. Huang, and D.R. MacFarlane, *Lithium doped -methyl--ethylpyrrolidinium bis(trifluoromethanesulfonyl)amide fast-ion conducting plastic crystals.* Journal of Materials Chemistry, 2000. **10**(10): p. 2259-2265.

150. Henderson, W.A., et al., *An Alternative Ionic Conductivity Mechanism for Plastic Crystalline Salt–Lithium Salt Electrolyte Mixtures.* Advanced Energy Materials, 2012. **2**(11): p. 1343-1350.
151. Zhu, H. and M. Forsyth, *Ion Vacancies and Transport in 1-Methylimidazolium Triflate Organic Ionic Plastic Crystal.* The Journal of Physical Chemistry Letters, 2020. **11**(2): p. 510-515.
152. Huang, J., et al., *Conduction in ionic organic plastic crystals: The role of defects.* Solid State Ionics, 2006. **177**(26): p. 2569-2573.
153. Shen, K.-H. and L.M. Hall, *Ion Conductivity and Correlations in Model Salt-Doped Polymers: Effects of Interaction Strength and Concentration.* Macromolecules, 2020. **53**(10): p. 3655-3668.
154. Wheatle, B.K., et al., *Influence of Dielectric Constant on Ionic Transport in Polyether-Based Electrolytes.* ACS Macro Letters, 2017. **6**(12): p. 1362-1367.
155. Wheatle, B.K., N.A. Lynd, and V. Ganesan, *Effect of Polymer Polarity on Ion Transport: A Competition between Ion Aggregation and Polymer Segmental Dynamics.* ACS Macro Letters, 2018. **7**(10): p. 1149-1154.
156. Nguyen, H.-D., et al., *Nanostructured multi-block copolymer single-ion conductors for safer high-performance lithium batteries.* Energy & Environmental Science, 2018. **11**(11): p. 3298-3309.
157. Stacy, E.W., et al., *Fundamental Limitations of Ionic Conductivity in Polymerized Ionic Liquids.* Macromolecules, 2018. **51**(21): p. 8637-8645.
158. Kubisiak, P., P. Wróbel, and A. Eilmes, *Molecular Dynamics Investigation of Correlations in Ion Transport in MeTFSI/EMIM–TFSI (Me = Li, Na) Electrolytes.* The Journal of Physical Chemistry B, 2020. **124**(2): p. 413-421.
159. Sau, K. and P.P. Kumar, *Role of Ion–Ion Correlations on Fast Ion Transport: Molecular Dynamics Simulation of Na2Ni2TeO6.* The Journal of Physical Chemistry C, 2015. **119**(32): p. 18030-18037.
160. Spohr, H.V. and G.N. Patey, *The influence of water on the structural and transport properties of model ionic liquids.* J Chem Phys, 2010. **132**(23): p. 234510.
161. Kubisiak, P., P. Wróbel, and A. Eilmes, *Molecular Dynamics Investigation of Correlations in Ion Transport in MeTFSI/EMIM-TFSI (Me = Li, Na) Electrolytes.* J Phys Chem B, 2020. **124**(2): p. 413-421.
162. Dong, D., et al., *How efficient is Li+ ion transport in solvate ionic liquids under anion-blocking conditions in a battery?* Physical Chemistry Chemical Physics, 2018. **20**(46): p. 29174-29183.
163. Angell, C.A., *Diffusion—Conductance Relations and Free Volume in Molten Salts.* The Journal of Physical Chemistry, 1965. **69**(2): p. 399-403.
164. Popov, I., et al., *Controlling the Ion Transport Number in Solvent-in-Salt Solutions.* Journal of Physical Chemistry B, 2022. **126**(24): p. 4572-4583.
165. Kianfar, E. and S.J.F.C.E. Mafi, *Ionic liquids: properties, application, and synthesis.* 2021: p. 22-31.

166. Shah, F.U., R. An, and N.J.F.i.C. Muhammad, *Properties and applications of ionic liquids in energy and environmental science*. 2020, Frontiers Media SA. p. 627213.
167. Zheng, Y., et al., *Ionic Liquid Electrolytes for Next-generation Electrochemical Energy Devices.* EnergyChem, 2022. **4**(3): p. 100075.
168. Flieger, J. and M.J.I.J.o.M.S. Flieger, *Ionic liquids toxicity—benefits and threats.* 2020. **21**(17): p. 6267.
169. Stenger-Smith, J.D., J.A.J.A.E.P. Irvin, Ionic Liquids,, and MOFs, *Ionic liquids for energy storage applications.* 2009: p. 102.
170. Xu, C. and Z. Cheng, *Thermal Stability of Ionic Liquids: Current Status and Prospects for Future Development.* 2021. **9**(2): p. 337.
171. Kazemiabnavi, S., et al., *Electrochemical Stability Window of Imidazolium-Based Ionic Liquids as Electrolytes for Lithium Batteries.* The Journal of Physical Chemistry B, 2016. **120**(25): p. 5691-5702.
172. De Vos, N., C. Maton, and C.V. Stevens, *Electrochemical Stability of Ionic Liquids: General Influences and Degradation Mechanisms.* 2014. **1**(8): p. 1258-1270.
173. Kim, E., et al., *Ionic liquid electrolytes for electrochemical energy storage devices.* 2021. **14**(14): p. 4000.
174. Salanne, M., *Ionic Liquids for Supercapacitor Applications.* Topics in Current Chemistry, 2017. **375**(3): p. 63.
175. Eftekhari, A., *Supercapacitors utilising ionic liquids.* Energy Storage Materials, 2017. **9**: p. 47-69.
176. Kurundawade, S.R., et al., *Chapter 13 - Applications of ionic liquids in fuel cells and supercapacitors*, in *Advanced Applications of Ionic Liquids*, J.A. Siddique, et al., Editors. 2023, Elsevier. p. 353-364.
177. Yasuda, T. and M.J.M.b. Watanabe, *Protic ionic liquids: Fuel cell applications.* 2013. **38**(7): p. 560-566.
178. Alashkar, A., et al., *A critical review on the use of ionic liquids in proton exchange membrane fuel cells.* 2022. **12**(2): p. 178.
179. Sourjah, A., et al., *New organic ionic plastic crystals utilizing the morpholinium cation.* 2023.
180. Pringle, J.M., et al. *Development of Organic Ionic Plastic Crystals As Solid-State Electrolytes*. in *Electrochemical Society Meeting Abstracts ecee2019*. 2019. The Electrochemical Society, Inc.
181. Janikowski, J., et al., *Organic ionic plastic crystals and low viscosity ionic liquids based on the dicyano (nitroso) methanide anion.* 2012. **77**(11): p. 1039-1045.
182. Li, Q., et al., *Organic ionic plastic crystal-based electrolytes for solid-state dye-sensitized solar cells.* 2012. **22**(14): p. 6674-6679.
183. Iftikhar, H., et al., *Progress on Electrolytes Development in Dye-Sensitized Solar Cells.* 2019. **12**(12): p. 1998.

184. Pringle, J., et al. *New Solid-State Electrolytes Based on Organic Ionic Plastic Crystals*. in *Electrochemical Society Meeting Abstracts prime2020*. 2020. The Electrochemical Society, Inc.
185. Yang, K., et al., *Organic Ionic Plastic Crystal-polymer Solid Electrolytes with High Ionic Conductivity and Mechanical Ability for Solid-state Lithium Ion Batteries.* 2018. **3**(44): p. 12595-12599.
186. Sun, J., B. Luo, and H. Li, *A Review on the Conventional Capacitors, Supercapacitors, and Emerging Hybrid Ion Capacitors: Past, Present, and Future.* 2022. **3**(6): p. 2100191.
187. Deshmukh, K., et al., *Dielectric Spectroscopy*. Spectroscopic Methods for Nanomaterials Characterization, ed. S. Thomas, et al. Vol. 2. 2017, Amsterdam: Elsevier Science Bv. 237-299.
188. Popov, I., S. Cheng, and A.P. Sokolov, *Broadband Dielectric Spectroscopy and Its Application in Polymeric Materials*, in *Macromolecular Engineering*. p. 1-39.
189. Schönhals, A. and F. Kremer, *Broadband Dielectric Measurement Techniques (10-6 Hz to 1012 Hz)*, in *Broadband Dielectric Spectroscopy*, F. Kremer and A. Schönhals, Editors. 2003, Springer Berlin Heidelberg: Berlin, Heidelberg. p. 35-57.
190. Friedrich Kremer, A.S., *Broadband Dielectric Spectroscopy*. 1 ed. Springers Berlin, Heidelberg. 2003: Springers Berlin, Heidelberg.
191. Woodward, W.H.H., *Broadband Dielectric Spectroscopy—A Practical Guide*, in *Broadband Dielectric Spectroscopy: A Modern Analytical Technique*. 2021, American Chemical Society. p. 3-59.
192. Feldman, Y., A. Puzenko, and Y. Ryabov, *DIELECTRIC RELAXATION PHENOMENA IN COMPLEX MATERIALS*, in *Fractals, Diffusion, and Relaxation in Disordered Complex Systems, Part A*, W.T. Coffey and Y.P. Kalmykov, Editors. 2006, John Wiley & Sons Inc: Hoboken. p. 1-+.
193. Popov, I., et al., *Controlling the Ion Transport Number in Solvent-in-Salt Solutions.* J Phys Chem B, 2022. **126**(24): p. 4572-4583.
194. Dyre, J.C., *The random free-energy barrier model for ac conduction in disordered solids.* Journal of Applied Physics, 1988. **64**(5): p. 2456-2468.
195. Schrøder, T.B. and J.C. Dyre, *ac Hopping Conduction at Extreme Disorder Takes Place on the Percolating Cluster.* Physical Review Letters, 2008. **101**(2): p. 025901.
196. Singh, M.K. and A. Singh, *Chapter 9 - Thermal characterization of materials using differential scanning calorimeter*, in *Characterization of Polymers and Fibres*, M.K. Singh and A. Singh, Editors. 2022, Woodhead Publishing. p. 201-222.
197. Gill, P., T.T. Moghadam, and B. Ranjbar, *Differential scanning calorimetry techniques: applications in biology and nanoscience.* J Biomol Tech, 2010. **21**(4): p. 167-93.
198. Willard, H.H., et al., *Instrumental methods of analysis, 7th edition*. 1988, United States: Florence, KY (US); Wadsworth Publishing Company.

Medium: X; Size: Pages: (896 p) 2011-03-24 Wadsworth Publishing Co., 7625 Empire Drive, Florence, KY 41042.
199. Lipol, L.S. *Determination of the thermal behavior of PET bottle by using the Differential Scanning Calorimetry (DSC)*. 2018.
200. Goodenough, J.B. and K.-S. Park, *The Li-Ion Rechargeable Battery: A Perspective.* Journal of the American Chemical Society, 2013. **135**(4): p. 1167-1176.
201. Suo, L., et al., *A new class of solvent-in-salt electrolyte for high-energy rechargeable metallic lithium batteries.* Nature communications, 2013. **4**(1): p. 1-9.
202. Zeng, X. and J. Li, *Innovative application of ionic liquid to separate Al and cathode materials from spent high-power lithium-ion batteries.* J Hazard Mater, 2014. **271**: p. 50-6.
203. Shah, F.U., R. An, and N. Muhammad, *Editorial: Properties and Applications of Ionic Liquids in Energy and Environmental Science.* Front Chem, 2020. **8**: p. 627213.
204. Yoo, K.S., *Synthesis of TiO2 Materials Using Ionic Liquids and Its Applications for Sustainable Energy and Environment.* J Nanosci Nanotechnol, 2016. **16**(5): p. 4302-9.
205. Sippel, P., et al., *Importance of liquid fragility for energy applications of ionic liquids.* Sci Rep, 2015. **5**: p. 13922.
206. Rauber, D., et al., *Structure-Property Relation of Trimethyl Ammonium Ionic Liquids for Battery Applications.* 2021. **11**(12): p. 5679.
207. Ishai, P.B., et al., *Electrode polarization in dielectric measurements: a review.* Measurement Science and Technology, 2013. **24**(10): p. 102001.
208. Dyre, J.C., *Studies of ac hopping conduction at low temperatures.* Physical Review B, 1994. **49**(17): p. 11709-11720.
209. Dyre, J.C. and T.B. Schrøder, *Universality of ac conduction in disordered solids.* Reviews of Modern Physics, 2000. **72**(3): p. 873-892.
210. Schrøder, T.B. and J.C. Dyre, *Scaling and Universality of ac Conduction in Disordered Solids.* Physical Review Letters, 2000. **84**(2): p. 310-313.
211. Sangoro, J.R. and F. Kremer, *Charge Transport and Glassy Dynamics in Ionic Liquids.* Accounts of Chemical Research, 2012. **45**(4): p. 525-532.
212. Sangoro, J.R., et al., *Diffusion in ionic liquids: the interplay between molecular structure and dynamics.* Soft Matter, 2011. **7**(5): p. 1678-1681.
213. Popov, I., et al., *Critical Role of Anion–Solvent Interactions for Dynamics of Solvent-in-Salt Solutions.* The Journal of Physical Chemistry C, 2020. **124**(16): p. 8457-8466.
214. Tokudaa, H., et al., *Physicochemical Properties and Structures of Room Temperature Ionic Liquids. 1. Variation of Anionic Species.* The Journal of Physical Chemistry B, 2004. **108**(42): p. 16593-16600.
215. Liu, H. and E. Maginn, *A molecular dynamics investigation of the structural and dynamic properties of the ionic liquid 1-n-butyl-3-methylimidazolium bis(trifluoromethanesulfonyl) imide.* J. Chem. Phys., 2011. **135**: p. 124507.

216. Urahata, S.M. and M.C.C. Ribeiro, *Single particle dynamics in ionic liquids of 1-alkyl-3-methylimidazolium cations.* The Journal of Chemical Physics, 2004. **122**(2).
217. Lorenz, M., et al., *Local Volume Conservation in Concentrated Electrolytes Is Governing Charge Transport in Electric Fields.* Journal of Physical Chemistry Letters, 2022. **13**(37): p. 8761-8767.
218. Kilchert, F., et al., *A Volume-based Description of Ion Transport: The Role of Incompressibility.* 2022.
219. Pfeifer, S., et al., *Quantification of cation-cation, anion-anion and cation-anion correlations in Li salt/glyme mixtures by combining very-low-frequency impedance spectroscopy with diffusion and electrophoretic NMR.* Physical Chemistry Chemical Physics, 2021. **23**(1): p. 628-640.
220. Roling, B., et al., *Ion Dynamics in Concentrated Electrolyte Solutions: Relating Equilibrium Fluctuations of the Ions to Transport Properties in Battery Cells.* 2022: p. e12533.
221. Popovic, J.J.M.C. and Physics, *Dry Polymer Electrolyte Concepts for Solid-State Batteries.* 2022. **223**(8): p. 2100344.
222. York, M., et al., *Recent advances in solid-state beyond lithium batteries.* 2022. **26**(9): p. 1851-1869.
223. Jin, L., et al., *Structure and Transport Properties of a Plastic Crystal Ion Conductor: Diethyl(methyl)(isobutyl)phosphonium Hexafluorophosphate.* Journal of the American Chemical Society, 2012. **134**(23): p. 9688-9697.
224. Pringle, J.M., *Recent progress in the development and use of organic ionic plastic crystal electrolytes.* Physical Chemistry Chemical Physics, 2013. **15**(5): p. 1339-1351.
225. Pringle, J.M., et al., *Organic ionic plastic crystals: recent advances.* Journal of Materials Chemistry, 2010. **20**(11): p. 2056-2062.
226. Jin, L., et al., *Molecular insights: structure and dynamics of a Li ion doped organic ionic plastic crystal.* Phys Chem Chem Phys, 2013. **15**(45): p. 19570-4.
227. Zhou, Z.-B. and H. Matsumoto, *Lithium-doped, organic ionic plastic crystal electrolytes exhibiting high ambient-temperature conductivities.* Electrochemistry Communications, 2007. **9**(5): p. 1017-1022.
228. MacFarlane, D.R. and M.J.A.m. Forsyth, *Plastic crystal electrolyte materials: new perspectives on solid state ionics.* 2001. **13**(12-13): p. 957-966.
229. Thomas, M.L., et al., *Organic ionic plastic crystals: flexible solid electrolytes for lithium secondary batteries.* 2023.
230. Sirigiri, N., et al., *Factors controlling the physical properties of an organic ionic plastic crystal.* Materials Today Physics, 2022. **22**: p. 100603.
231. Popov, I., et al., *Collective Ion Dynamics in Ionic Plastic Crystals: The Origin of Conductivity Suppression.* The Journal of Physical Chemistry C, 2023. **127**(32): p. 15918-15927.

232. Popov, I., et al., *Collective Ion Dynamics in Ionic Plastic Crystals: The Origin of Conductivity Suppression.* 2023.
233. Das, S., et al., *Brillouin light scattering study of microscopic structure and dynamics in pyrrolidinium salt based ionic liquids.* Solid State Ionics, 2021. **363**: p. 115603.
234. Madsen, I.C., N.V. Scarlett, and N.A. Webster, *Quantitative phase analysis*, in *Uniting Electron Crystallography and Powder Diffraction*. 2012, Springer. p. 207-218.
235. Bish, D.L. and S.J.J.o.A.C. Howard, *Quantitative phase analysis using the Rietveld method.* 1988. **21**(2): p. 86-91.
236. Loaiza, L.C. and P. Johansson, *Li-Salt Doped Single-Ion Conducting Polymer Electrolytes for Lithium Battery Application.* 2022. **223**(8): p. 2100419.
237. Pitawala, J., et al., *Phase behaviour, transport properties, and interactions in Li-salt doped ionic liquids.* Faraday Discuss, 2012. **154**: p. 71-80; discussion 81-96, 465-71.
238. Sun, L., et al., *Ionic liquid‐based redox active electrolytes for supercapacitors.* 2022. **32**(27): p. 2203611.
239. Ramesh, S., R. Shanti, and E. Morris, *Studies on the thermal behavior of CS:LiTFSI:[Amim] Cl polymer electrolytes exerted by different [Amim] Cl content.* Solid State Sciences, 2012. **14**(1): p. 182-186.
240. Martinelli, A., et al., *Phase behavior and ionic conductivity in lithium bis(trifluoromethanesulfonyl)imide-doped ionic liquids of the pyrrolidinium cation and Bis(trifluoromethanesulfonyl)imide anion.* J Phys Chem B, 2009. **113**(32): p. 11247-51.

VITA

Md Dipu Ahmed was born and raised in Dhaka, Bangladesh. After the completion of bachelor and master in science degree in Applied Chemistry and Chemical Engineering from university of Dhaka, He worked as analytical development chemist in a FDA approved pharmaceutical industry namely Eskayef Pharmaceuticals Ltd. Dipu had strong desire to pursue advance degree from the United States and attended the graduate school at the University of Tennessee Knoxville (UTK) in chemistry department under polymer science in spring 2021. He worked with Dr. Sokolov group on different projects including concentrated ionic systems. He got lab safety cultural awards twice from environmental health and safety dept from UTK in spring 2023 and summer 2023. He will obtain his master's degree working on development of understanding of ionic corrections on conductivity in concentrated ionic systems.